A review on catalytic methane combustion at low temperatures

He, Li; Fan, Yilin; Bellettre, Jerome; Yue, Jun; Luo, Lingai

Published in:
Renewable and Sustainable Energy Reviews

DOI:
10.1016/j.rser.2019.109589

Publication date:
2020

Renewable and Sustainable Energy Reviews 119 (2020) 109589

Contents lists available at ScienceDirect

Renewable and Sustainable Energy Reviews

journal homepage: http://www.elsevier.com/locate/rser

A review on catalytic methane combustion at low temperatures: Catalysts, mechanisms, reaction conditions and reactor designs

Li He [a,b], Yilin Fan [a], Jérôme Bellettre [a], Jun Yue [b,**], Lingai Luo [a,*]

[a] Université de Nantes, CNRS, Laboratoire de thermique et énergie de Nantes, LTeN, UMR 6607, F-44000, Nantes, France
[b] Department of Chemical Engineering, Engineering and Technology Institute Groningen, University of Groningen, 9747 AG Groningen, the Netherlands

ARTICLE INFO

Keywords:
Natural gas
Catalytic methane combustion
Catalysts
Mechanism
Reaction conditions
Reactor

ABSTRACT

Natural gas (with methane as its main component) provides an attractive energy source because of its large abundance and its high heat of combustion per mole of carbon dioxide generated. However, the emissions released from the conventional flame combustion (essentially NO_x) have harmful impacts on the environment and the human health. Within the scope of rational and clean use of fossil energies, the catalytic combustion of natural gas appears as one of the most promising alternatives to flammable combustion. The presence of catalysts enables complete oxidation of methane at much lower temperatures (typically 500 °C), so that the formation of pollutants can be largely avoided. This work presents a literature review on the catalytic methane combustion. Various aspects are discussed including the catalyst types, the reaction mechanisms and kinetic characteristics, effects of various influencing operational factors and different reactor types proposed and tested. This paper may serve as an essential reference that contributes to the development of well-designed reactors, equipped with appropriate catalysts, and under well-handled operating conditions to realize the favorable (kinetic) performance, for their future applications and propagation in different industrial sectors.

1. Introduction

One of the major concerns over economic growth and social development nowadays is the constantly increasing energy demand [1]. The study of U.S. Energy Information Administration has forecasted an increase of 28% in the world's energy consumption from 2015 to 2040 [2]. While there is a constant progress year by year for the development of renewable energies, the use of fossil sources (petroleum, coal and natural gas) is still dominant, and remains indispensable in the near future [3].

Among the fossil energy resources, the natural gas presents a particular interest because of its higher energy content (55.7 kJ g^{-1} if fully based on methane as its main component) than coal (39.3 kJ g^{-1}) and petroleum (43.6 kJ g^{-1}) as well as its reduced CO_2 emission (50% less than coal and 30% less than petroleum). Moreover, the proven natural gas reserves worldwide are abundant, reaching about 193.5 trillion cubic meters at the end of 2017 [4]. As a result, natural gas has accounted for the largest increment (24%) in the main energy consumption in the past decade until 2017, and has been suggested as a substitute for oil and coal as a future leading energy source for the next 20 years [5]. In response to this, there is a rapidly growing number of research & development efforts yearly on the deployment of natural gas for their use in various sectors including industrial, residential, power, transport and many others [6].

Besides the natural gas fields, the synthetic natural gas (SNG) can also be derived from coal gasification, CO_2 methanation and biomass gasification/digestion [7,8]. Fig. 1 shows the main reaction network of SNG in the industry. Biomass is particularly promising as a substitute for fossil resources owing to its benefits of energy security and environmental friendliness. On one hand, the SNG can be obtained from

Abbreviations: 3DOM, Three-dimensionally ordered microporous; $AB_xAl_{(12-x)}O_{19}$ (x = 1, 3, 6, 9, 12), Hexaaluminate formula; ABO_3 (or $A^IB^VO_3$, $A^{II}B^{IV}O_3$, or $A^{III}B^{III}O_3$), Perovskites formula; BET, Brunauer, Emmett and Teller method, specific surface area of catalyst, unit: $m^2 \cdot g^{-1}$; BHA, Barium hexaaluminate; CMC, Catalytic methane combustion; DP, Deposition precipitation; DRIFT, Diffuse reflectance infrared spectroscopy; HDP, Homogeneous deposition precipitation; HTF, Heat transfer fluid; ITM, Ion transport membrane reactor; NGVs, Natural gas vehicles; SEM, Scanning electron microscope; SOFCs, Solid oxide fuel cells; SNG, Synthetic natural gas.

* Corresponding author.
** Corresponding author.
E-mail addresses: yue.jun@rug.nl (J. Yue), Lingai.Luo@univ-nantes.fr (L. Luo).

https://doi.org/10.1016/j.rser.2019.109589
Received 26 April 2019; Received in revised form 29 October 2019; Accepted 11 November 2019
Available online 30 November 2019

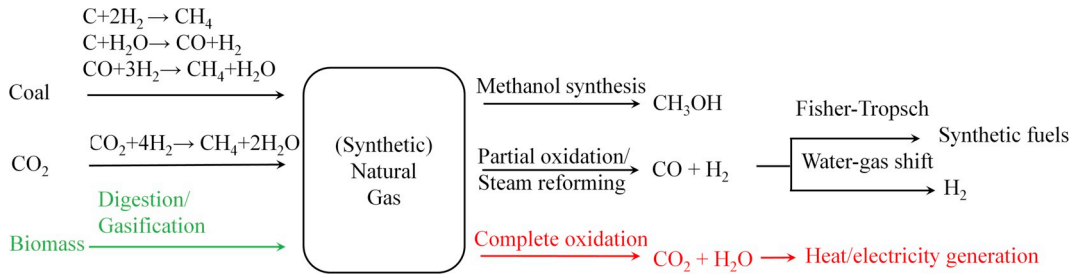

Fig. 1. Main reaction network of synthetic natural gas.

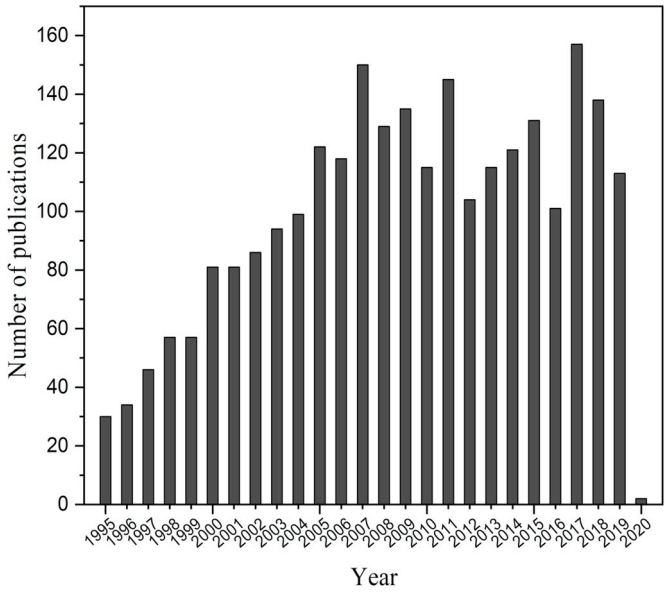

Fig. 2. Number of publications on the catalytic methane combustion (source: Scopus; keyword: catalytic methane combustion; date: 17 October 2019).

upgrading biogas that is generated from biomass digestion (e.g. manure) and/or from carbohydrate fermentation by bacteria in an anaerobic environment [9–11]. On the other hand, the SNG can be produced via gasification of biomass (e.g. wood, straw and crops) followed by the process of methanation [12,13]. The syngas and methanol can be synthesized by partial oxidation and steam reforming reaction, producing consequently synthetic fuels and hydrogen. Meanwhile, the combustion of methane can provide the heat and electricity due to the strongly exothermic nature of the reaction.

The conventional flame combustion of (synthetic) natural gas occurs typically at above 1400 °C and releases harmful pollutants (such as NO_x, CO and hydrocarbon). The impact of NO_x on human health (respiratory diseases) has been widely recognized [14]. Its emission also has harmful environmental impacts including the formation of photochemical smog and acid rain [15]. More and more stringent regulations are thus applicable over European countries. For example, in September 2018, the maximum NO_x emission level has been reduced from 70 mg·kWh^{-1} (class 5) to 56 mg·kWh^{-1} for all domestic boilers sold in Europe [16]. As a result, the complete oxidation of natural gas in the presence of catalysts (i.e. the catalytic combustion) appears as one of the most promising alternative solutions for the rational and clean use of fossil energies. The activation energy is reduced from 100–200 kJ mol^{-1} (conventional combustion) to 40–80 kJ mol^{-1} (catalytic combustion), leading to a lower working temperature (<600 °C). In this regard, less pollutant emissions could be reached (~5 ppm compared with 150–200 ppm for conventional combustion). Hence, the catalytic combustion of methane or natural gas as a clean technology has received increasing research attention [17], indicated by the significantly increasing number of yearly publications over the past two decades (Fig. 2).

Various application areas of catalytic methane combustion (CMC) have been proposed and attempted, as illustrated in Fig. 3 and briefly described below.

(i) Natural gas vehicles (NGVs) [18–21] (ca. 300–700 °C): NGVs have the advantages in the abatement of greenhouse gas emissions and smog emissions compared to gasoline or diesel-driven vehicles. Three-way catalysts are applied on NGVs mainly for exhaust purification in practice.

(ii) Gas turbine [22–27] (ca. 700–1400 °C): Methane combustion is widely used as the fuel on the gas turbine. The combusted gas is used to drive a turbine for power generation. For example, 25 kW electricity output can be obtained with 0.8 vol% methane in the air [24].

(iii) Solid oxide fuel cells (SOFCs) [28] (ca. 500–1000 °C): The preheated compressed air passes into the cathode of the battery while the compressed methane mixed with the overheated steam enters into the anode of the fuel cell. The methane electrochemical conversion in SOFCs, if properly controlled, could obtain a high conversion efficiency and an environmental benefit due to a significant decrease in pollutant emissions.

(iv) Domestic heating systems [29–32] (ca. 300–700 °C): the heat released from the exothermic CMC reaction is utilized to drive the domestic heating systems, such as the central boilers or gas stoves. A high energy conversion efficiency and eco-friendly water boiler prototype with a hot water yield of 11.5 kg min^{-1} has been reported [33].

(v) Coupling with endothermic reaction (ca. 300–700 °C): the reaction heat from CMC is commonly used to drive an endothermic reaction so as to maintain the continuous autothermal operation [34]. Novel reactor designs have been proposed for coupling the CMC with an endothermic reaction (methane steam reforming [35,36], dehydrogenation of propane to propylene [37], dehydrogenation of ethane to ethylene [38,39], etc.), owing to the optimized energy integration and the process intensification.

It may be discovered that compared to the conventional flame combustion, the presence of catalysts enables a decrease of the working temperature (<1400 °C). Depending on the target application, the operational temperature for CMC can be further divided into a relatively lower range (about 300–700 °C) and a relatively higher one (about 700–1400 °C). The low-temperature CMC becomes more attractive due to the remarkable abatement of pollutant emissions and the prolonged catalyst lifetime. For instance, the reusability and the reproducibility of catalysts, especially for noble metal catalysts, are shortened at high temperatures. In this field, developing catalysts with high catalytic activity, low light-off temperature and good thermal stability even for such low temperature operations is still a challenging issue.

A great number of researches have been devoted to catalyst development [18,40,41] and reactor design [42–44] for CMC. Noble metal catalysts (e.g. Pt, Pd and Rh) have been widely investigated owing to their high catalytic activity. Hexaaluminate and perovskite catalysts,

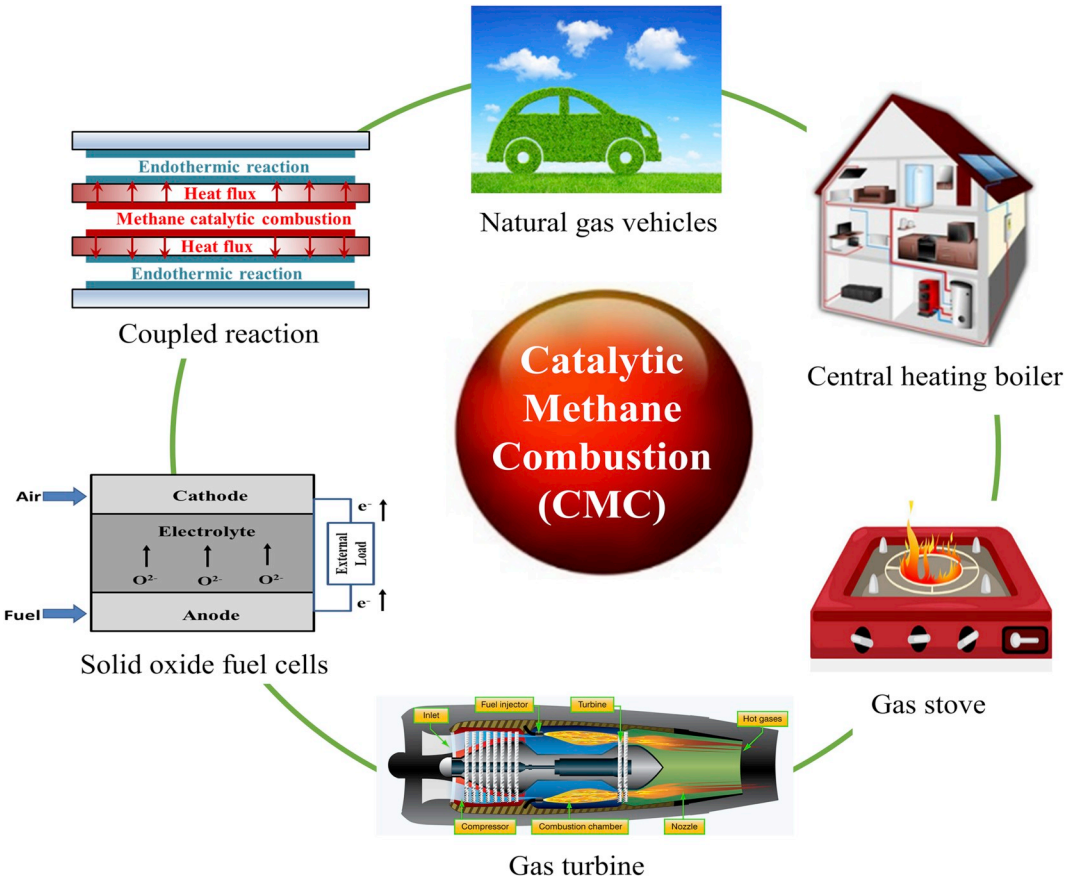

Fig. 3. Main applications of CMC.

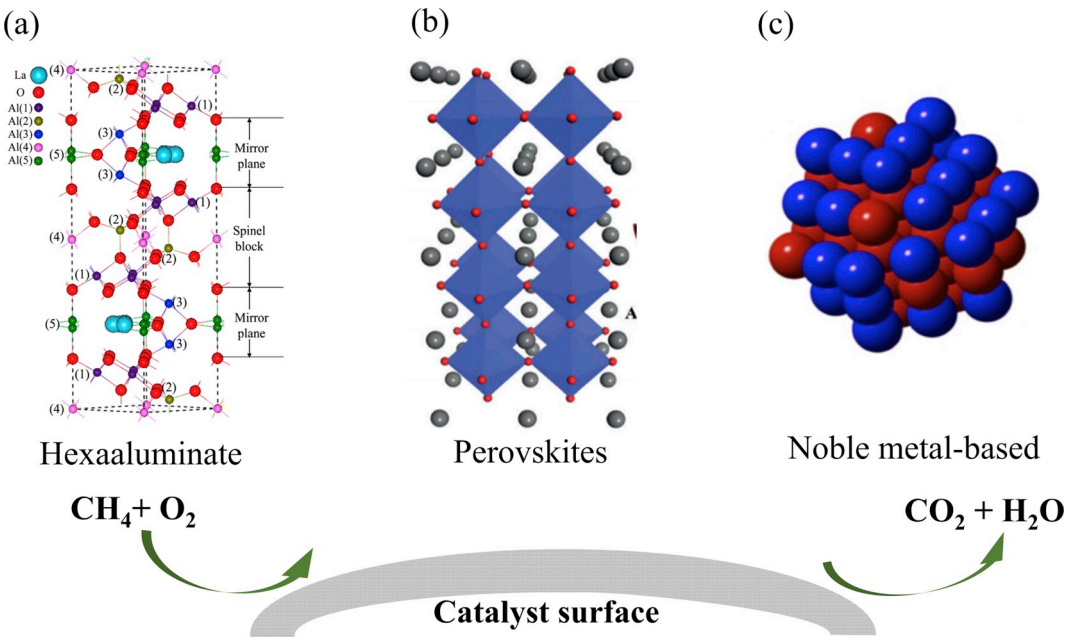

Fig. 4. Schematic structure of catalysts for CMC. (a) hexaaluminate ($LaFeAl_{11}O_{19}$) [68]; (b) perovskites ($La_{0.5}Sr_{0.5}CoO_{3-\delta}$) [69]; (c) noble metal-based (Pd–Ru) catalyst [70].

due to their relatively lower catalytic activity and high thermal stability, are commonly used for high temperature applications (600–1400 °C). Optimization of reaction conditions over various catalysts has been broadly investigated [19], such as the effect of light-off temperature, reactant concentration, oxygen to methane molar ratio, residence time, etc. Moreover, the mechanistic studies mainly focusing on kinetic models for various catalysts have been well elaborated in earlier literatures [45–48]. The reactor designs (e.g. micro/mini-structured reactor)

Table 1
Summary of some published reviews related to CMC.

Reference	Main contents
Gélin & Primet 2002 [18]	Noble metal catalysts for methane complete oxidation at low temperatures (1) Pd, Pt-based catalysts with silica and alumina support (2) Kinetics, active sites nature (Pd, Pt), mechanism (3) Particle size effect (4) Sulfur poisoning effect (5) Improved support: ZrO_2, SnO_2, CeO_2, Co_3O_4, etc. (6) Bimetallic system: Pd–Pt catalyst
Choudhary et al. 2002 [40]	Catalysts for oxidation of methane and lower alkanes (1) Noble metal-based catalysts: Pd, Pt, Rh, Au (2) Metal oxide catalysts Single metal oxides: CuO, MgO, Co_3O_4, etc. Mixed metal oxides: perovskites, hexaaluminate, doped metal oxides
Ciuparu et al. 2002 [57]	CMC over Pd-based catalysts (1) Catalyst characterization, deactivation, reaction conditions, etc. (2) Transformation of Pd and PdO phases (3) Catalytic mechanism
Li & Hoflund 2003 [41]	Complete oxidation of methane at low temperatures over noble/non-noble metal catalysts (1) Kinetics and mechanism over Pd/Al_2O_3 (2) Effect of Ce additives on the activity (3) Effect of CO_2 and H_2O on the activity (4) Perovskite-type oxides
Rahimpou et al. 2012 [34]	Coupling exothermic and endothermic catalytic reactions (1) Reactor type: fixed bed, fluidized bed, etc. (2) Various alternatives for thermal coupling (3) Various coupling catalytic reactions, including: CMC reaction coupled with: methane steam reforming (with H_2O or CO_2) or dehydrogenation of propane to propylene or dehydrogenation of ethane to ethylene or methane partial oxidation coupled with methane steam reforming, etc.
Zhu et al. 2014 [53]	Perovskite preparation and application in heterogeneous catalysis (1) Structure and properties, characterizations (2) Synthesis with morphologies: bulk, nanosized, porous, nanospheres, etc. (3) Applications: NO decomposition; NO reduction; NO oxidation; N_2O decomposition CH_4 combustion; CO oxidation; oxidative reforming of hydrocarbon; volatile organic compound combustion
Chen et al. 2015 [17]	Catalysts for methane combustion (1) Noble metal catalyst: Pd-based catalyst: active nature, support effect, additive effect, sulfur poisoning Pt-based catalyst: chlorine effect, particle size, SO_2, H_2/propane addition Au-based catalyst: Au state, different preparation methods effects Bimetallic system: Pt–Pd, Pd–Rh, Pd–Au, etc. (2) Metal oxide catalyst: Single metal oxide-based catalysts: CuO, Co_3O_4, MnO_x, CeO_2 Perovskite catalysts: substitution effect, sulfur poisoning, and preparation methods Spine catalysts: catalytic activity, cation substitution, etc. Hexaaluminate catalyst: preparation methods, cation substitution, etc. Kinetics and reaction mechanism over metal oxide catalysts
Tian et al. 2016 [52]	Hexaaluminate structure and catalytic performance (1) Structure: β-Al_2O_3 and magnetoplumbite structures, prosperities (2) Synthesis: sol-gel, co-precipitation, reverse microemulsion, etc. (3) Catalytic performances: methane combustion, methane partial oxidation, N_2O decomposition
Gür 2016 [28]	Methane conversion in SOFCs: (1) Catalytic methane oxidation (2) Electrochemical conversion of methane (3) Major challenges for methane conversion on catalytic anodes
Cruellas et al. 2017 [58]	Advanced reactor concepts for oxidative coupling of methane (1) Concept and type of reactors for methane oxidative coupling (2) Heat management system (3) Applications
Yang & Guo 2018 [59]	Nanostructured perovskite oxides (1) CMC reaction mechanism (2) Properties and structure design of perovskite (3) Recent advances of perovskite for CMC
Current review	*Various aspects on CMC* *(1) Catalysts: hexaaluminates, perovskite, noble metal* *(2) Reaction mechanism and kinetics* *(3) Reaction operational conditions: effect of temperature, ratio of oxygen to methane, space velocity, natural gas composition, pressure* *(4) Reactor types: fixed-bed reactor, wall-coated reactor (folded plate-type, tube-coated type, monolithic, microchannel plate-type), membrane bed, fluidized bed*

Table 2
Comparison of main catalysts used for methane combustion.

Reference	Catalyst type	BET surface area ($m^2 \cdot g^{-1}$)[a]	Calcination temperature (°C)	Reaction temperature (°C)	Advantages	Disadvantages	Applications
[52]	Hexaaluminate	0–30	900–1300	<1000	- High thermal stability - Doped cation substitution (improved catalytic activity) - Different oxygen species - Relatively low cost	- Low surface area - High light-off temperature	High temperature reaction (e.g., partial/complete oxidation of methane, N_2O decomposition)
[53,73]	Perovskite	0–30	700–1100	<1000	- High thermal stability - Doped cation substitution - higher oxygen mobility and species - Relatively low cost	Ditto	Ditto
[18,40,41]	Noble metal (e.g. Pt, Pd, Rh)	>100	450–600	<600	- High catalytic activity - High surface area - Low light-off temperature	- Catalyst sintering - Relatively high cost	Low temperature reaction (e.g., partial/complete oxidation, methane steam reforming)

Note.
[a] Average specific surface area measured by BET (Brunauer, Emmett and Teller) method is shown here, but may vary depending on the preparation method.

with coupled endothermic reaction have become a hotspot direction in recent decade [49–51]. Reviews papers related to CMC have also been published, as summarized in Table 1. Nevertheless, most of them primarily focus on the improvement of catalytic activity (e.g. noble metal-based catalysts [17,18,40,41], hexaaluminates/perovskite catalysts [52,53]). Other review papers may involve the CMC in one or several sub-sections, but they are mainly devoted to a specific topic, e.g. heating system [54,55], SOFCs [28], coupling exothermic/endothermic reactions [34], SNGs [9,56], etc.

The present review on CMC aims at filling the literature gap by providing a comprehensive and combined understanding of catalysts, mechanisms, reaction conditions and reactor designs. In particular, the present paper has the following objectives:

- A brief introduction of the catalyst types, their advantages/disadvantages, associated reaction mechanisms and kinetic characteristics.
- A complete survey on the effects of various operational factors on the performance of CMC, including temperature, space velocity, O_2/CH_4 ratio, natural gas composition and pressure.
- A review on different reactor types used for CMC, with a special focus on microchannel reactor-heat exchangers.

This paper may serve as an essential reference that contributes to the development of well-designed reactors, equipped with appropriate catalysts and under well-handled operating conditions, towards realizing their favorable (kinetic) performance and for their future application and propagation in different industrial sectors.

2. Catalysts for methane combustion

2.1. Catalyst category

Catalysts play an important role in terms of catalytic activity and reaction rate on the CMC, and are mainly categorized into metal oxide catalysts (e.g. hexaaluminate, perovskites, and single-metal oxides) and noble metal-based catalysts. The research interests on perovskites and noble metal catalysts are remarkably increasing over the years, with the latter being the most popular. The main advantages and disadvantages of catalysts are summarized in Table 2.

2.1.1. Mixed oxide catalysts

(1) *Hexaaluminate* [52,60–63] possesses a typical lamellar structure consisting of alternatively packed spinel blocks and conduction layers (mirror symmetry plane), as shown in Fig. 4a. It can be represented by the formula $AB_xAl_{(12-x)}O_{19}$ ($x = 1, 3, 6, 9, 12$), wherein A is a large cation (e.g., of Na, K, Ba, La) residing in the conduction layer and B is the transition metal ion (e.g., of Mn, Fe, Co, Cu or Ni) or noble metal ion (e.g., of Ir, Ru, Pd or Rh) which substitutes A cation in both the spinel block and the conduction layer. Magnetoplumbite and β-alumina are two common structures for hexaaluminate in terms of the different arrangement, charge and radius of ions in the conduction layer [64]. Magnetoplumbite structure consists of A cation, O, Al in the conduction layers, while β-alumina consists of A cation and O. Importantly, the cation-substituted hexaaluminate with high sintering resistance greatly improves the catalytic activity in methane combustion due to the availability of the valent variation of transition metals (e.g. Mn, Ba, La, etc.) in the crystal lattice [65–67].

Hexaaluminate has been applied for CMC since 1987, owing to its exceptionally high thermal stability and strong resistance to thermal shock [71]. Thus, hexaaluminate is considered as the most suitable catalyst for high temperature applications (e.g. for gas turbines). Other main applications include the methane partial oxidation, the dry reforming of methane and the decomposition of N_2O. Although a great improvement of specific surface has been achieved, efforts are still required so as to synthesize hexaaluminate with simple procedures, as well as an excellent catalytic activity.

(2) *Perovskites* [72–74] are represented by a standard formula as ABO_3 (or more complicated as $A^IB^VO_3$, $A^{II}B^{IV}O_3$ or $A^{III}B^{III}O_3$). A as a larger cation is commonly composed of alkaline/rare earth elements (e.g. of La, Sr, Bi, etc.), residing on the edge of the structure for its stabilization with less effect on the catalytic activity. B as a smaller cation consists of transition metal that is surrounded by octahedral of oxygen anions, functioning as the main catalytic center. Their structure is schematically shown in Fig. 4b. The microstructure of mixed oxide catalyst is beneficial for their oxygen mobility and catalytic activity [75]. The presence of defect structure in oxygen vacancies, the existence of unusual valence and the availability of reversibly released oxygen have been considered relevant to the enhanced catalytic activity, even comparable to that of noble metal catalysts [76,77]. It can be explained by the fact that the oxygen vacancies are directly relevant to the adsorbed oxygen species over the catalyst surface. The more oxygen vacancies, the more adsorbed oxygen formed over the surface, leading to the higher catalytic activities in methane oxidation. A recent work reported by Miao et al. [78] reveals that more active oxygen species could be obtained using $La(Mn, Fe)O_{3+\lambda}$ perovskite catalyst, and the catalytic

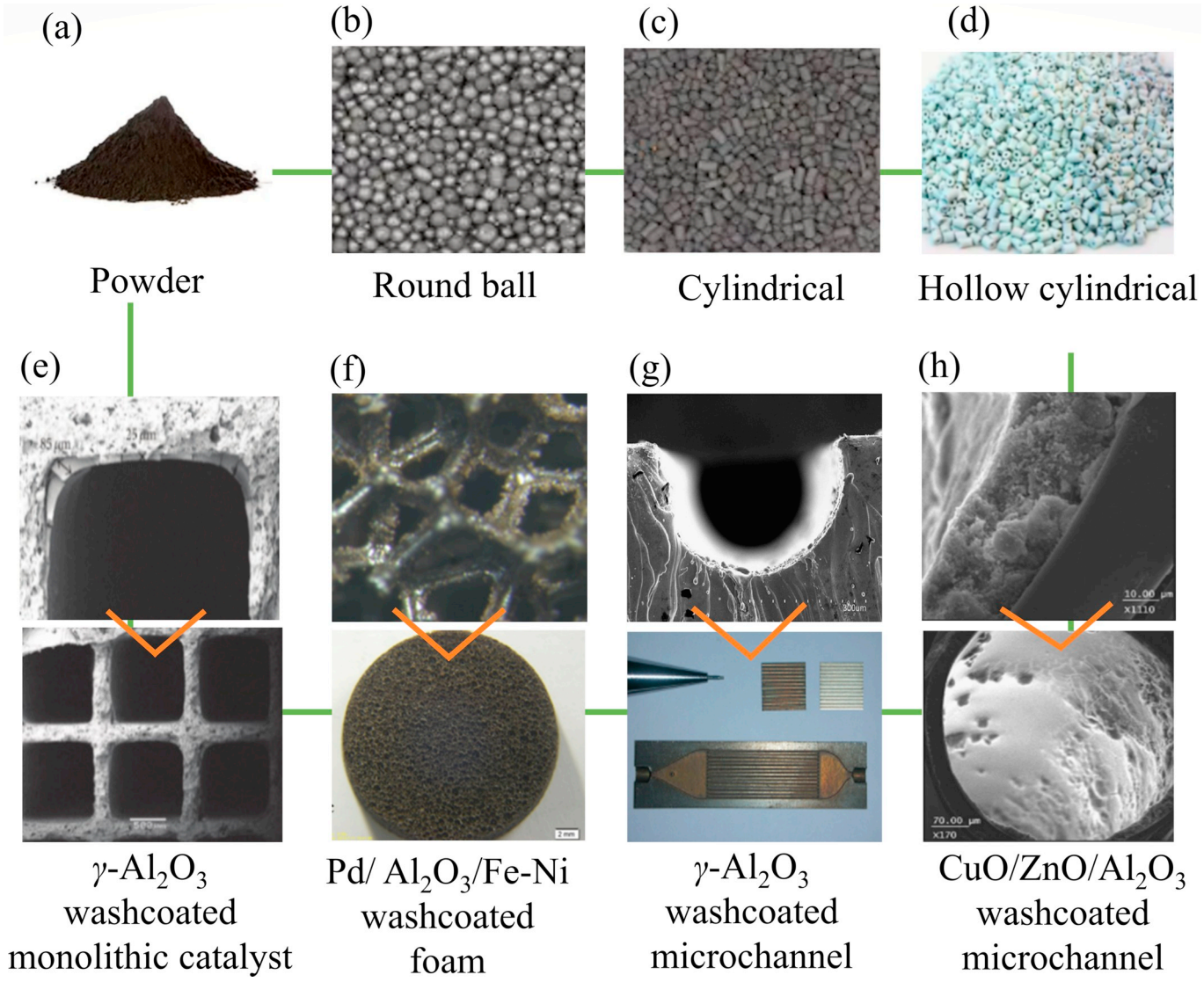

Fig. 5. Various shaping of catalysts. (a) Powder catalyst; (b) Pellet catalyst; (c) Round ball catalyst; (d) Ring shape catalyst; (e) SEM images of γ-Al_2O_3 washcoated layer on cordierite monolith [112]; (f) Microscopic image of Pd/Al_2O_3/Fe–Ni foam [113]; (g) SEM (scanning electron microscope) images of γ-Al_2O_3 washcoated microchannel [114]; (h) SEM images of CuO/ZnO/Al_2O_3 washcoated capillary microreactor [115].

activity of CMC thereby was significantly improved. The cation-substitution of perovskites effectively increases the oxygen vacancies by varying the distribution of B oxidation state [79,80]. Different aspects of perovskites have been addressed in several review papers, including the structure, synthesis and applications [53,59,81], the acid-base catalytic properties of perovskites [82], and the lanthanum-based perovskites [83]. The mechanism and kinetics may be found in the book of Granger et al. [84].

A lower calcination temperature is required for the perovskite phase than the hexaaluminate phase [85]. Perovskite catalysts are featured by their high thermal stability as well as the improved specific surface area, displaying a better catalytic activity in CMC. The higher catalytic performance is mainly ascribed to the foreign-cation substitution, the produced oxygen lattice and the deficiency over catalyst surface. A promising direction of improvement is designing perovskite catalysts with featured morphologies (e.g., nano-sized, porous, hollow), favoring their potential industrial applications.

2.1.2. *Noble metal catalysts*

Noble metal catalysts have been most intensively investigated for CMC, owing to their high catalytic activity at low temperatures [57,86–88]. Their basic structure is shown in Fig. 4c. Pd, Pt, Rh, Au and Co as the active component have been widely studied in the literature. Among them, Pd and Pt-based catalysts were reported as the most active one by far. Various support materials, such as ZrO_2, CeO_2, Al_2O_3, SnO_2, TiO_2, were considered. The base/acid properties of the support affect the catalytic activity by interacting with the oxidized/metallized state of noble metals. It was reported that the decreased acidity strength of Al_2O_3 support (with Pd as the active component) could enhance the performance of CMC [89]. Moreover, the introduction of additives (e.g. of La, Mn, Ce, Mg, V) could stabilize the catalyst support and active sites, and prolong the catalyst life. It has been reported by Farrauto et al. [90,91] that the CeO_2 addition is favorable to prevent the catalyst deactivation. The PdO species on the catalyst surface thereby are stabilized due to the increased temperature of PdO decomposition. Moreover, the improved storage and exchange of oxygen species in the presence of CeO_2 effectively promote the Pd reoxidation, resulting in a higher catalytic performance [92]. The recent study by Toso et al. [93] illustrated that the stability of Pd/$Ce_{0.75}Zr_{0.25}O_2$ catalyst exposure to the water was improved by well-dispersed small Pd nanoparticles. More detailed reviews can be found in the literature [17,18,41].

The formation of active sites is mainly dependent on the support

composition, properties, and the preparation method. With respect to Pd and Pt-based catalysts, Pd is supposed to be superior to Pt, not only for the CMC but also for the oxidation of higher alkanes and olefins [94]. It is commonly considered that Pd in the oxidized state (PdO) is the most active and stable (up to 800 °C) [95]. Farrauto et al. [90] proposed that at least two different PdO species were present on the Al_2O_3 support. Dispersed PdO decomposed in a temperature range between 750 and 800 °C, whereas crystalline PdO decomposed from 800 to 850 °C. Hicks et al. [96] identified at least two different phases by infrared spectra. The crystalline palladium with a smaller size presented 10 to 100 higher catalytic activity than dispersed PdO phase. Similarly, the Pt crystalline phase has a higher catalytic activity than that in the dispersed PtO_2 phase due to the formation of chemisorbed oxygen in the crystalline phase [96].

Moreover, bi- or trimetallic catalysts have been reported to have higher catalytic activity and stability compared to monometallic ones [97–101]. For example, Pd–Pt/Al_2O_3 catalyst is more active and stable than Pd/Al_2O_3 [102,103]. It has been reported that Pt–Pd catalysts showed a higher activity even than Pd–Ag, Pd–Co, Pd–Ni and Pd–Rh over the Al_2O_3 support [97]. A better synergetic effect and the formation of bi-metal structure have proved to improve the catalyst activity and life-time. Other factors such as the support structure, the particle size and the surface morphology also have significant influence on the catalytic performance. More details on the influence of these factors can be found in the references [19,104–106].

The electrochemical field-assisted CMC is a relatively novel direction in recent years owing to the synergetic effect. Electrocatalysis process commonly involves the oxidation and reduction reactions via direct electrons transformation (i.e. the produced electrical current). Electrolytes as promoting species can modify the electronic properties of the catalyst surface via the formation of favorable bonds between reactants and the electrodes. The decrease of the activation energy through the synergetic effect between electric field and catalysis results in the enhancement of reaction rate for CMC [107–109]. Li et al. [109] reported that the reaction rate of CMC over the Mn_xCo_y catalyst was remarkably accelerated by the improved reducibility of Co^{3+} in the electric field, promoting the methane activation at low temperature. The light-off temperature (T_{50} = 255 °C) over $PdCe_{0.75}Zr_{0.25}O_x$ catalyst can be significantly reduced because of the enhanced reducibility of PdO_x species in electric field (e.g. 3 mA current) [110]. More details on the electrochemical-assisted CMC may be found in a recent reference [111].

Although noble metal catalysts present advantages such as high specific surface area, high dispersion of active component and mild reaction conditions, the catalyst deactivation (due to sintering, particle size growth, poisoning, etc.) and the high cost are the main limitations for their large-scale application in the industry.

2.2. Shaping of catalyst

The shaping of catalysts could significantly affect the pressure drop and the reactant-catalyst mass transfer in the reactor. Fig. 5 shows a variety of catalyst shapes used for CMC. Fine powders are more suitable for being incorporated into minireactors or microreactors with higher catalyst surface area. However, powder catalysts (Fig. 5a) could lead to a high pressure drop if packed in a long (e.g., several meters) fixed-bed reactor, or possibly be blown out when used in a fluidized-bed reactor. To decrease the pressure drop, the catalyst is commonly shaped into larger bodies, e.g. pellet, round ball, cylindrical shape (Fig. 5b–d). Moreover, a sufficient mechanical strength of the catalyst support is essential for the catalyst's long-term structural durability.

Washcoated catalysts have received an increasing attention owing to its high surface area, low pressure drop and better usage of catalyst. This type of catalyst is usually used in monolithic reactors (Fig. 5e) [112,116], foam reactors (Fig. 5f) [113,117], multichannel microreactors (Fig. 5g) [118–120] and tube reactors (Fig. 5h) [32,121]. The recent progress of washcoated and packed-bed microreactors is reviewed in the reference [50]. The washcoated catalyst is commonly deposited as a thin layer on structured surfaces using typically a dip-coating method [122]. Other methods, such as suspension method [120,123–125], sol-gel technique [126,127], chemical vapor deposition [128,129], physical vapor deposition [130,131]are also widely used. In our previous work [120], the preparation of a well-adhered Pt/γ-Al_2O_3 catalytic coating in microreactors has been elaborated by applying various binders, particle size, pH conditions, etc. The preparation of the suspension and the pretreatment of the substrate hosting the catalytic layer have to be adapted to obtain a high thermal stability and a well dispersion of the coating [118,120,132].

Table 3
Main literature results on kinetic parameters for CMC.

Reference	Catalyst	Reactant	Temperature (°C)	Conversion (%)	E_a (kJ·mol^{-1})	Reaction rates (μmol·g^{-1}·min^{-1})
[19]	0.5% Pt/Al_2O_3	O_2/CH_4 = 2:1	350–425	1.8–13.7	101 ± 10	
	1% Pt/Al_2O_3				104 ± 1.0	
	2% Pt/Al_2O_3				91.4 ± 5	
	4% Pt/Al_2O_3				98.1 ± 11	
	0.5% Pt/Al_2O_3				108 ± 1.5	
	1% Pt/Al_2O_3	O_2/CH_4 = 5:1	350–500	0–28	121 ± 10	
	2% Pt/Al_2O_3				100 ± 5	
	4% Pt/Al_2O_3				83.8 ± 5	
[175]	$NiFe_2O_4$	CH_4: 3 vol% O_2: 7.2 vol%	350–400	~2–13	210.8	
[176]	$Co_{(0.95)}ZrO_2$		750–800		23	11 880
	$Co_{(1.9)}ZrO_2$		750–800		26	18 000
	$Co_{(1.9)}La/ZrO_2$		770–820		29	52 200
[177]	Ru/γ-Al_2O_3	CH_4: 0.8 vol%	361	10%	116	2.53
	Ru_{90}–Re_{10}/γ-Al_2O_3	O_2: 22 vol%	337	10%	104	5.17
	Ru_{75}–Re_{25}/γ-Al_2O_3	N_2: 78 vol%	359	10%	117	2.00
[178]	γ-Al_2O_3	CH_4: 0.5–3 vol%			21 200	
	Cu/γ-Al_2O_3 (600 °C)		525	50%		1.11 × 10^{11} 0.91 × 10^{11}
	Cu/γ-Al_2O_3 (800 °C)		540	50%	21 330 Cal mol^{-1}	
[179]	$AuPd_{1.95}/CoCr_2O_4$	CH_4: 2.5 vol%	305	10%		60
		O_2: 20 vol%	353	50%		
		N_2: 77.5 vol%	394	90%		
[180]	$ZrO_2/LaMnO_3$	CH_4: 3 vol%	417	10%	19.3	3.30
		O_2: 10 vol%	539	50%		
		N_2: balance	632	90%		
[181]	Cu–Cr/$CuCr_2O_4$	air/CH_4 = 30	550		105.9 ± 10.4	
			600		118.2 ± 0.6	

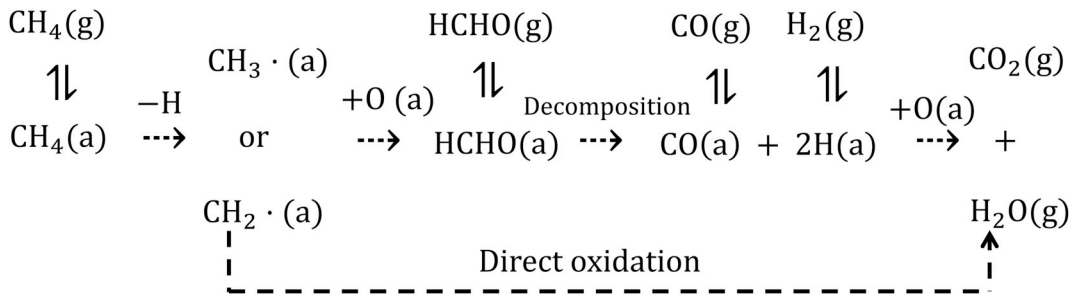

Fig. 6. Reaction routes of methane catalytic oxidation over noble metal catalysts. The bracket (a) indicates the adsorbed state and (g) the gas phase [147].

3. Mechanism and kinetic study of CMC

Compared to other higher alkanes, methane is the most stable alkane molecule with high ionization potential (12.5 eV), low electron affinity (4.4 eV) and high C–H bond energy (434 kJ mol^{-1}), rendering it extremely difficult to be activated under mild conditions. A high reaction temperature (>1400 °C) is often required for carrying out conventional methane flame combustion. Hence, mechanistic and kinetic studies are important for guiding the catalyst design and the process optimization in order to achieve an efficient combustion at relative low temperature levels (<600 °C) [133–135]. The reaction has been reported to be zero order in oxygen and first order in methane [136]. The kinetic model and the elementary steps were elaborated in the literature [137–143], and the main kinetics parameters are summarized in Table 3.

Regarding the noble metal catalyst, a great number of studies have been devoted to revealing the mechanism of catalytic methane oxidation [48,144–146]. The classic reaction routes over noble metal catalysts are shown in Fig. 6 [147]. CH_4 molecules are first adsorbed on the catalyst and dissociated to the adsorbed methyl (CH_3·) or methylene (CH_2·) species, which further interact with the adsorbed oxygen, either to directly produce CO_2 and H_2O, or to form the adsorbed CO and H_2 via formaldehyde (HCHO) as the intermediate [148,149]. The adsorbed CO and H_2 further interact with the adsorbed oxygen to form the final product (CO_2 and H_2O) based on the reactant ratios (theoretically, partial oxidation occurs at O_2/CH_4 molar ratio < 2). The adsorbed CO is predominant with the increasing methane coverage, whereas CO_2 formation is more favorable at high oxygen coverages. However, due to the swift dissociation of CO, the variation of the surface concentrations of methane and oxygen is negligible. Experimental measurements over Pt/Al_2O_3 catalysts have indicated that the reaction rate determining step was shifted from the oxygen desorption to the methane adsorption with the increasing catalyst surface temperature [141]. Given the higher methane adsorption energy than oxygen [150–152], at the beginning the oxygen adsorption reaction ($O_2 + 2\ Pt(*) \rightarrow 2O(*) + 2\ Pt$; * is the molecule adsorbed on the surface), this rate determining step may be additionally due to the competitive adsorption of oxygen that inhibits the methane oxidation by excluding the weakly adsorbed methane on the active sites [147]. At high oxygen atom coverages, methane is converted through the proposed reaction ($CH_4 + O(*) + Pt(*) \rightarrow CH_3(*) + OH(*) + Pt$). As a result, the surface temperature increases due to the release of the reaction heat. The number of the adsorbed oxygen atoms is generally decreased with the increasing temperature and the reaction of the methane adsorption ($CH_4 + 2\ Pt(*) \rightarrow CH_3(*) + H(*) + 2\ Pt$) becomes more prominent. The light-off phenomenon thus happens once the favorable coverage of methane and oxygen on the catalyst surface is reached [133,153].

Three types of mechanism and the corresponding kinetic models have been proposed for CMC in the literature, including the Langmuir-Hinselwood mechanism [154–156], the Eley-Rideal mechanism [157] and the Mars-van Krevelen mechanism [158–161]. The rate-determining step for both the Langmuir-Hinselwood and Eley-Rideal mechanisms is commonly considered as the superficial reaction. The reaction rate is associated to the electronic properties of transition ions over the catalyst surface. On the contrary, the CMC is considered as the interfacial reaction by the Mars-van Krevelen mechanism; the reaction rate is mainly correlated to the lattice oxygen vacancies.

Regarding the Langmuir-Hinselwood mechanism, the molecules of both gas phase reactants are adsorbed on the catalyst surface and react via surface diffusion. The formed products are then desorbed from the catalyst surface to complete the reaction. The kinetic models of CMC over Pt/Al_2O_3 catalyst proposed by Trimm and Lam [162] well fit the Langmuir-Hinselwood mechanism, indicating that both the adsorbed methane and oxygen were involved in the reaction. Their study confirmed that the temperature increase was mainly to change the reaction path from the oxygen adsorption to methane adsorption [162]. However, Jodłowski et al. [163] observed that methane over $Co–Pd/\gamma\text{-}Al_2O_3$ catalyst was only adsorbed with pre-adsorbed oxygen over the surface (under oxygen-rich conditions) by using the DRIFT (diffuse reflectance infrared spectroscopy), suggesting that the Langmuir-Hinshelwood mechanism should not be recommended.

The Eley-Rideal mechanism suggests that only one gas phase reactant has to be adsorbed onto the catalyst surface. The adsorbed reactant then interacts with the other reactant which is still in the gas phase. Subsequently, the formed products are desorbed from the catalyst surface. Seimanides and Stoukides [157] reported that this mechanism could well predict the CMC over Pd/ZrO_2 catalyst in the range of 450–600 °C. It is likely to be the only adsorbed atomic oxygen that reacts with the gaseous methane. Veldsink et al. [164] illustrated that the Eley-Rideal mechanism was adequate to describe the experiment data, and the reaction rate equation over $CuO/\gamma\text{-}Al_2O_3$ catalyst was proposed without the limitation of heat and mass transfer.

The Mars-van Krevelen mechanism is widely supported by a large amount of experimental results on CMC [165,166]. Different from the above two mechanisms, the Mars-van Krevelen mechanism suggests that the adsorbing surface is an active participant. Firstly, one of the reactants in the gas phase forms a chemical bond with the catalyst surface in the form of a thin layer (e.g. of metal oxide). Then, the remaining gas phase reactant can interact with the chemically bonded reactant, leaving behind a vacancy upon desorption of the products. However, it is not easy to distinguish between Mars-van Krevelen and Eley-Rideal mechanisms because of the existence of both the lattice and adsorbed oxygen species on the catalyst surface. Pfefferle et al. [160] further reported that one ^{16}O atom (lattice phase) in PdO was bounded to two Pd atoms, using the in-situ technology of isotopically labeled reaction. It was found that the ^{16}O atom in PdO was responsible to oxidize methane rather than the adsorbed ^{18}O atom in the gas phase. This conclusion is in line with the findings of Au-Yeung et al. [167]. In addition, the variation in the oxidation valence of Pd plays an important role in the reaction, indicating that the Mars-van Krevelen mechanism is more adequate to be used for the CMC [57,168,169]. Similarly for $NiCo_2O_4$ perovskite catalyst, Tao et al. [77] reported that the chemisorbed lattice oxygen played an important role. The oxidized products (CO_2 and H_2O) were generated

Table 4
Summary of catalysts and reaction conditions for methane oxidation in various reactors.

Reference/ year[a]	Catalyst	Preparation method	BET surface area ($m^2 \cdot g^{-1}$)	Reactor (material, size)	Reactant	Total flow rate ($mL \cdot min^{-1}$)	Space velocity	T_{10} (°C)[b]	T_{50} (°C)[b]	T_{90} (°C)[b]	T*x* (°C)[b] *X* = conv%	Remarks
Hexaaluminate catalyst												
[65] 1989	$BaAlAl_{11}O_{19-\alpha}$	Hydrolysis of metal alkoxides	15.3	Fixed-bed (quartz)	CH_4: 1 vol% In air	800	48 000 h^{-1}	710		730		- Mn-substituted catalyst presented the best catalytic performance
	$BaCrAl_{11}O_{19-\alpha}$		15.7					700		770		
	$BaMnAl_{11}O_{19-\alpha}$		13.7					540		740		
	$BaFeAl_{11}O_{19-\alpha}$		11.1					560		780		
	$BaCoAl_{11}O_{19-\alpha}$		15.2					690		720		
	$BaNiAl_{11}O_{19-\alpha}$		11.1					710		770		
[209]	BHA	Sol-gel	<20	Flow reactor	CH_4: 1 vol%		60 000 h^{-1}	710		~750		- Reverse microemulsions method presented a higher surface area and an excellent catalytic activity
2000	BHA	Reverse-micro emulsion	40–160		In air			590	~650	~750		
	CeO_2-BHA							~400		600		
[210]	$BaAl_{12}O_{19-\alpha}$	Co-precipitation and supercritical drying		Fixed-bed (quartz, i.d. 10 mm)	CH_4: 1 vol%, O_2: 4 vol%, N_2: balance		15 000 h^{-1}	630	750	841		- Introduction of CeO_2 increased the surface area and enhanced the catalytic activity
2007	$BaMnAl_{11}O_{19-\alpha}$							470	580	655		
	$BaMn_2Al_{10}O_{19-\alpha}$							433	537	619		
	$CeO_2/BaAl_{12}O_{19-\alpha}$		83.5					535	618	690		
	$CeO_2/BaMnAl_{11}O_{19-\alpha}$		55.9					468	576	645		
	$CeO_2/BaMn_2Al_{10}O_{19-\alpha}$		47.8					426	534	611		
	$CeO_2/BaFeAl_{10}O_{19-\alpha}$		75.3					436	530	597		
Perovskite catalyst												
[211]	0 wt %Pd/ $LaMnO_3{\cdot}2ZrO_2$	Incipient wetness impregnation	29.82	Fixed-bed (quartz, i.d. 4 mm)	CH_4: 2 vol%, O_2: 14 vol%, He: balance	50			520			- ZrO_2 introduction increased the support thermal resistance - Incipient wetness impregnation exhibited a higher catalytic performance
2005	0.5 wt%Pd/ $LaMnO_3{\cdot}2ZrO_2$		28.88						509			
	1 wt %Pd/ $LaMnO_3{\cdot}2ZrO_2$		29.30						485			
	2 wt %Pd/ $LaMnO_3{\cdot}2ZrO_2$		28.64						432			
	3 wt %Pd/ $LaMnO_3{\cdot}2ZrO_2$		27.43						461			
	0.5 wt %Pd/$La_2Zr_2O_7$								531			
	1 wt %Pd/$La_2Zr_2O_7$	Solution combustion							518			
	2 wt %Pd/$La_2Zr_2O_7$								476			
	3 wt % Pd/$La_2Zr_2O_7$								498			
[212]	La_2CuO_4 -260	Co-precipitation		Fixed-bed (quartz, i.d. 4 mm)	CH_4: 2 vol%, O_2: 20 vol%, N_2: balance		50 000 mL g^{-1} h^{-1}	548	662	739		- An enhanced activity of La_2CuO_4 due to the Sr^{2+} doping - Excellent performance are attributed to more adsorbed oxygen species, better reducibility and single crystallinity.
2010	La_2CuO_4 -220							587	677	759		
	La_2CuO_4 -180							625	722	766		
	$LaSrCuO_4$ -260							482	620	667		
[213]	$BaZr_{(1-x)}Me_xO_3$	Modified citrate method		Fixed-bed (quartz, i.d. 7 mm)	CH_4: 0.5 vol %, O_2: 4 vol %, N_2: 16 vol %, He: balance	150	150 000 mL g^{-1} h^{-1}					- Catalytic performance of substituted transition metals: Pd, Ru > Rh > Co > Mn > Ni
2012	Me = 5% Rh		15.3						625		T_{20} = 530	
	Me = 5% Pd		18.3						600		T_{20} = 520	
	Me = 15% Rh		7.3						660		T_{20} = 570	
	Me = 20% Rh		13.1						650		T_{20} = 570	
	Me = 2.73% Mn		10.7						710		T_{20} = 635	
	Me = 2.91% Ni		n.a.						790		T_{20} = 690	
	Me = 5.92% Ni		n.a.						700		T_{20} = 625	
	Me = 4.91% Ru		5.6						600		T_{20} = 520	
	Me = 1% Pt		3.1						730		T_{20} = 645	
	Me = 2.93% Co		13.8						640		T_{20} = 570	
	Me = 5.86% Co		38.5						775		T_{20} = 675	
	$BaZrO_3$		6.3									

(*continued on next page*)

Table 4 (*continued*)

Reference/ year[a]	Catalyst	Preparation method	BET surface area ($m^2 \cdot g^{-1}$)	Reactor (material, size)	Reactant	Total flow rate ($mL \cdot min^{-1}$)	Space velocity	T_{10} (°C)[b]	T_{50} (°C)[b]	T_{90} (°C)[b]	T*x* (°C)[b] *X* = conv%	Remarks
[214] 2014	$MgCr_2O_4$	Sol-gel	1.1	Fixed-bed	CH_4: 1 vol%		48 000 mL g^{-1} h^{-1}	400		684		-$MgCr_2O_4$ exhibited a higher activity than $CoCr_2O_4$ due to the presence of Cr^{6+} and bulk structure
	$CoCr_2O_4$		0.4		In air			480		750		
	MgO							618.8		742.4		
	Cr_2O_3							593.6		736.7		
[77] 2015	$NiCo_2O_4$	Co-deposition precipitation	218.7 (calculated surface area with average size of 4.5 nm)	Fixed-bed (quartz, i.d. 6 mm)	CH_4: 5 vol%, O_2: 25 vol%, Ar: balance	200	24 000 mL g^{-1} h^{-1}	~230	~262		T_{100}: 350	-$NiCo_2O_4$ showed a higher catalytic performance than Pd/Al_2O_3 under the same conditions
					CH_4: 0.2 vol %, O_2: 5 vol %, CO_2: 15 vol%, H_2O: 10 vol%, Ar: balance			~240	~300		T_{100}: 425	
					CH_4: 0.2 vol %, O_2: 5 vol %, NO: 0.15 vol%, H_2O: 10 vol %, Ar: balance			~300	~335		T_{100}: 475	
[215] 2016	3DOM	Templating method	32.4	Fixed-bed (quartz, i.d. 6 mm)	CH_4: 5 vol%, O_2: 30 vol%, Ar: balance	42.8	50000 mL g^{-1} h^{-1}	344	384	508		-Au addition weakened the bond between intermediates and Pd atoms, and enriched the adsorbed oxygen species over the catalyst surface, thus enhancing the reaction rate
	$La_{0.6}Sr_{0.4}MnO_3$1Au/ 3DOM		32.6					338	375	402		
	$La_{0.6}Sr_{0.4}MnO_3$1Pd/ 3DOM		32.0					323	358	378		
	$La_{0.6}Sr_{0.4}MnO_3$1AuPd/ 3DOM		33.6					304	350	382		
	$La_{0.6}Sr_{0.4}MnO_3$2AuPd/ 3DOM		33.3					280	331	354		
	$La_{0.6}Sr_{0.4}MnO_3$3AuPd/ 3DOM $La_{0.6}Sr_{0.4}MnO_3$		33.8					265	314	336		
[216] 2016	$LaFeO_3$	Nitrate-citrate combustion synthesis		Fixed-bed (quartz)	CH_4: 5 vol%, O_2: 50 vol%, N_2: 45 vol%	1000	240 000 h^{-1}		~650		T_{25}: 600	- Perovskite nanopowder synthesized by solution combustion
	$La_{0.8}Sr_{0.2}FeO_3$								~550		T_{65}: 600	
	$La_{0.6}Sr_{0.4}FeO_3$								~640		T_{35}: 600	- Partial substitution of La^{3+} by Sr^{2+} greatly increased the catalytic activity
[217] 2018	CeO_2	Support	28.9	Fixed-bed (stainless steel, i.d. 8 mm)	CH_4: 10 vol %, O_2: 25 vol %, Ar: balance		24 000 mL g^{-1} h^{-1}	523	641			- Catalytic activity of different methods: CeO_2 (Plasma treatment) > $CoAlO_x/CeO_2$ (Impregnation combustion) > $CoAlO_x/CeO_2$ (Microwave in-situ grown) > $CoAlO_x/CeO_2$ (Impregnation)
	$CoAlO_x/CeO_2$	Impregnation	20.1					460	511	614		
	$CoAlO_x/CeO_2$	Microwave in-situ grown	28.4					418	481	601		
	$CoAlO_x/CeO_2$	Impregnation combustion	27.7					405	464	590		
	$CoAlO_x/CeO_2$	Plasma treatment	27.2					335	415	580		
[76] 2018	$LaMnO_3$	Sol-gel	11	Fixed-bed (quartz, no size reported)	CH_4: 0.6 vol %, O_2: 21 vol %, Ar: balance	133	40 000 h^{-1}	313	379	443		-Effect of different preparation methods on the catalytic performance: - Chemical combustion ≈ Solvothermal > Sol-gel > Spray-pyrolysis - Catalytic performance 1% Pd/Al_2O_3 > $LaMnO_3$/ $La_{0.8}Sr_{0.2}MnO_3$ > 0.5% Pt/Al_2O_3
	$La_{0.8}Sr_{0.2}MnO_3$		27					270	333	397		
		Chemical combustion	15					237	351	375		
			18					266	329	389		
		Microwave-assisted solvothermal	16					269	331	392		
			19					280	363	439		
		Spray-pyrolysis	6					330	410	496		
			11					359	452	537		
	0.5 wt% Pt/Al_2O_3							278	446	499		

(*continued on next page*)

Table 4 (*continued*)

Reference/ year[a]	Catalyst	Preparation method	BET surface area ($m^2 \cdot g^{-1}$)	Reactor (material, size)	Reactant	Total flow rate ($mL \cdot min^{-1}$)	Space velocity	T_{10} (°C)[b]	T_{50} (°C)[b]	T_{90} (°C)[b]	T*x* (°C)[b] *X* = conv%	Remarks
	1 wt% Pd/Al_2O_3							205	252	296		
[218]	Bulk $LaMnAl_{11}O_{19}$	Polymethyl	12	Fixed-bed	CH_4: 2.5 vol	16.7	20 000 mL g^{-1} h^{-1}	475	615	–		- Catalytic activity:
2018	3DOM $LaMnAl_{11}O_{19}$	methacrylate	27.7	(quartz, i.d.	%, O_2: 20 vol			432	540	651		1.91$AuPd_{1.80}$/3DOM $LaMnAl_{11}O_{19}$
	0.44$AuPd_{1.86}$/3DOM $LaMnAl_{11}O_{19}$	templating method	26.7	8 mm)	%, N_2: balance			355	432	510		> 0.94$AuPd_{1.86}$/3DOM $LaMnAl_{11}O_{19}$ > 0.44$AuPd_{1.86}$/
	0.94$AuPd_{1.86}$/3DOM $LaMnAl_{11}O_{19}$		24.4					332	375	443		3DOM $LaMnAl_{11}O_{19}$ > 3DOM $LaMnAl_{11}O_{19}$ > Bulk $LaMnAl_{11}O_{19}$
	1.91$AuPd_{1.80}$/3DOM $LaMnAl_{11}O_{19}$		28.2					305	342	402		
[219]	CeO_2	Co-precipitation	64	Fixed-bed	CH_4: 1 vol%,	100	30 000 mL g^{-1} h^{-1}					- Catalytic activity:
2018	$Ce_{0.95}Fe_{0.05}O_{2-\delta}$		98	(quartz)	O_2: 20 vol%,							$Ce_{0.6}Fe_{0.4}O_{2-\delta}$ > $Ce_{0.65}Fe_{0.35}O_{2-\delta}$ > $Ce_{0.7}Fe_{0.3}O_{2-\delta}$ > $Ce_{0.8}Fe_{0.2}O_{2-\delta}$ > $Ce_{0.9}Fe_{0.1}O_{2-\delta}$ > $Ce_{0.95}Fe_{0.05}O_{2-\delta}$ > CeO_2
	$Ce_{0.9}Fe_{0.1}O_{2-\delta}$		70		N_2: balance							
	$Ce_{0.8}Fe_{0.2}O_{2-\delta}$		83									
	$Ce_{0.7}Fe_{0.3}O_{2-\delta}$		109							458		
	$Ce_{0.65}Fe_{0.35}O_{2-\delta}$		110									
	$Ce_{0.6}Fe_{0.4}O_{2-\delta}$		114					333	378	438		
Noble metal catalyst and metal oxides												
[19]	4 wt% Pt/Al_2O_3	Dry		Fix-bed (i.d.	O_2/	200					T_{14}: 400	- Methane conversion in order of
1994		impregnation		5 mm)	CH_4 = 5:1						$T_{49.2}$: 475	O_2/CH_4 molar ratio: 5:1 < 2:1 < 1:1
											$T_{93.8}$: 550	
	4 wt% Pd/Al_2O_3				O_2/						T_8: 375	- Methane conversion in order of
					CH_4 = 2:1						T_{28}: 425	O_2/CH_4 molar ratio: 5:1 > 2:1 > 1:1
											T_{96}: 450	
					O_2/						T_4: 350	
					CH_4 = 1:1						T_{59}: 375	
											$T_{94.6}$: 475	
					O_2/						T_{23}: 300	
					CH_4 = 5:1						$T_{40.6}$: 325	
											$T_{94.5}$: 400	
					O_2/CH_4 1:1						$T_{9.1}$:300	
											$T_{50.7}$:375	
											$T_{91.1}$:500	
[220]	Pd-ZSM-5	Ion-exchange		Fixed-bed	CH_4: 1 vol%	74	30 000 h^{-1}	~220	~255	~270		- Catalytic activity:Pd-ZSM-5>PdO/Al_2O_3
1994	PdO/Al_2O_3			(quartz, o. d.1/4 inch at inlet, 3/8 inch at outlet)	In air			~275	~325	~350		- Higher metal dispersion and lattice oxygen of PdO/Al_2O_3 catalyst
[178]	γ-Al_2O_3	Wet	180	Fluidized bed	CH_4: 0.5 vol	Gas velocity:						- Unreacted CH_4 > 100 ppm at
2002	Cu/γ-Al_2O_3(600 °C)	impregnation	170	(stainless	% In air	0.4–0.8 cm s^{-1}			525			0.8 m s^{-1} gas velocity and below
	Cu/γ-Al_2O_3(800 °C)		144	steel, i.d. 100 mm)					540			700 °C
												- Unreacted CH_4 < 10 ppm at 0.4 m s^{-1} gas velocity and below 700 °C
[221]	Pd/Al_2O_3	Washcoated	334	Fixed-bed	CH_4: 1 vol %		5800 h^{-1}	300	367	497		- Catalytic activity and thermal
2004	Pd/Al_2O_3–$ZrSiO_4$	monolith	217	(quartz, i.d.	In air			285	360	415		resistance increased by introducing
	Pd/Al_2O_3–SiO_2		356	26 mm)				285	360	447		SiO_2 and $ZrSiO_4$
[92]	Pd–3CeO_2/Al_2O_3	Sol-gel	680	Fixed-bed					648			- The higher Ce content, the higher
2004	Pd–5CeO_2/Al_2O_3		343						623			catalytic activity
	Pd–3La_2O_3/Al_2O_3		369						705			- La addition resulted in a lower
	Pd–5La_2O_3/Al_2O_3		650						723			catalytic activity due to less oxygen donor species present
[222]	2 wt% Pd/CeO_2	Deposition-precipitation	58.8	Fix-bed (quartz)	CH_4: 1 vol% In air		50 000 h^{-1}	224	257		T_{100}: 300	- Highest catalytic activity with 2 wt % Pd/CeO_2 prepared by DP method
2005	2 wt% Pd/CeO_2	Impregnation	53.6					458	557			- Strong interaction between Pd and

(*continued on next page*)

Table 4 (*continued*)

Reference/ year[a]	Catalyst	Preparation method	BET surface area ($m^2 \cdot g^{-1}$)	Reactor (material, size)	Reactant	Total flow rate ($mL \cdot min^{-1}$)	Space velocity	T_{10} (°C)[b]	T_{50} (°C)[b]	T_{90} (°C)[b]	T*x* (°C)[b] *X* = conv%	Remarks
	2 wt% Pd/Al_2O_3	Deposition-precipitation	193					307	349		T_{100}: 410	CeO_2 produced a large amount of active oxygen
[103] 2005	Pd/Al_2O_3	Incipient wetness impregnation	102	Flow reactor			250 000 h^{-1}					- Effect of pressure on catalytic performance: 5 bar: ~5.8% conversion 7.5 bar: ~3.5% 10 bar: ~2.5% 12.5 bar: ~2.2% 15 bar: ~1.7%
	$PdPt/Al_2O_3$		91									5 bar: ~7.2% 7.5 bar: ~5.2% 10 bar: ~4% 12.5 bar: ~3.6% 15 bar: ~3.5%
[184] 2007	Pd/HZSM-5	Precipitation	498.1	Fixed-bed (quartz)	CH_4: 2 vol%, O_2: 8 vol%, N_2: balance		48 000 h^{-1}	317	351		T_{100}: 351	- The highest catalytic activity with Pd–Ce/HZSM-5 - The addition of CeO_2 promoted the catalytic activity
	Pd–Ce/HZSM-5		493.5					290	336		T_{100}: 336	
	Pd–La/HZSM-5		438.4					331	387		T_{100}: 387	
	Pd–Sm/HZSM-5		455.0					326	374		T_{100}: 374	
	Pd–Nd/HZSM-5		462.2					322	371		T_{100}: 371	
	Pd–Tb/HZSM-5		419.1					329	388		T_{100}: 388	
	$Pd/\gamma\text{-}Al_2O_3$							352	443		T_{100}: 443	
	Pd/SiO_2							410	526		T_{100}: 526	
[223] 2008	Au/Fe_2O_3	Deposition-precipitation	33	Fixed-bed (quartz)	CH_4: 1 vol% In air	100	51 000 h^{-1}	410	496		T_{95}: 565	- Catalyst prepared by HDP method showed a higher catalytic activity than DP method for methane combustion
	Au/Fe_2O_3	Homogeneous deposition precipitation	24					302	387		T_{95}: 488	
	Fe_2O_3		51					468	575		T_{95}: 650	
[224] 2009	$Co_{10}Mn_0$	Co-precipitation Powder	62.55	Fixed-bed (quartz i.d. 8 mm)	CH_4: 1 vol%, O_2: 10 vol%, N_2: balance	150	36 000 h^{-1}		297	339	T_{20}: 265	- Appropriate Mn addition led to disorders in the spinel structure, and thus increased crystal defections and increased activity
	Co_5Mn_1		147.65						293	324	T_{20}: 280	
	Co_3Mn_1		158.46						306	333	T_{20}: 282	
	Co_1Mn_1		150.25						350	386	T_{20}: 323	
	Co_1Mn_3		154.49						351	392	T_{20}: 323	
	Co_0Mn_{10}		183.94						358	393	T_{20}: 331	
[225] 2009	Pd/SiO_2	Sol-gel	688	Fixed-bed (quartz, i.d. 12 mm)	CH_4: 0.3 vol %, O_2: 2.4 vol%, He: balance (SO_2-free)	50	60 000 mL g^{-1} h^{-1}		355			- The combination of TiO_2 and SiO_2 promoted the catalytic performance - TiO_2 and SiO_2 increased the catalyst SO_2 poisoning tolerance
	Pd/Ti5Si		328						332			
	Pd/Ti10Si		284						312			
	Pd/Ti15Si		243						321			
	Pd/Ti20Si		170						326			
	Pd/TiO_2		38						337			
	Pd/SiO_2				CH_4: 0.3 vol %, O_2: 2.4 vol%, He: balance (with 10 vol ppm SO_2)				395			
	Pd/Ti5Si								379			
	Pd/Ti10Si								365			
	Pd/Ti15Si								n.a.			
	Pd/Ti20Si								381			
	Pd/TiO_2								346			
[118] 2009	Pt–W/γ-Al_2O_3 commercial	Washcoated	214	Microchannel	CH_4: 9.1 vol %	107	74 000 h^{-1}	399	493		T_{100}: 600	- Pt–W/γ-Al_2O_3 showed 100% methane combustion and 99% CO_2 formation at 600 °C for 60 h test, 98% CH_4 conversion after 100 h
	Pt–W/γ-Al_2O_3 home-made		123					430	528		T_{100}: 625	
	Pt–Mo/γ-Al_2O_3 commercial		242					443	526		T_{100}: 625	
	Pt–Mo/γ-Al_2O_3 home-made		150					470	554		T_{100}: 650	
	2 wt% $Pd/CeO_2{\cdot}2ZrO_2$					50						

(*continued on next page*)

Table 4 (*continued*)

Reference/ year[a]	Catalyst	Preparation method	BET surface area ($m^2 \cdot g^{-1}$)	Reactor (material, size)	Reactant	Total flow rate ($mL \cdot min^{-1}$)	Space velocity	T_{10} (°C)[b]	T_{50} (°C)[b]	T_{90} (°C)[b]	T*x* (°C)[b] *X* = conv%	Remarks
[226] 2010	Fresh	Solution combustion synthesis	74.6	Fixed-bed (quartz, i.d. 4 mm)	CH_4: 2 vol%, O_2: 16 vol%, He: balance			340	382	429		- Lower catalytic activity with catalyst aging time: Pd/$CeO_2 \cdot 2ZrO_2$; - Increased catalytic activity with catalyst aging time: Pd/$LaMnO_3 \cdot 2ZrO_2$ Pd/$BaCeO_3 \cdot 2ZrO_2$
	1week aged		65.8					336	383	419		
	2 weeks aged		34.8					345	421	498		
	2 wt% Pd/ $LaMnO_3 \cdot 2ZrO_2$											
	Fresh		132.5					450	570	645		
	1week aged		69.8					500	625	690		
	2 weeks aged		21.6					360	450	550		
	2 wt% Pd/ $BaCeO_3 \cdot 2ZrO_2$											
	Fresh		26.4					414	512	592		
	1week aged		22.7					540	628	694		
	2 weeks aged		15.4					330	443	540		
[88] 2010	$Pd_{(1.0)}/Al_2O_3$	Impregnation		Fixed-bed (quartz, i.d. 8 mm)	CH_4: 0.1 vol %, O_2:16.74 vol %, N_2: 83.16 vol%		10 000 h^{-1}		474	520		- Trimetallic catalytic activity depended on noble metal composition: PtPdRh/Al_2O_3> PtRh/Al_2O_3>Pd/Al_2O_3
	$Pt_{(1.5)}Rh_{(0.3)}/Al_2O_3$								415	460		
	$Pt_{(1.0)}Pd_{(0.75)}Rh_{(0.25)}/Al_2O_3$ (molar ratio)								388	442		
[227] 2015	CoAlO-500 °C	Deposition	88.6	Fixed-bed (quartz, i.d. 6 mm)	CH_4: 2 vol%, O_2: 20 vol%, N_2: 78 vol%	41.6	30 000 mL g^{-1} h^{-1}	462	538	618		- Catalytic activity: CoAlO - 700 °C < CoAlO - 600 °C < CoAlO - 500 °C <Ag–CoAlO - 500 °C <Ag–CoAlO - 700 °C <Ag–CoAlO - 600 °C - The highest catalytic activity with Ag–CoAlO-600 °C due to abundant Co^{3+} and adsorbed oxygen
	CoAlO-600 °C		262.6					471	562	629		
	CoAlO-700 °C		29.1					477	585	656		
	Ag NPs:											
	Ag–CoAlO-500 °C		96.2					393	516	571		
	Ag–CoAlO-600 °C		69.5					343	444	522		
	Ag–CoAlO-700 °C		212.4					371	475	555		
[201] 2015	2.94$Au_{0.50}$Pd/meso-Co_3O_4		114.5	Fixed-bed (quartz)	SO_2 addition		20 000 mL g^{-1} h^{-1}	230	280	324		*SO_2 addition (irreversible)* −100 ppm SO_2 addition: Conversion drop from 90.5% to 73.6% after 31 h - *regeneration:* CH_4 conversion slightly increased to 74.2% after 16 h
								263	312	378		
								242	288	334		
								269	321	397		
					H_2O addition							*H_2O addition (reversible)* −2 vol% H_2O addition: Conversion drop from 93% to 91% −5 vol% H_2O addition: Conversion drop from 91% to 90% −10 vol% H_2O addition: Conversion drop from 90% to 89%
					CO_2 addition							*CO_2 addition (reversible)* −2.5 vol% CO_2 addition: ca.2% decrease in methane conversion after 13 h −5 vol% CO_2 addition: ca.1% decrease in methane conversion after 4 h *-regeneration* restore to original ca.90.5% of methane conversion
[113] 2015	Fe–Ni	Washcoated		Tubular (inner i.d. 20 mm, outer: i.d. 32 mm)	CH_4: 5 vol%	50		T_{10}: 550				- Catalyst activity vs. Pd loading: 4.8% > 3.2%
	3.2 wt% Pd/Al_2O_3/ Fe–Ni				CH_4: 5 vol%	50		T_{10}: 350	T_{35}: 400		T_{98}: 500	- CH_4 conversion decreased with the increasing flow rate

(*continued on next page*)

Table 4 (*continued*)

Reference/ year[a]	Catalyst	Preparation method	BET surface area ($m^2 \cdot g^{-1}$)	Reactor (material, size)	Reactant	Total flow rate ($mL \cdot min^{-1}$)	Space velocity	T_{10} (°C)[b]	T_{50} (°C)[b]	T_{90} (°C)[b]	T*x* (°C)[b] *X* = conv%	Remarks
	4.8 wt% Pd/Al_2O_3/ Fe–Ni				CH_4: 5 vol%	50		T_{16}: 350	T_{40}: 400		T_{98}: 550	- CH_4 conversion slightly increased with the increasing CH_4 concentration
	4.8 wt% Pd/Al_2O_3/ Fe–Ni				CH_4: 5 vol%	100		T_{10}: 400	T_{50}: 500		T_{95}: 550	
	4.8 wt% Pd/Al_2O_3/ Fe–Ni				CH_4: 5 vol%	150		T_9: 400	T_{45}: 500		T_{65}: 550	
	4.8 wt% Pd/Al_2O_3/ Fe–Ni				CH_4: 5 vol%	200		T_7: 400	T_{35}: 500		T_{62}: 550	
	4.8 wt% Pd/Al_2O_3/ Fe–Ni				CH_4: 2 vol%	50		T_{10}: 350	T_{60}: 450		T_{88}: 500	
	4.8 wt% Pd/Al_2O_3/ Fe–Ni				CH_4: 3 vol%	50		T_{12}: 350	T_{68}: 450		T_{90}: 500	
	4.8 wt% Pd/Al_2O_3/ Fe–Ni				CH_4: 4 vol%	50		T_{15}: 350	T_{70}: 450		T_{93}: 500	
[177] 2016	3 wt%Re/γ-Al_2O_3	Wet impregnation		Fixed bed (i.d. 8 mm)	CH_4: 0.8 vol %, In air	100	60 000 h^{-1}	535	650		T_{95}: 800	- Pretreatment of catalyst greatly affected the activity - Re addition improved the activity
	5 wt%Pd/γ-Al_2O_3 (degussa)		316					300	331		T_{95}: 403	
	5 wt%Ru/γ-Al_2O_3 (fluka)		90					386	436		T_{95}: 555	
	5 wt0%Ru/γ-Al_2O_3		183					361	407		T_{95}: 525	
	Ru_{90}–Re_{10}/γ-Al_2O_3		174					337	391		T_{95}: 506	
	Ru_{75}–Re_{25}/γ-Al_2O_3		147					359	411		T_{95}: 538	
[228] 2016	0.5 wt% Pd/γ-Al_2O_3			Fluidized bed (i.d. 102 mm)	CH_4: 0.15 vol %	velocity 0.1 m s^{-1}					$T_{62.2}$: 450 $T_{94.5}$: 550	- At 550 °C, 0.3 %CH_4 velocity from 0.1–0.25 m s^{-1}, CH_4 conversion: 98%–73%
[229] 2016	Co_3O_4 - 200 °C		136.2		CH_4: 1 vol%, O_2: 20 vol%		18 000 mL g^{-1} h^{-1}		270			- Catalytic activity: Co_3O_4 - 200 °C > Co_3O_4 - 400 °C > Co_3O_4 - 600 °C
	Co_3O_4 - 400 °C		41.5						292			
	Co_3O_4 - 600 °C		7.4						373			
[179] 2017	3DOM $CoCr_2O_4$ (Three-dimensionally ordered macroporous)		33.2	Fixed-bed (quartz, i.d. 6 mm)	CH_4: 2.5 vol %, O_2: 20 vol %, N_2:	16.7	20 000 mL g^{-1} h^{-1}	320	370	440		- Catalytic performance decreased with the increasing space velocity - 1.93$AuPd_{1.95}$/3DOM $CoCr_2O_4$ presented the best activity - Addition of H_2O(g) and SO_2 resulted in catalyst deactivation
	0.98$AuPd_{1.93}$/3DOM $CoCr_2O_4$		35.6		77.5 vol%			310	362	410		
	1.93$AuPd_{1.95}$/3DOM $CoCr_2O_4$		34.9					305	353	394		
	1.98$AuPd_{1.96}$/Bulk $CoCr_2O_4$		8.8					325	385	467		
	Bulk $CoCr_2O_4$		7.2					335	400	490		
	1.93$AuPd_{1.95}$/3DOM $CoCr_2O_4$						10 000 mL g^{-1} h^{-1}	~290	~345	~382		
	1.93$AuPd_{1.95}$/3DOM $CoCr_2O_4$						40 000 mL g^{-1} h^{-1}	~325	~380	~43		
[230] 2017	$Pd/CoAl_2O_4/Al_2O_3$	Galvanic deposition Impregnation		Fixed-bed (Pyrex glass, i.d. 4 mm)	CH_4: 0.4 vol %, O_2: 10 vol %, He: balance	100	300 000 mL g^{-1} h^{-1}	266	~295			- Catalyst by galvanic deposition method performed better
								285	~335			
[231] 2017	Pd/ZrO_2	Sonochemically aided impregnation synthesis	24.23	Fixed-bed	CH_4: 2000 ppm in air		150 000 mL g^{-1} h^{-1}				$T_{\sim 95} = 300$	- Catalytic activity: Co/ZrO_2 > Pd/ZrO_2/SDS > Cr/ZrO_2 > Cu/ZrO_2 > Cu/ZrO_2/SDS > Cr/ZrO_2/SDS > Co/ZrO_2/SDS > Pd/ZrO_2
	Co/ZrO_2		22.91								$T_{\sim 35} = 300$	
	Cu/ZrO_2		24.76								$T_{\sim 14} = 300$	
	Cr/ZrO_2		22.93								$T_{\sim 22} = 300$	
	Pd/ZrO_2/SDS		25.10								$T_{\sim 20} = 300$	
	Co/ZrO_2/SDS		24.97								$T_{\sim 8} = 300$	
	Cu/ZrO_2/SDS		22.28								$T_{\sim 10} = 300$	
			23.04								$T_{\sim 14} = 300$	

(*continued on next page*)

Table 4 (*continued*)

Reference/ year[a]	Catalyst	Preparation method	BET surface area ($m^2 \cdot g^{-1}$)	Reactor (material, size)	Reactant	Total flow rate ($mL \cdot min^{-1}$)	Space velocity	T_{10} (°C)[b]	T_{50} (°C)[b]	T_{90} (°C)[b]	Tx (°C)[b] X = conv%	Remarks
	Cr/ZrO_2/SDS (SDS: sodium dodecyl sulphate)											
[232] 2019	CoO_x @ SiO_2 - 400 °C	Deposition	389	Fixed-bed (quartz)	CH_4: 2 vol%, O_2: 20 vol%, N_2: balance	250	15 000 mL g^{-1} h^{-1}				T_{100} = 330	- Catalytic activity: CoO_x @ SiO_2 - 400 °C > CoO_x @ SiO_2 - 600 °C > CoO_x @ SiO_2 - 800 °C
	CoO_x @ SiO_2 - 600 °C		290								T_{100} = ~380	
	CoO_x @ SiO_2 - 800 °C		225								T_{-85} = ~400	

Notes.
[a] Mentioned studies in Table 4 are listed in the order of published year.
[b] $T_{10}/T_{50}/T_{90}$: the temperature at which the methane conversion is 10%, 50% and 90%.

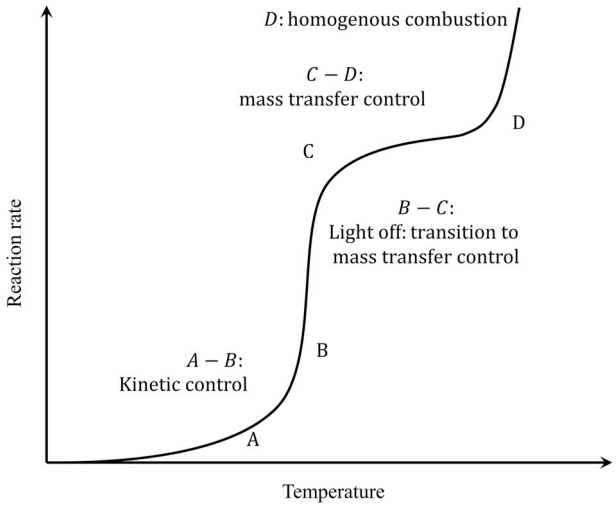

Fig. 7. Reaction rate as a function of temperature [186].

by the competitive adsorption, and surface vacancies subsequently left behind by the fast re-oxidation on the catalyst surface. Note that the DRIFT associated with Raman and X-ray fluorescence spectroscopies has been applied as important in-situ technologies by Jodłowski et al. [163] for the CMC over Co–Pd/Al_2O_3 catalyst. The proposed mechanism is slightly different from the Mars-van Krevelen mechanism, in that only the adsorbed active oxygen species on the catalyst surface was responsible to oxidize methane instead of the bulk oxygen atoms. Furthermore, the presence of –OCH_3 species was detected, rather than HCHO and H_2 in the gas phase. These results are also supported by other studies [170, 171].

Therefore, there is no unanimous mechanism so far to fully elaborate the CMC, given the whole processes being rather complex and strongly dependent on the reaction conditions and used catalysts [172,173]. The Mars-van Krevelen mechanism seems to be more widely accepted than the Langmuir-Hinselwood and Eley-Rideal mechanisms. In this respect, more in-depth understanding is still needed to better elucidate the reaction pathway [174]. More details on the reaction mechanisms may be found in the literature [138–143].

4. Effect of operational conditions on CMC

In this section, main factors that should be carefully assessed are reviewed so as to determine the appropriate working conditions for

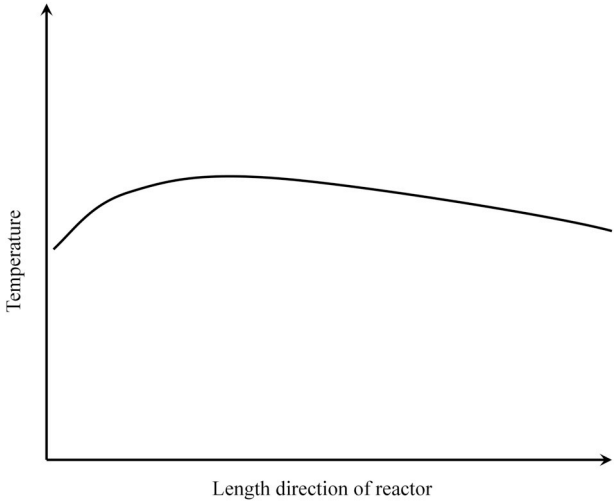

Fig. 8. Temperature distribution along the reactor length.

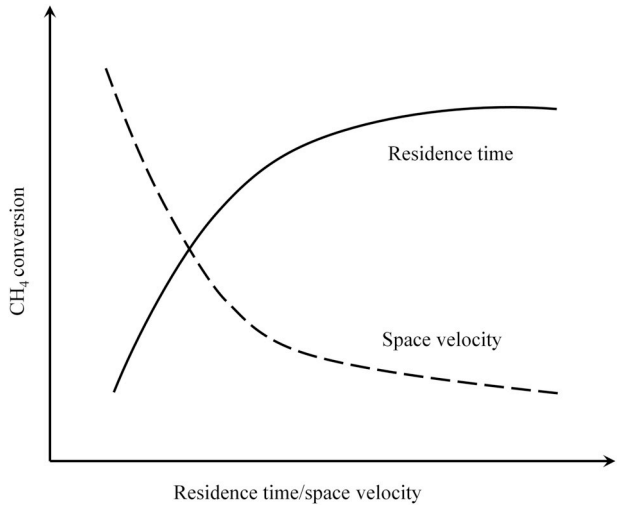

Fig. 9. CH_4 conversion as a function of the space velocity or residence time.

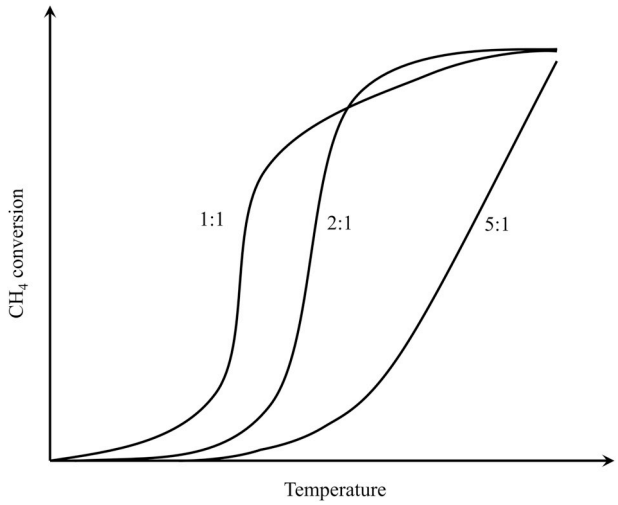

Fig. 10. CH_4 conversion as a function of temperature under different oxygen-to-methane molar ratios over Pt/Al_2O_3 catalyst [19].

CMC, including the temperature, the ratio of methane to oxygen, the flow rate, the reactant composition and the pressure. The reaction behavior addressed in this section, unless otherwise specified, is assumed to be intrinsic. A summary of the studies over various catalysts and the key influential factors can be found in Table 4.

4.1. Effect of temperature

In general, the intrinsic reaction rate for CMC is correlated to temperature and activation energy according to the Arrhenius equation [182,183]. The reaction rate presents a great increase with the increasing reaction temperature.

Light-off temperature is one of the most crucial parameters used to indicate the catalyst activity [118,184,185]. Fig. 7 shows the reaction regime as a function of the temperature. At the beginning, the temperature over the catalyst is low and thus the reaction rate is limited by the intrinsic kinetics (regime A-B). The light-off is commonly defined by the regime where the temperature has no significant change when the conversion is increased from 10%, 20% up to 50% (regime B–C) [186]. As light-off happens at comparatively high temperature levels, the intrinsic reaction rate rapidly increases but gradually the mass transfer rate cannot keep up with (regime B–C). Hence, the overall reaction rate tends to be limited more by the mass transfer rate. Upon further increase of the reaction temperature, the intrinsic reaction rate is increased so fast that the reaction falls in the mass transfer controlled regime (regime C-D). In this regime, the rate of increase in the overall reaction rate becomes slower. Eventually at substantially high temperature levels, the homogeneous combustion of methane dominates (regime D). The latter two regimes impose high requirements on the reactor design in terms of maintaining the catalyst stability and enhancing the mass and heat transfer rates. The effect of high working temperatures on the shortened life-time due to the catalyst sintering should be considered, especially for noble metal catalysts.

As for wall-coated plate-type/microchannel reactor, the temperature distribution along the catalytic reactor commonly displays a rapid increase at the entrance region, and a smooth decrease along the reactor length thereafter, as shown in Fig. 8. This is because that methane is mainly converted at the front section of the reactor [187]. However, the peak temperature region moves slowly towards the downstream with the increasing oxygen/methane ratio. The variation of temperature along the reactor mainly depends on the reactant flow pattern and the reactor structure, which will be elaborated in the following section 5.

Moreover, the pollutant emission could be significantly affected by the operational temperature. With the presence of N_2 in the reactant feed, it was reported that NO_x emission showed a growing trend with the increasing temperature [188]. The formation of CO is often due to the incomplete methane combustion under low temperatures and/or with a methane rich mixture.

In addition, it is worth noting that the catalyst deactivation is significantly influenced by the operational temperature. For instance, the active PdO phase is decomposed to the less active metallic palladium (PdO → Pd) at above 800 °C, followed by the agglomeration and deactivation of catalysts [95]. It is thus essential to maintain the operational temperature below the thermal decomposition temperature of PdO. Another solution is to increase the decomposition temperature by optimizing the catalyst, e.g. by introducing metal oxides [189]. Farrauto et al. [90] pointed out that the addition of ZrO_2 into PdO/Al_2O_3 catalyst exhibited a superior synergistic effect between the temperature hysteresis and the active site reformation. The decomposition temperature of PdO was thus increased to ca. 900 °C. In order to regenerate the catalyst, Farrauto et al. [90] suggested that the reoxidation temperature of metallic Pd occurred at ca. 650 °C, and methane conversion increased after reoxidation process [90]. Another reason causing the catalyst deactivation at low temperatures (e.g. below 450 °C) may be the overwhelming accumulation of hydroxyl group over the catalyst surface [190]. It hinders the migration and exchange of the active oxygen species between the catalyst support and active sites (PdO/Pd), resulting in the catalyst sintering. This is further confirmed by the water vapor effect on the methane conversion to be discussed in the section 4.4.

4.2. Effect of space velocity and residence time

Theoretically, the methane conversion presents an inverse proportion to the space velocity, as shown in Fig. 9. It was observed that the methane conversion at 400 °C increased from 72% to 100% over Au–Pd catalyst when decreasing the space velocity of reactants from 40 000 to 10 000 $mL \cdot g_{cat}^{-1} \cdot h^{-1}$ [179] (cf. the detailed experimental data in Table 4). A similar tendency over various catalysts has also been reported by other researchers [88,113]. This can be theoretically explained by the fact that the more accessibility of reactants (at longer residence times) over the active sites of catalyst favors the conversion of the adsorbed methane molecules. However, the side reactions and coke deposition are more likely to occur under long residence times [191].

The methane conversion is directly relevant to the intrinsic reaction kinetics and mass transfer. The internal mass transfer mostly depends on the catalyst properties (e.g. diffusion in the pore structure, size and volume). The external mass transfer from gas phase to the catalyst surface is limited by the residence time (i.e., the flow rate of reactants). As for the exothermic reaction, the effect of the temperature gradient on the

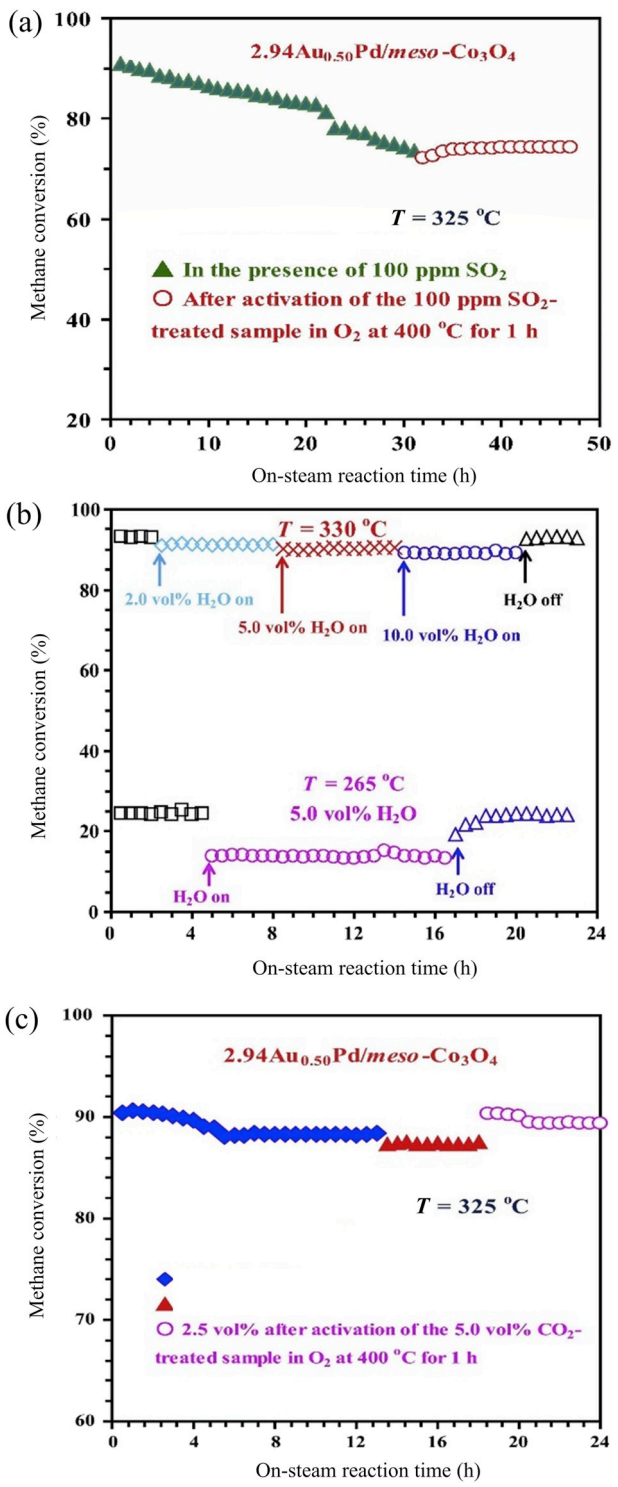

Fig. 11. Effect of (a) SO_2 (b) H_2O (c) CO_2 on the methane conversion. T in figures indicated the reaction temperature. Conditions: Au–Pd/Co_3O_4 catalyst, space velocity, 20 000 $mL \cdot g_{cat}^{-1} \cdot h^{-1}$ [201].

reaction rate should also be considered. It has been reported that at a certain temperature, a steady-state conversion rate could be reached with the increasing flow rate. After that, a further increase in the flow rate could not have any influence on the methane conversion. The mass transfer limitation is thus negligible at higher flow rates [192].

Moreover, in order to obtain sufficient reaction heat for heating purposes, higher reactant space velocity is required, but usually accompanied with a lower methane conversion. Hence, a compromise between the space velocity and the methane conversion should be reached for a certain application.

4.3. Effect of oxygen to methane molar ratio

The selectivity variation of products strongly depends on the molar ratio of oxygen to methane. Mouaddib et al. [193] investigated the effect of oxygen to methane molar ratio in the range of 4 to 0.66 over Pd/Al_2O_3 catalyst. It was observed that CO was formed under oxygen deficient conditions ($O_2/CH_4 < 2$) due to the side reaction of methane steam reforming. And CO became a main product when O_2/CH_4 molar ratio reached 0.66 [193]. Similarly, Lee et al. [186] reported that CO was formed over Pt/Al_2O_3, Pd/Al_2O_3 and Rh/Al_2O_3 catalysts in the presence of oxygen deficient mixtures as feedstock. The selectivity of CO also depended on the reaction temperature. With the increasing reaction temperature, the CO selectivity constantly increased and became a main product under low O_2/CH_4 molar ratio. But the methane conversion was independent to the presence of CO in the feedstock [186].

Burch et al. [19] investigated the effect of different molar ratios of oxygen to methane on Pt/Al_2O_3 and Pd/Al_2O_3 catalysts. Pt/Al_2O_3 catalyst became more active from the oxygen-rich (O_2/CH_4 = 5:1) condition to methane rich (O_2/CH_4 = 1:1) condition, because the less oxidized platinum was more active than the oxidized platinum. As for Pt-based catalyst, Drozdov et al. [194] further explained that a weaker bond existed between oxygen and metallic platinum than that with platinum oxides. Thus, Pt-based catalyst is less active in oxygen-rich mixtures. On the contrary, as for Pd-based catalyst, it has been found that the oxygen is weakly bound to palladium oxides compared with metallic palladium [194]. Thus, the Pd-based catalyst is more active in oxygen-rich mixture [19,195].

The methane conversion at different oxygen-to-methane molar ratios does not display the same augmentation as the reaction temperature increases. More interestingly, the light-off phenomenon was observed to be significantly influenced by the oxygen to methane molar ratio and the resulted degree of reactant surface coverages [19]. It was found that the methane conversion over Pt/Al_2O_3 increased with the decreasing oxygen-to-methane molar ratio (e.g., from 5:1 to 1:1 as shown in Fig. 10; cf. detailed experimental results listed in Table 4) at lower temperatures (ca. 300–425 °C, in terms of different Pt loading) [19]. At higher temperatures (ca. 450–550 °C), the methane conversion at such a molar ratio of 1:1 became lower than that at 2:1, due to the insufficient oxygen supply, and the light-off was observed in the latter case. This phenomenon could be explained by the fact that the favorable concentration of CH_4 and O_2 over the catalyst surface and/or the more significant local heat release greatly accelerate the reaction rate. However, no light-off was found under an oxygen-to-methane molar ratio of 5:1 because the excessively adsorbed oxygen resulted in a non-optimized surface coverage of methane, eventually hindering the light-off. The competitive adsorption between the adsorbed methane and oxygen species could affect the methane conversion. The lower methane conversion at the case of 5:1 ratio (Fig. 10) could be explained by the fact that more adsorbed oxygen species over the catalytic surface suppress the methane absorption due to the high methane adsorption energy [147,150].

Regarding the pollutant emissions, a lean reactant mixture is preferred in order to lower the emissions of CO, NO_x and the unburned hydrocarbon [196]. It has been reported that CO was detected at a methane concentration higher than 9.5 vol% and carbon deposition occurred on catalyst surfaces at a methane concentration above 26.5 vol % [197].

4.4. Effect of (synthetic) natural gas composition

Besides methane, natural gas is commonly composed of varying amounts of higher alkanes (e.g., ethane, propane) and other species depending on the resources. In this section, the effect of H_2S, H_2O, NO and CO_2 on the catalytic methane conversion is discussed, more details

Table 5
Summary of thermal parameters for various reactors.

Reference	Reactor	Catalyst	Reactant	Tx (°C) X = conv %	Heat transfer	Heat released	Heat recovery efficiency	Input power	Gas exhaust	Remarks
[29] 1999	Monolith (Fig. 16b)	One monolith Two monoliths	Air/CH_4 1.1–1.5			15–40 W cm^{-2}			NO_x: 5 ppm CO: 0 ppm NO_x: 0 ppm CO: 0 ppm CH_4: 0 ppm	- Long coating → CO emission - Short coating → NO_x emission - Completely catalytic boiler: No emissions, and lower sensitivity to gas quality
[187] 1999	Monolith	Pd–NiO/Al_2O_3	E_a: 1.0 1.25 1.5 2.0			6.2–13.4 kcal h^{-1} cm^{-2}	~90% ~100% ~100% ~100%			- E_a 1.0–1.5: catalytic combustion E_a: 1.75–2.0: flame occurred E_a > 2.1: flame blown off E_a 1.25–1.75: stable catalytic combustion - Over 95% methane was converted within 8 mm from the entrance
[32] 2003	Fin reactor (Fig. 14a)	Pd/ZrO_2	0.19 m s^{-1} 0.11 m s^{-1} 0.15 m s^{-1} 0.23 m s^{-1} 0.12–0.31 m s^{-1}	T_{35}: 400 T_{70}: 450 T_{78}: 500 T_{80}: 600 $T_{99.9}$: 500 $T_{99.9}$: 500 T_{76}: 500 $T_{98.5}$: 500	Air as HTF (heat transfer fluid)		$T_{fin\ surface}$: ~300–750 °C T_{outlet}: ~727–927 °C			- <500 °C: methane conversion was greatly affected by the inlet temperature - >500 °C: methane conversion was slightly affected by the inlet temperature - Higher flowrate → more heat removed → lower surface temperature → decreased conversion - Surface area should be as large as possible
[33] 2005	Monolith	$Co_3O_4/Fe_2O_3/MnO_2$	CH_4: O_2: N_2 1:4:5	T_{10}: 358 °C T_{90}: 378 °C	T_{inlet}: 16.8 °C T_{outlet}: 42.0 °C (to heat water: 11.2 kg min^{-1})	19.9 kW 80 W cm^{-2}	101.1%		CO: 0.01% NO_x: 22 ppm O_2: 5.6% Hydrocarbon: 0 ppm	- Burner with two heat exchanger on two sides of monolith catalyst is able to enhance the heat efficiency and reduce the pollutant
[282] 2006	Monolith (450 × 200 × 700 mm)	Pt-based	1.00 m^3 s^{-1} 1.17 m^3 s^{-1} 1.33 m^3 s^{-1} 1.50 m^3 s^{-1} 1.67 m^3 s^{-1} (natural gas flow rate)		$T_{exhaust}$: 73 °C $T_{exhaust}$: 90 °C $T_{exhaust}$: 93 °C $T_{exhaust}$: 106 °C $T_{exhaust}$: 114 °C		99%–99.5%	3.5 kW 4.0 kW 4.6 kW 5.2 kW 5.7 kW	NO: 3 ppm, CO:1, SO_2:1 NO: 2 ppm, CO:1, SO_2:1 NO: 2 ppm, CO:0, SO_2:2 NO: 0 ppm, CO:0, SO_2:2 NO: 0 ppm, CO:0, SO_2:4	- E_a:2.08, 6.88% heat loss at an exhaust temperature of 114 °C - High combustion efficiency and near-zero emission
[242] 2007	Fixed-bed central heat exchange (Fig. 12c)	MnO_2		99.9%	T_{inlet}: 833 °C T_{outlet}: 683 °C	1.89 MW[a]	63.3%			- Heat recovery efficiency: hot gas withdrawal > central heat exchange - MnO_2 > Pd catalyst - Conversion: central heat exchange > hot gas withdrawal
	Hot gas withdrawal (Fig. 12d)	MnO_2		97.1%	T_{inlet}: 878 °C T_{outlet}: 60 °C	2.85 MW	95.5%			
		Pd		92.4%	T_{inlet}: 670 °C T_{outlet}: 60 °C	2.16 MW	72.0%			
[283] 2007	Fixed-bed	Pd/ $LaMnO_3{\cdot}2ZrO_2$	E_a: 2–45%		T_{inlet}: 30–60 °C			10–25 kW		- Great improvement of catalytic performance was

(*continued on next page*)

Table 5 (*continued*)

Reference	Reactor	Catalyst	Reactant	T*x* (°C) X = conv %	Heat transfer	Heat released	Heat recovery efficiency	Input power	Gas exhaust	Remarks
					T_{outlet}: 50–80 °C					observed after sulfur aging
[31] 2009	Fixed-bed (i.d.: 50 mm L: 120 mm)	$Pd/LaMnO_3/ZrO_2$	E_a: 5%[b]	T_{50}: 570 T_{50}: 382	T_{inlet}: 30 °C			10 kW	~65–85 $mg{\cdot}kWh^{-1}$	- NO increased at low input power
		$Pd/CeO_2/ZrO_2$ $Pd/BaCeO_3/ZrO_2$ (catalyst coating on FeCrAl fibre mat)		T_{50}: 512	T_{outlet}: 50 °C (heat up water)			22 kW 35 kW 10 kW 22 kW 35 kW 10 kW 22 kW 35 kW	~150–160 ~160–175 ~40–50 ~45–50 ~55–65 ~0 ~0 ~0	- NO decreased at high air excess
			E_a: 30%							
			E_a: 60%							
[245] 2009	Fixed-bed hot gas withdrawal without returning cold gases	Pd-washcoated monolith	3000 ppm	$T_{97\text{-}99}$: 400 $T_{97\text{-}99}$: 420-460		9.8 MW	10–100%			- Stability: withdrawal hot gas at bed end > withdrawal hot gas at center; no returning cold gas > returning - At the end of bed without returning cold gas showed the best conversion and heat recovery efficiency
			5000 ppm	$T_{98\text{-}99}$: 430-550 $T_{99\text{-}100}$: 440-650		16.4 MW				
			7000 ppm	$T_{98\text{-}100}$: 400-500		23.0 MW				
			9000 ppm			29.5 MW				
	With returning cold gases		3000–9000 ppm				0–73%			
[284] 2015	Fixed-bed L: 40 mm	Pt/Al_2O_3 $Pt/ZSM\text{-}5$	Flow rate: 800 mL min^{-1}	T_{76}: ~230	$Q^c_{surface}$ ~7 W			35.2 W		- 20 mm catalyst bed length showed better catalytic performance and combustion efficiency than 40 mm and 10 mm bed length, because it balanced the catalyst spatial density and the residence time
			1400 mL min^{-1}	T_{57}: ~395	~9.6 W			61.7 W		
	L: 20 mm		2000 mL min^{-1}	T_{36}: ~350	~8.2 W			88.1 W		
			800 mL min^{-1}	T_{58}: ~310	~7.7 W			35.2 W		
			1400 mL min^{-1}	T_{80}: ~335	~8.9 W			61.7 W		
	L: 10 mm		2000 mL min^{-1}	T_{90}: ~350	~9.2 W			88.1 W		
			800 mL min^{-1}	T_{33}: ~250	~6.4 W			35.2 W		
			1400 mL min^{-1}	T_{25}: ~255	~6.8 W			61.7 W		
			1800 mL min^{-1}	T_{18}: ~210	~6.2 W			79.2 W		
[275] 2015	Membrane reactor	$Pd/\gamma\text{-}Al_2O_3$	3–4% CH_4 In air	$T_{73.5\text{-}91.2}$: 555–575 °C	Yield of H_2: 103–153 $kg{\cdot}day^{-1}{\cdot}kg^{-1}_{cat}$					- 91% methane conversion in steam reforming, and 99.99% purity hydrogen can be obtained by the provided heated from methane combustion
	Coupled with steam reforming rector (Fig. 17d)	$Ru\text{–}MgO\text{–}La_2O_3/\gamma\text{-}Al_2O_3$		$T_{\sim 91}$: 570 °C						

Note.
a. Amount of heat flux withdrawal.
b. E_a: air excess.
c. $Q_{surface:}$ heat release rate transferred via combustor surface.

can be found in the references [179,198].

Noble metal catalysts are easily poisoned when exposed to natural gas containing sulfur compounds (Fig. 11a). For instance, the irreversible deactivation by SO_2 might be attributed to its occupation of the active sites, and/or the transformation of the highly active compound PdO on the catalyst surface to less active $PdSO_3$ or $PdSO_4$. Similar results were also reported in the literature [199,200]. The highly challenging issue of the resistance to poisoning by sulfur containing compounds present in trace amounts in the natural gas (odorizer) should be fully addressed. Developing catalysts with improved resistance to sulfur poisoning and possible desulfurization pretreatment are possible measures.

The presence of water vapor acts as an inhibitor for CMC [165,202]. It was observed that the methane conversion over the $Au\text{–}Pd/Co_3O_4$ catalyst dropped remarkably when water vapor was introduced, but this process is reversible when the water vapor is removed (Fig. 11b) [201]. Specifically, the hydroxyl group was formed by reaction of the chemisorbed oxygen species with the water vapor over the catalyst surface, preventing thereby the exchange of the oxygen species between the active sites and the support [190,203]. Moreover, the hydroxyl group also hindered the desorption of CO_2 and H_2O over the catalyst surface due to the competitive adsorption. The kinetic study by Geng et al. [203] illustrated that the reaction order with respect to methane decreased from 1.07 to 0.86 after the water vapor addition, and the reaction order

Table 6
Advantages and disadvantages of various reactor types for CMC.

Reactor type	Advantages	Disadvantages
Fixed-bed	- Easy operation - Low cost - Suitable for industrial uses - Enhanced catalyst spatial density	- Low reactor surface area - Poor temperature uniformity - High pressure drop
Micro/mini structured	- High surface-to-volume ratio - High mass/heat transfer rate - Low pressure drop - Inherent safety (e.g. hazardous reaction mixtures can be handled safely due to channel dimensions below the quenching distance) - Compact design	- High manufacture cost - Not easy to replace the catalyst if washcoated
Monolithic	- Regular and well-defined structure - High surface-to-volume ratio - High mass/heat transfer rate - Low pressure drop - High thermal stability - Low cost	- Not easy to replace the catalyst if washcoated
Membrane	- Reaction and product separation in one reactor - By changing oxygen permeation and partial pressure to achieve the high conversion, and products are easy to withdrawal under high pressures	- High cost of membrane replacement
Fluidized bed	- Enhanced gas-solid catalyst contact - Enhanced heat/mass transfer - Low pressure drop - Good temperature distribution	- Large-scale device - Catalyst mass loss and high heat loss - Reactor bed temperature fluctuation

in water also decreased from −0.72 to −0.95 with the increasing water concentration. Thus, improving the catalyst stability in the presence of water vapor becomes one important challenge to deal with wet CMC. Recently, Toso et al. [93] reported that the solution combustion synthesis could improve the stability and water resistance of Pd-ceria and Pd-ceria-zirconia catalysts compared to the traditional impregnation method. Ciuparu et al. [204] also suggested that the influence of water vapor became insignificant at above 723 K.

Sadokhina et al. [205] observed the enhanced activity with NO addition under wet conditions. This can be explained by the reaction between NO and hydroxyl species to form HNO_3 on the catalyst surface, compensating the inhibition effect of water addition.

The reversible inhibition effect of CO_2 addition is depicted in Fig. 11c. The negative influence of CO_2 addition on the methane conversion is ascribed to the accumulation of carbonate species on the catalyst surface, thus preventing a further adsorption of CH_4 and O_2 over the surface [201] (cf. detailed experimental data in Table 4).

4.5. Effect of operating pressure

Most published studies have performed the CMC at the atmospheric pressure. High working pressure conditions (up to 30 bar or higher) are primarily applied for gas turbine purpose.

The methane conversion decreased (from ~7.2% to ~3.5%) with the increasing pressure (from 5 bar to 15 bar) over Pd–Pt/Al_2O_3 catalyst (cf. more details listed in Table 4) [103]. Moreover, it was reported that the effect of working pressure varied with the temperature [206]. At lower temperatures (500–600 °C), an increase in the pressure led to the decreased methane conversion and the lower combustion efficiency. In this case, the higher specific surface area was commonly required at high pressures so as to obtain a higher conversion. At higher temperatures (>700 °C), homogenous combustion takes place. A higher combustion efficiency could thereby be obtained with an increasing pressure [206, 207], probably due to the increasing mass throughputs [208].

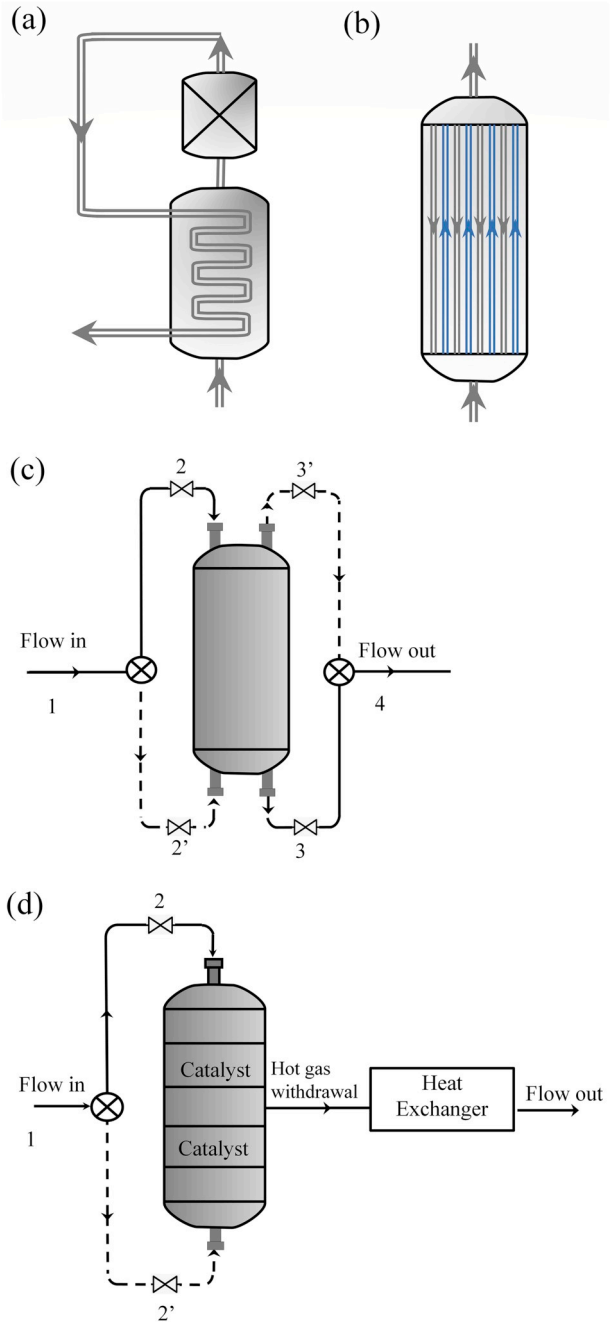

Fig. 12. Autothermal fixed-bed reactor with (a) a separate heat exchanger; (b) an integrated heat exchanger; (c) a periodic flow reversal mode (central heat exchange); (d) hot gas withdrawal on two side ends of the catalyst section.

5. Types of catalytic reactors

In this section, some representative types of reactor used for CMC are discussed. Special focuses are laid on the geometry, the way of reaction heat recovery and the improvement of thermal efficiency by the enhancement of heat and mass transfer. Table 5 recapitulates some key facts of the relevant studies reported in the literature and Table 6 provides a comparison on the advantages and disadvantages of these reactors.

5.1. Fixed-bed reactor

A fixed-bed catalytic reactor is commonly made up of a cylindrical

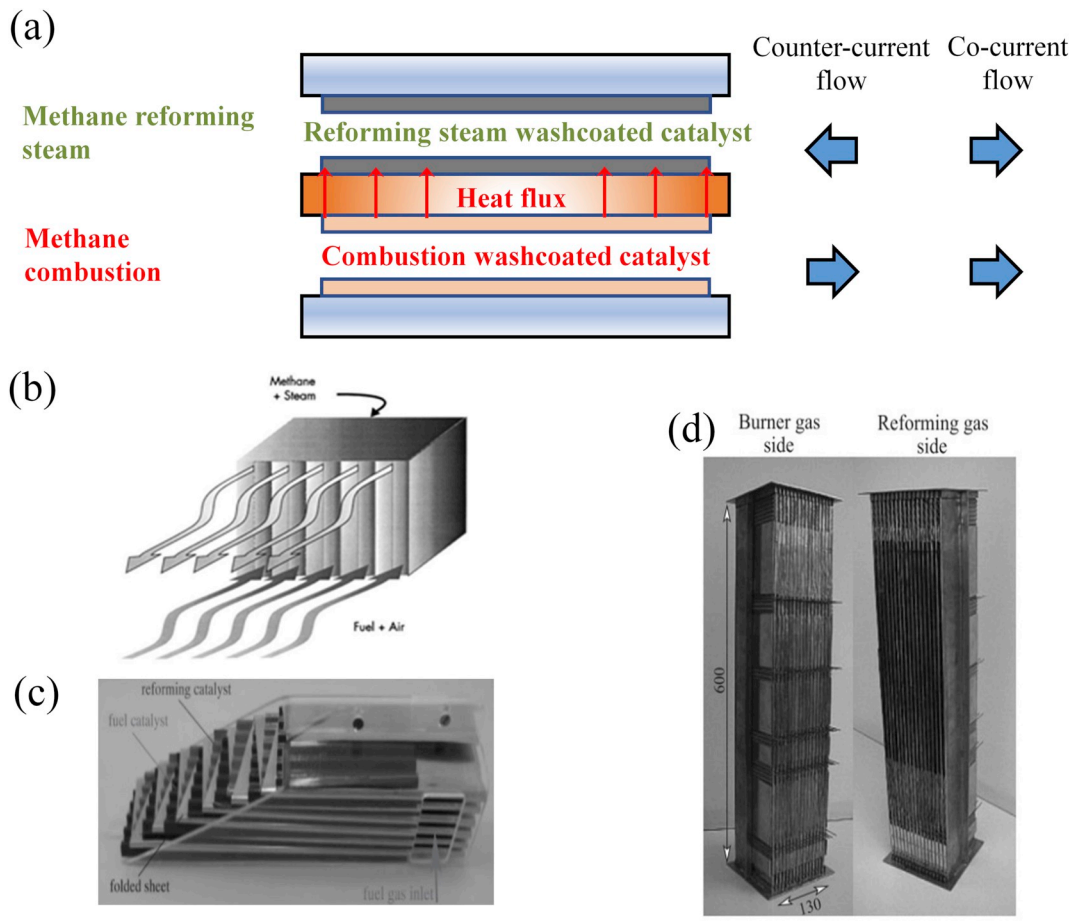

Fig. 13. Wall-coated reactor. (a) co-current and counter-current flow modes of wall-coated reactor; (b) folded metal sheet [251]; (c) folded sheet reactor with corrugated spacers as catalyst carriers [44]; (d) pilot-scale multifunctional folded sheet reactor [252].

tube with a certain amount of catalysts being fixed in certain locations inside the tube. The shapes of catalyst can be powder, spherical, cylindrical or randomly shaped pellets. This type of reactor is the most commonly used, suitable not only for catalyst activity test and kinetic study, but also for practical applications in the chemical and process industries. The advantages of fixed-bed reactors include easy operation, low cost, high catalyst spatial density, etc. Poor temperature distribution, low surface area, and high-pressure drop are their main disadvantages.

Besides being used individually as a single-stage reactor, several fixed-bed reactor modules may be combined to form a multi-stage reactor system. Different catalysts may be used for each stage. A two-stage combustor combining a conventional flame reactor with a catalytic reactor has been proposed by Sadamori et al. [206,233], with the purpose of improving the combustion efficiency and further reducing the gas exhaust emission. In their study, three monolithic catalysts with Pd and/or Pt based catalysts were loaded in the catalytic stage. Combustion efficiency higher than 99.5% and the NO_x emission less than 2 ppm (80% reduction) could be achieved by controlling the inlet temperature between 500 and 700 °C. In terms of thermal behavior, the conventional stationary fixed-bed reactor with a separated heat exchanger (Fig. 12a) has the problem such that the reaction heat is difficult to be fully utilized. Multifunctional or extended autothermal reactors having higher interfacial surface areas and more efficient heat transfer thus become more attractive, especially for strongly or moderately exothermic reactions [234]. This concept combines catalytic reaction with an effective thermal management (i.e. heat removal or addition) in an integrated and compact device (Fig. 12b), so as to largely reduce the heat losses. Compared to the ex-situ configuration, lower CO and NO_x emissions and higher heat power could be achieved for the multifunctional reactor with an integrated heat exchanger [31]. Detailed information about the autothermal fixed-bed reactor can be found in the literature [235–237].

In order to further enhance the heat transfer capability, the fixed-bed reactor can be operated in the reversal flow mode [238,239], where the feeds are alternately introduced from either end of the reactor (Fig. 12c). The continuous heat extraction is a viable way to provide necessary amount of heat in the reactor, and to maintain the catalyst activity without overheating. A high amount of heat withdrawal could result in a high instability of the reaction due to a remarkably decreased temperature of the reactor. Moreover, a periodic steady state in temperature can be achieved by switching the direction of reactant flow. The reversal time is one of the significant factors not only to stabilize the reactor and the heat exchanger but also to maintain a stable temperature in the catalytic section. A longer reversal time is commonly accompanied with a higher heat loss. On the contrary, a shorter reversal time can result in a lower heat generation and a reduced methane conversion [240,241]. Many simulations studied the relative position of the catalyst bed and the heat exchanger as well as the flow pattern in order to find out the most efficient way to recover heat from reversal-flow reactors [242–244]. Gosiewski et al. [242] found that a higher heat recovery efficiency can be approached by the hot gas withdrawal (Fig. 12d) than by the central heat exchange (Fig. 12c). Detail experimental data are listed in Table 5. Their results showed that more than 70% of heat can be recovered when withdrawing only around 30% of the hot gas. Furthermore, Hunter et al. [245] studied different patterns of heat recovery with respect to the heat withdrawal location (central or end) and the possibilities of returning the cooled gas to exchange heat. It was

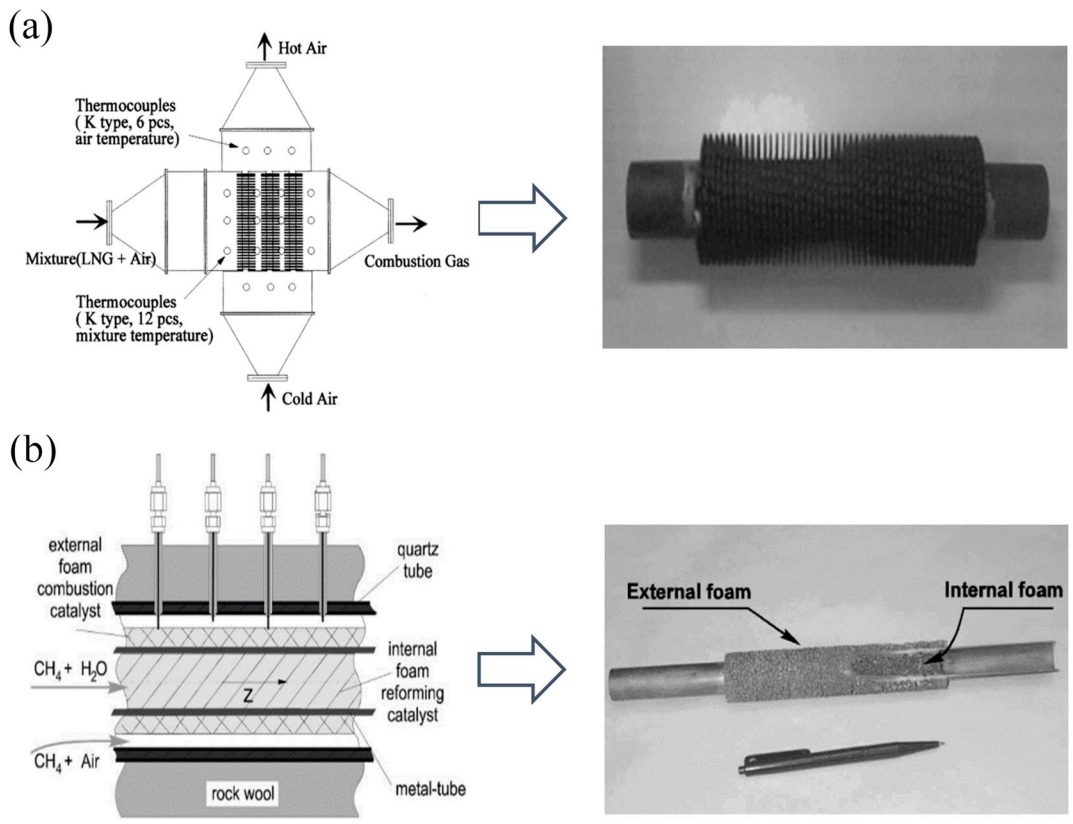

Fig. 14. Coated-tubular reactor. (a) tube-fin geometry and laboratory prototype [32]; (b) external surface coated with Ni–Cr catalyst, and internal surface coated with Ni catalyst [121].

found that a higher heat recovery efficiency could be obtained by positioning the heat exchanger at the two side ends of the catalytic bed without any returned cold gas (Fig. 12e). Hence, a high thermal recovery efficiency and the best methane conversion may be achieved by considering both the flow reversal mode (e.g. the hot gas withdrawal at the end of the catalyst bed) and the reversal time. More description of the flow-reversal reactors can be found in the references [236,242, 246–248].

5.2. Wall-coated reactor

Conventional fixed-bed reactors have the drawback of limited heat transfer rate due to the low surface-to-volume ratio. On the contrary, the wall-coated reactors have features like lower pressure drop and higher surface area by depositing the catalyst layer on the reactor wall surface, so as to augment the catalyst contact surface area and to enhance the mass/heat transfer. Hence, this type of reactor is more suitable to be employed for coupling exothermic reactions with endothermic reactions. A lower temperature difference and a shorter distance between the heat source (exothermic reaction) and heat sink (endothermic reaction) are beneficial to increase the heat exchange efficiency. The so-called wall-coated reactor could be further divided into (folded) plate-type, tubular-type, micro/mini channel plate-type and monolithic reactors.

5.2.1. (Folded) plate-type reactor

Fig. 13a shows a basic plate-type reactor coupling CMC with methane steam reforming reaction. The two reactions happen on the opposite sides of the same plate with overlapped temperature profiles. The two flow modes (i.e., co-current and counter-current) were intensively investigated [249]. The hot spots could be avoided by optimizing the overlapping zone of reactions with the proper co-current arrangement. However, the complete overlapping is not able to be achieved by utilizing the counter-current flow mode. Regarding the distance between plates (thickness: 0.5 mm), it has been reported that no significant effect on the catalytic performance was observed when the plate distance varied between 1 and 4 mm [250].

A folded sheet structure reactor for the coupled CMC and steam reforming reaction was investigated by Polman et al. [251]. A relatively simple design with two separated chambers was formed by the folded metal sheet, as shown in Fig. 13b. In order to avoid the high heat loss and to enhance the heat transfer, a novel folded sheet reactor with rectangular adjacent channels was proposed by Kolios et al. [44]. The spacers with rectangular ducts in between are responsible to support the whole structure, providing additional effective heat exchange areas as well (increased by a factor of 3). The gas distributor with channels is located on the right side of the entire reactor, as shown in Fig. 13c [44]. Fig. 13d shows a pilot-scale multifunctional folded sheet reactor combining methane combustion with methanol reforming [252].

5.2.2. Coated tubular reactor

A novel tube-type reactor (i.d. 25 mm, o.d. 38.5 mm) with external fins (fin height 14.3 mm) was proposed by Seo et al. (Fig. 14a) [32]. The external surfaces of tube with fins were coated with Pd/ZrO_2 catalysts for CMC while the cold air as the heat transfer fluid (HTF) was circulated inside the tube to remove the released reaction heat. From practical point of view, this compact design with a high surface area is capable of achieving 100% methane conversion and a high heat transfer rate under high methane flow rate conditions. Moreover, nearly 100% methane conversion could be obtained by 16 finned-tube reactors even under high gas velocity conditions (0.12–0.31 m s^{-1}). However, the same conversion for 10 finned-tube reactors is required under a much lower velocity (<0.11 m s^{-1}). Moreover, it has been reported that the conversion at 400 °C decreased from 88% to 70% with the increasing

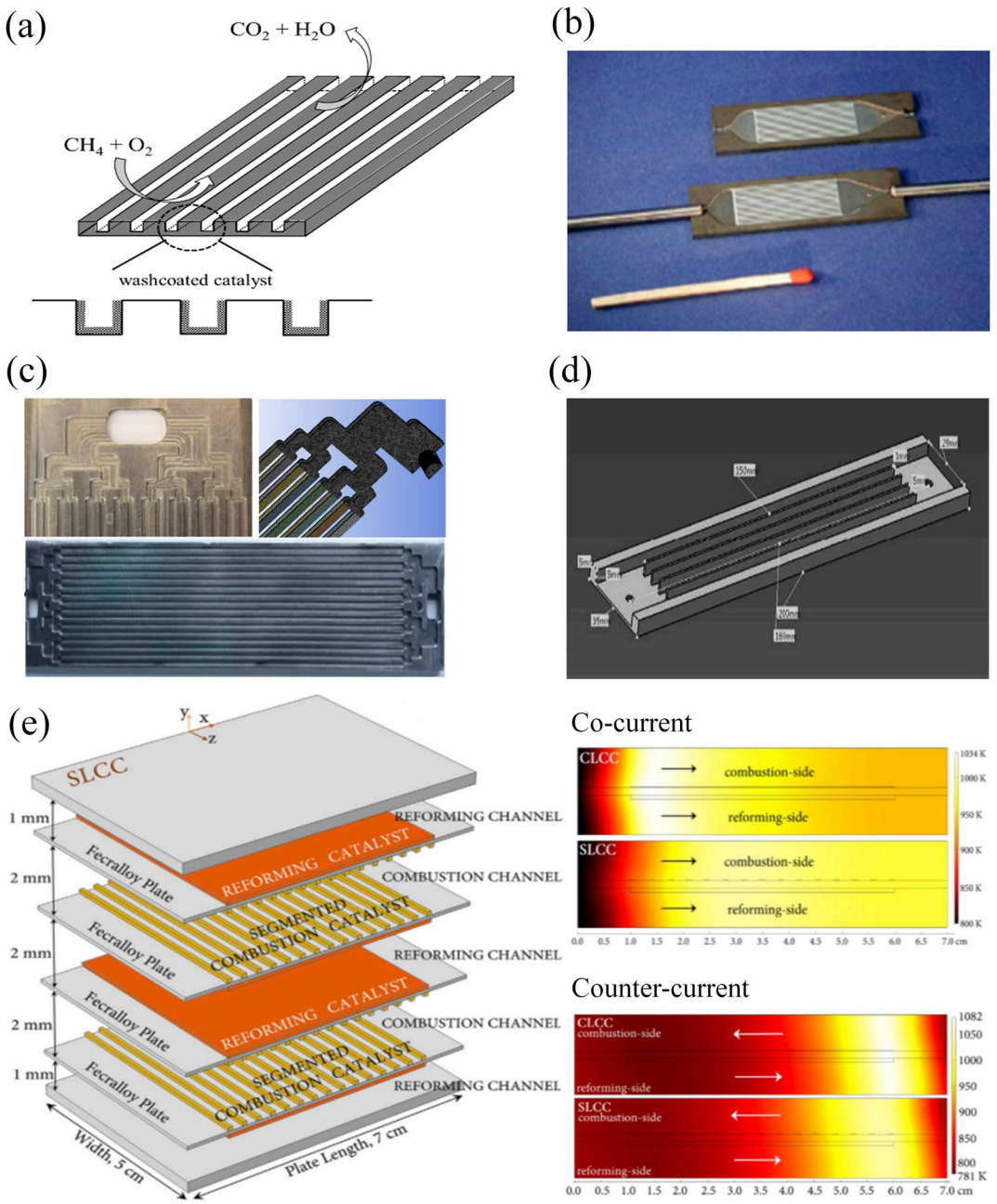

Fig. 15. Microchannel reactor. (a) basic geometry; (b) Washcoated Pt–W/Mo–Al_2O_3 catalyst on a microchannel reactor for CMC [118]; (c) Pt/γ-Al_2O_3 catalyst on multichannel reactor for CMC [120]; (d) coupling steam reforming over a microchannel reactor [262]; (e) integration of multi-plates coupling with methane steam reforming over a microchannel reactor [119].

catalyst thickness from 1 mm to 3 mm (cf. more details shown in Table 5). A washcoated finned tubular reactors with thinner catalyst thickness (e.g., <1 mm) was more favorable to reach a high conversion.

Ismagilov et al. [121] investigated a tubular reactor (i.d. 18 mm, o.d. 20 mm) with coated metal foams both on the external (Ni–Cr) and internal (Ni) tube surfaces (Fig. 14b). A stable catalytic performance and uniform temperature distribution in the reactor could be obtained by optimizing the gas mixture composition and the catalyst thickness. Moreover, the thickness of catalytic layer in the range of 4–5 mm was favorable to reach a more stable combustion than that of 2.5 mm. Thus, a suitable surface area and catalyst thickness are required not only for increasing the diffusion rate of reactants, but also for higher catalytic combustion efficiency.

Unlike the traditional straight combustor, Yan et al. [253] numerically investigated three different designs of the micro tube combustors for CMC. The improved combustion efficiency can be obtained from the design of multi-step separated baffles (two groups of three separated zones). One of the key advantages of this design is that the separated baffles provided chances for the premixed methane and air to enter the reaction zone from different locations, which enhanced the combustion efficiency and heat recirculation.

5.2.3. *Micro/mini channel plate-type reactor*

Micro/mini channel reactor has attracted more attention in the past several decades [254–256]. The high surface area of microchannel reactors as well as excellent mass/heat transfer presents great benefits for the catalytic performance [257–259]. Thus, highly exothermic reactions are better handled in the microchannel reactor, due to the suppression of the hot spot formation. However, it is worth noting that the high surface area may also result in the thermal quenching problem due to the high

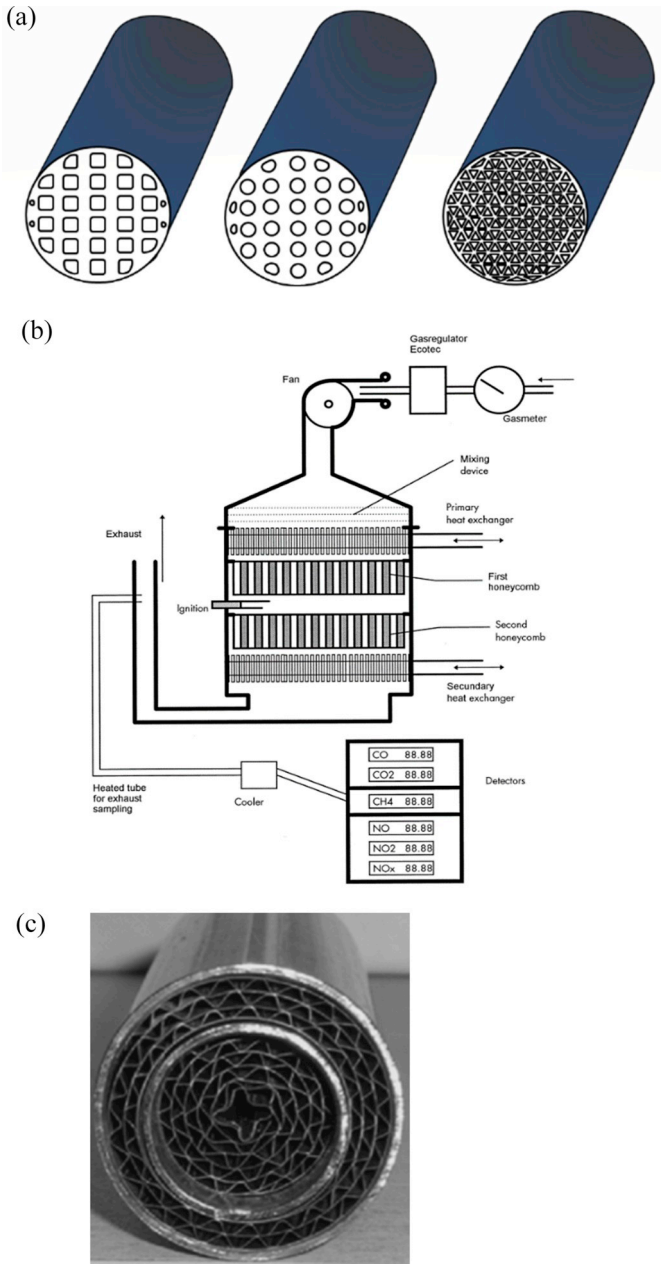

Fig. 16. Monolithic reactor. (a) various internal channel shapes (square/round/triangle); (b) catalytic monolithic reactor with two monolithic exchangers [29]; (c) folded-wall monolithic reactor coupled with steam reforming reaction [35].

heat loss if the reactor is not properly insulated. An extra heat source may have to be provided to the microchannel reactor when the released heat from CMC is insufficient to compensate the heat loss to maintain a continuous combustion in practice [258,260,261].

Fig. 15a shows a basic geometry of microreactor with washcoated catalyst on multiple straight channels, where the CMC reaction takes place. O'Connell et al. [118] investigated methane combustion on a microstructured reactor (51 cm length × 14 cm width) with the microchannels (500 μm × 250 μm, 14 channels in total) over washcoated Pt–W/Mo–Al_2O_3 catalyst, as shown in Fig. 15b. A methane conversion of 50% has been obtained at 493 °C under the total flow rate of 107 mL min^{-1}. The CMC was experimentally investigated by He et al. [120] in a parallel microchannels reactor (317.5 mm length × 50 mm width × 3 mm thickness) over washcoat Pt/γ-Al_2O_3 catalyst, as shown in Fig. 15c. A methane conversion of 95.75% could be obtained at 450 °C and 110 mL min^{-1} (at a residence time of 14.41 s). A compact microchannel reactor (15 cm × 3.9 cm × 1.5 cm) was used for the coupled CMC with methane steam reforming, as shown in Fig. 15d [262]. Each plate consists of 5 parallel straight channels (10 cm × 0.5 cm × 0.5 cm). The methane catalytic reactor with Pt–Sn/Al_2O_3 catalyst is located on the two sides of the steam reforming reactor with Ni/$CaAl_2O_4$ catalyst. The heat released from the CMC was provided for steam reforming reaction to produce hydrogen. The improved heat efficiency of 67% and methane conversion of 96% were obtained under optimized feed ratio (1.5) of combustion to reforming and at 700 °C. Enough hydrogen was expected to be generated to operate a 30 W fuel cell. Mundhwa et al. [119,263] proposed a microstructured reactor design (Fig. 15e) composed of two methane combustion reactors with segmented channels (1 mm × 5 cm × 20 μm, 20 channels) and two reforming reactor without channels. The plates were stacked alternatively one above another to form the autothermal microstructured reactor. Washcoated Pt/Al_2O_3 catalysts were applied in methane combustion microchannels while Ni/Al_2O_3 catalysts were coated on the steam reforming side. Based on this design, about 7–8% less reactants and 70% less catalysts were required for methane combustion to power a 1 kW fuel cell. A better methane conversion and heat transfer efficiency (in terms of better temperature distribution) could be obtained under the co-current flow mode (Fig. 15e). Contrarily, the counter-current flow mode generated undesirable high temperatures, resulting in the degraded catalyst life-time.

In order to improve the stability of methane combustion, Nui et al. [264] proposed different trapezoidal bluff bodies in the microchannel reactor. The numerical results presented that the combustion recirculation zone was broadened due to the formation of vortex by increasing the blockage ratio of bluff bodies.

The thickness of the catalyst layer has a significant impact on the catalytic performance. The increased thickness of the catalyst layer usually results in a decrease in the methane conversion due to the increased internal mass transfer limitation [121]. However, Rodrigues et al. [261] reported that a higher catalytic activity could be obtained by the thicker catalyst film. The porous catalyst prepared by the electrodeposited method offered the reactants easier access to the inner surface.

5.2.4. Monolithic reactor

Monolithic reactors with open structures present a low pressure drop, high surface-to-volume ratio, high mass/heat transfer rates and high thermal stability. Thus, this type of reactor is widely applied to gas turbines and automobiles for power generation and/or for pollutant emission purification [265,266]. Numerous types of interconnected channels (e.g. square/round/triangle, as shown in Fig. 16a) and various types of substrate (e.g., honeycombs, foams or fibers) are oriented to different applications [267,268]. A higher monolithic surface area can be obtained by triangular interconnected channels. It was reported that monolith with a high specific surface area (400 cells·cm^{-2}) presented enhanced mass and heat transfer characteristics compared to the lower one (60 cells·cm^{-2}) [269]. Ceramic and metallic substrates are the most common materials used in studies due to the high mechanical stability and the low thermal expansion.

Usually, the catalyst was loaded on the upper section of the reactor and the heat exchanger was located on the bottom. The thermal efficiency was found to be between 20% and 30% for such system [270]. In order to better utilize the heat released from reaction, a two-stage monolith prototype with two heat exchangers was designed. This compact design of premixed burner comprises two honeycombs in between the two heat exchangers on the opposite side, similar model as shown in Fig. 16b [29]. The thermal efficiency for this design could reach 101.1%, implying an effective way to satisfactorily recover the released reaction heat [33]. Fig. 16c shows a monolith and folded wall reactor [35] for the CMC coupled with the steam reforming reaction, the inner pipe for CMC reaction and the annular part for steam reforming

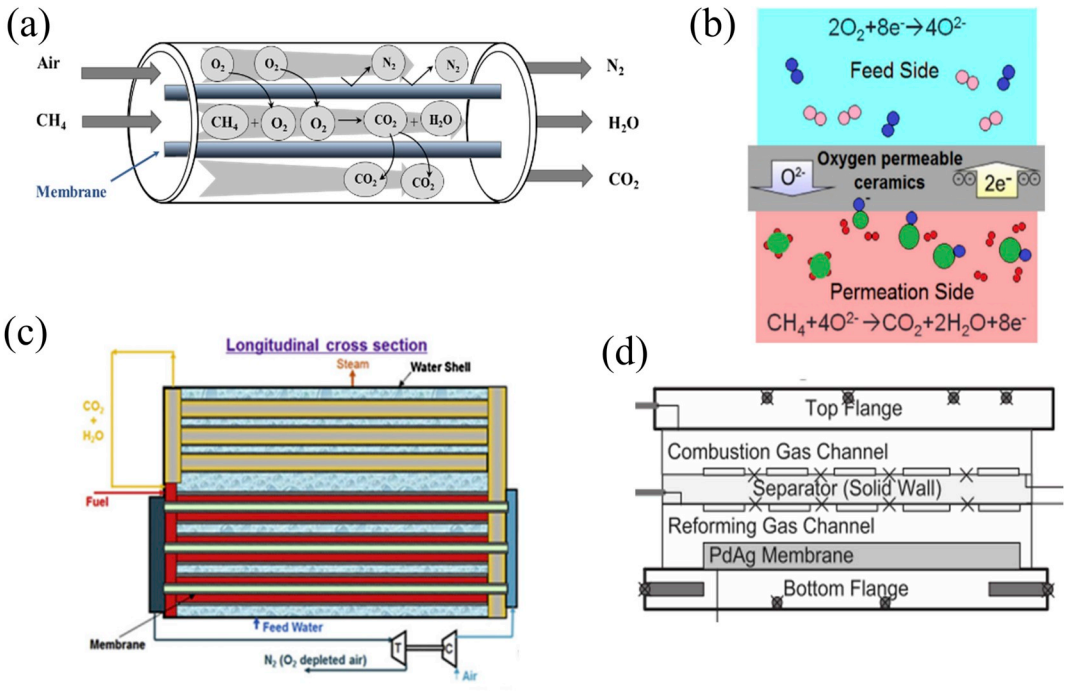

Fig. 17. Membrane reactor for CMC. (a) basic principle; (b) oxygen transport across the membrane [273]; (c) ion transport membrane reactor [274]; (d) multi-channel membrane reactor coupled with steam reforming reaction [275].

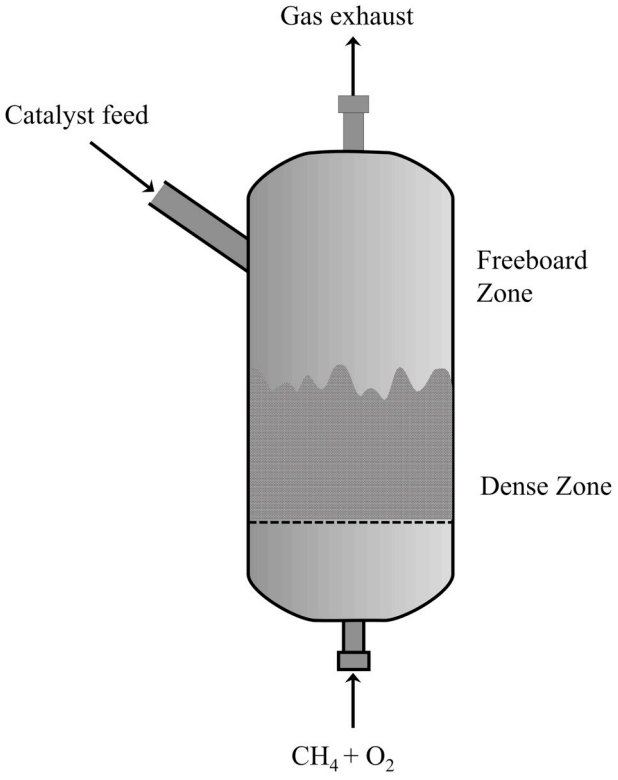

Fig. 18. Fluidized bed reactor for CMC.

reaction (co-flow model). The temperature difference can be managed by adjusting the feed ratio of methane steam reforming to combustion. Furthermore, the heat transfer can be obviously improved by proper channel arrangement or catalyst distribution.

5.3. Membrane reactor

A membrane reactor commonly comprises a membrane coated with catalysts or as a barrier that only allows certain component(s) to pass through. Lanthanum cobaltite perovskite ceramic is one of the most widely used materials for membranes. Other materials with improved properties, such as thin dual-phase membranes, ceramic metal dual-phase membranes and ion transport membranes are also very promising for enhanced oxygen permeation [271]. The increasing motivation for their industrial applications is the reduction of CO_2 emissions from methane combustion.

The basic principle of membrane reactor for CMC is shown in Fig. 17a. CH_4 and air pass through the membrane, and the permeated O_2 reacts with CH_4. CO_2 in the products can be successfully separated and captured. It has been reported that the nitrogen with a purity of 98–99% could be produced and the system remained stable over 120 h [272].The membrane reactor used for CMC could achieve a high methane conversion mainly by varying the partial pressure of oxygen permeation. However, the high costs of membrane reactors potentially limit their industrial applications.

The membrane reaction efficiency is affected by the feed flow rate, the temperature, and the permeability of oxygen. Fig. 17b depicts the oxygen transport over the membrane reactor [273]. The oxygen is firstly adsorbed on the surface of the membrane. The charged oxygen vacancy (O^{2-}) is diffused to the other side, due to the formation of the chemical potential gradient across the membrane. The electrons on the other side are transferred in a reversed-direction so as to compensate for the oxygen vacancies. The results of Falkenstein et al. [273] present that the oxygen permeation flux increased with the increasing methane flow rate and reaction temperature. However, the oxygen permeation flux remained fairly constant at high methane flow rates (e.g. >20 mL min^{-1}), probably due to the limitation of the effective membrane surface area. CO_2 selectivity was thus not significantly varied under higher flow rates in this case. This is in agreement with the results reported by Tan et al. [276], that is, the high methane and air flow rates resulted in a lower oxygen permeation and reaction rate over $La_{0.6}Sr_{0.4}Co_{0.2}Fe_{0.8}O_{3-\alpha}$ hollow fiber membrane reactor. Moreover, the membrane, coated with

platinum catalyst, showed that the membrane reactor effectively facilitated the oxygen permeation and improved the methane conversion, owing to the reduced oxygen permeation resistance [276].

Habib et al. [274] proposed a two-pass ion transport membrane reactor (ITM) for CMC, as shown in Fig. 17c. The first pass is responsible for oxygen permeation, where methane combustion and partial heat exchange between the mixture gas and the water also happened. The second pass is for further permeation. Moreover, the counter-current flow configuration in this ITM provided high methane conversion than that with the co-current flow configuration, owing to the higher oxygen permeation in the first case. In fact, the increased oxygen partial pressure and the accumulated oxygen flux may lead to the reduced oxygen permeation under the co-current flow mode. Moreover, the membrane reactors have also been applied for coupling with steam reforming [277] (Fig. 17d) or ammonia decomposition [278] reactions. An effective way to improve the performance for this system is to increase the membrane effectiveness and to reduce the membrane thickness.

5.4. Fluidized bed reactor

Fluidized bed reactor is a kind of typical catalytic reactors in which solid catalysts (frequently with a diameter of 10–300 μm) are fluidized during the reaction. It is capable of handling a larger amount of reactants or catalysts owing to the large reactor size, and the feed flow rate is required to suspend the catalysts. A porous plate as gas distributor is responsible for supporting the material in the fluidized bed, as shown in Fig. 18. The high gas flow results in an efficient contact between the reactants and the catalysts, leading to the enhanced heat and mass transfer rates on the catalyst surfaces. As a result, the non-uniform temperature distribution that commonly exists in fixed-bed reactor could be avoided. One of its main disadvantages is the great mass loss of the catalyst due to the in-bed attrition after long-term operation.

The experiment measurement by Yang et al. [279] illustrated that the methane conversion increased with the increasing temperature in the fluidized bed reactor, and decreased with the increasing methane inlet concentration. The methane conversion was also reported to decrease with the increasing gas velocity [228]. The fluctuation of temperature and the variation of mixture concentration may occur, due to the intensive motion of solid particles rising up and falling back [280]. Meanwhile, the enhanced mass and heat transfer can be realized between the reactants and the catalyst particles, due to the strong oscillations in the fluidized bed. Furthermore, the kinetic experiments conducted by Yang et al. [279] in the fluidized bed confirmed that the reaction was only controlled by the kinetics at a bed temperature below 450 °C, and by the mass transfer and kinetics together at temperatures above. Dubinina et al. [281] reported $CuO/Al_2O_3MgO–Cr_2O_3$ catalyst to be the one of the most promising catalysts in the fluidized bed reactor for CMC.

6. Summary and prospect

This work provides an extensive review on the CMC. Different catalysts, mechanisms, effect of operational parameters and reactor types are discussed. The main conclusions may be summarized as follows.

- Noble metal catalysts with high activity are favorable for CMC at low temperatures (<700 °C). The bi-metallic catalysts have a better catalytic activity due to the more active sites and electronic synergy effects. The hexaaluminate and perovskite mixed metal-oxide catalysts with different microstructured features exhibit a high thermal stability, thus more suitable for high temperature applications (700–1300 °C).
- The Mars-van Krevelen mechanism is more widely accepted than the Langmuir-Hinselwood and Eley-Rideal mechanisms. It has been observed by in-situ (spectroscopic) technologies that the adsorbed oxygen species in PdO catalyst are responsible for the methane oxidation, rather than oxygen in gas phase.
- The light-off temperature is mainly influenced by the operating temperature and the oxygen to methane molar ratio. It varies depending on different catalyst properties. The optimized O_2/CH_4 molar ratio is beneficial for a full methane conversion due to the optimized coverage of the adsorbed mixtures over the surface.
- The natural gas containing the sulfur compound, carbon dioxide and water vapor can suppress the catalytic activity due to the competitive adsorption and the blockage of active sites. The deactivation due to water and carbon dioxide is reversible whereas the sulfur poisoning is irreversible.
- The reversal flow mode for fixed-bed reactors with hot gas withdrawal at the end of the bed and without the return of cold gas is highly recommended in order to maximize the heat recovery and methane conversion.
- The recent development of mini/microstructured reactor with compact design has been broadly investigated for coupling the CMC with endothermic reaction (methane steam reforming) at different flow modes. The co-current flow mode presents a better thermal efficiency than the counter-current flow one.

Some scientific and technological barriers remain to be overcome for the widespread industrial application of CMC, which are also the key issues and challenges of the current research and development:

- To improve the thermal stability and to prolong the lifetime of noble metal catalysts by avoiding the possible sintering at high temperature levels.
- To improve the current understanding into CMC reaction mechanisms and the corresponding kinetic models, including the deactivation mechanism (e.g. CMC with the presence of water and sulfides etc.).
- To lower the light-off temperature and to maintain the long-term high catalytic activity of hexaaluminate and perovskite catalysts.
- To develop effective desulfurization pre-treatment and measures in order to extend the catalyst lifetime.
- To improve mechanical and chemical stabilities of the catalyst coating, and to cope with the deactivation issue by proposing replacement and/or regeneration methods.
- To further enhance the heat and mass transfer in compact and integrated catalytic reactor-heat exchangers.

Declaration of competing interest

None.

Acknowledgement

This work was supported by the Region Pays de la Loire (Chaire Connect Talent ODE) from French side; and the Ubbo-Emmius Fund 2015 from University of Groningen and the start-up package in the area of green chemistry and technology (for Jun Yue) from the Netherlands' side. For their permission to reproduce the figures, we thank the ACS (Figs. 4a and 6), John Wiley and Sons (Figs. 4b and 15c) and Elsevier (Figs. 4c, 5f and 5g, h, 7 and 11 and 12a and b, 13b and c, Figs. 13d, 14a and 14b, 15b, 15c and 15d, 16b and 16c, 17b and 17c, d).

References

[1] Karavalakis G, Durbin TD, Villela M, Miller JW. Air pollutant emissions of light-duty vehicles operating on various natural gas compositions. J Nat Gas Sci Eng 2012;4:8–16.
[2] U.S. Energy Information Administration. International energy outlook. https://www.eia.gov/todayinenergy/detail.php?id=32912. [Accessed 22 September 2014].

[3] Durand B. Petroleum, natural gas and coal: nature, formation mechanisms, future prospects in the energy transition. EDP Sciences 2019:101–52.
[4] Centre for Energy Economics Research and Policy. UK. BP Statistical review of world energy. https://www.bp.com/en/global/corporate/energy-economics/statistical-review-of-world-energy. [Accessed 19 April 2019].
[5] Zou C, Zhao Q, Zhang G, Xiong B. Energy revolution: from a fossil energy era to a new energy era. Nat Gas Ind B 2016;3(1):1–11.
[6] Petrov AW, Ferri D, Krumeich F, Nachtegaal M, van Bokhoven JA, et al. Stable complete methane oxidation over palladium based zeolite catalysts. Nat Commun 2018;9(1):2545–53.
[7] Mehrpooya M, Khalili M, Sharifzadeh MMM. Model development and energy and exergy analysis of the biomass gasification process (Based on the various biomass sources). Renew Sustain Energy Rev 2018;91:869–87.
[8] Ahmad F, Silva EL, Varesche MBA. Hydrothermal processing of biomass for anaerobic digestion-A review. Renew Sustain Energy Rev 2018;98:108–24.
[9] Naik SN, Goud VV, Rout PK, Dalai AK. Production of first and second generation biofuels: a comprehensive review. Renew Sustain Energy Rev 2010;14(2):578–97.
[10] Li H, Larsson E, Thorin E, Dahlquist E, Yu X. Feasibility study on combining anaerobic digestion and biomass gasification to increase the production of biomethane. Energy Convers Manag 2015;100:212–9.
[11] Sansaniwal S, Rosen M, Tyagi S. Global challenges in the sustainable development of biomass gasification: an overview. Renew Sustain Energy Rev 2017;80:23–43.
[12] Zwart R, Boerrigter H, Deurwaarder E, Van der Meijden C, Van Paasen S. Production of synthetic natural gas (SNG) from biomass. http://www.ecn.nl/docs/library/report/2006/e06018.pdf. [Accessed 3 June 2013].
[13] Vitasari CR, Jurascik M, Ptasinski KJ. Exergy analysis of biomass-to-synthetic natural gas (SNG) process via indirect gasification of various biomass feedstock. Energy 2011;36(6):3825–37.
[14] Ricciardolo FL, Sterk PJ, Gaston B, Folkerts G. Nitric oxide in health and disease of the respiratory system. Physiol Rev 2004;84(3):731–65.
[15] Najjar YS. Gaseous pollutants formation and their harmful effects on health and environment. Innov Energy Policies 2011;1:1–9.
[16] Official Journal of the European Union. Commission regulation (EU) No. 813/2013. http://data.europa.eu/eli/reg/2013/813/oj. [Accessed 2 August 2013].
[17] Chen J, Arandiyan H, Gao X, Li J. Recent advances in catalysts for methane combustion. Catal Surv Asia 2015;19(3):140–71.
[18] Gélin P, Primet M. Complete oxidation of methane at low temperature over noble metal based catalysts: a review. Appl Catal, B 2002;39(1):1–37.
[19] Burch R, Loader PK. Investigation of Pt/Al_2O_3 and Pd/Al_2O_3 catalysts for the combustion of methane at low concentrations. Appl Catal, B 1994;5(1):149–64.
[20] Gélin P, Urfels L, Primet M, Tena E. Complete oxidation of methane at low temperature over Pt and Pd catalysts for the abatement of lean-burn natural gas fuelled vehicles emissions: influence of water and sulphur containing compounds. Catal Today 2003;83(1–4):45–57.
[21] Hao H, Liu Z, Zhao F, Li W. Natural gas as vehicle fuel in China: a review. Renew Sustain Energy Rev 2016;62:521–33.
[22] Forzatti P. Status and perspectives of catalytic combustion for gas turbines. Catal Today 2003;83(1–4):3–18.
[23] Lyubovsky M, Smith LL, Castaldi M, Karim H, Nentwick B, et al. Catalytic combustion over platinum group catalysts: fuel-lean versus fuel-rich operation. Catal Today 2003;83(1–4):71–84.
[24] Su S, Yu XA. 25 kWe low concentration methane catalytic combustion gas turbine prototype unit. Energy 2015;79:428–38.
[25] Ismagilov ZR, Shikina NV, Yashnik SA, Zagoruiko AN, Kerzhentsev MA, et al. Technology of methane combustion on granulated catalysts for environmentally friendly gas turbine power plants. Catal Today 2010;155(1–2):35–44.
[26] Sadamori H. Application concepts and evaluation of small-scale catalytic combustors for natural gas. Catal Today 1999;47(1):325–38.
[27] Khidr KI, Eldrainy YA, EL-Kassaby MM. Towards lower gas turbine emissions: flameless distributed combustion. Renew Sustain Energy Rev 2017;67:1237–66.
[28] Gür TM. Comprehensive review of methane conversion in solid oxide fuel cells: prospects for efficient electricity generation from natural gas. Prog Energy Combust Sci 2016;54:1–64.
[29] Vaillant SR, Gastec AS. Catalytic combustion in a domestic natural gas burner. Catal Today 1999;47(1):415–20.
[30] Jugjai S, Rungsimuntuchart N. High efficiency heat-recirculating domestic gas burners. Exp Therm Fluid Sci 2002;26(5):581–92.
[31] Specchia S, Toniato G. Natural gas combustion catalysts for environmental-friendly domestic burners. Catal Today 2009;147:99–106.
[32] Seo YS, Yu SP, Cho SJ, Song KS. The catalytic heat exchanger using catalytic fin tubes. Chem Eng Sci 2003;58(1):43–53.
[33] Du X. Applied studies on methane catalytic combustion development of a natural gas premixed catalytic burner and boiler for household applications [Thesis in chinese]. Sichuan University; 2005.
[34] Rahimpour M, Dehnavi M, Allahgholipour F, Iranshahi D, Jokar S. Assessment and comparison of different catalytic coupling exothermic and endothermic reactions: a review. Appl Energy 2012;99:496–512.
[35] Mei H, Li C, Ji S, Liu H. Modeling of a metal monolith catalytic reactor for methane steam reforming-combustion coupling. Chem Eng Sci 2007;62(16):4294–303.
[36] Chen Y, Xu H, Jin X, Xiong G. Integration of gasoline preforming into autothermal reforming for hydrogen production. Catal Today 2006;116(3):334–40.
[37] Van Sint Annaland M, Scholts HAR, Kuipers JAM, Van Swaaij WPM. A novel reverse flow reactor coupling endothermic and exothermic reactions, part II: sequential reactor configuration for reversible endothermic reactions. Chem Eng Sci 2002;57(5):855–72.
[38] Venkataraman K, Redenius JM, Schmidt LD. Millisecond catalytic wall reactors: dehydrogenation of ethane. Chem Eng Sci 2002;57(13):2335–43.
[39] Zanfir M, Gavriilidis A. Modelling of a catalytic plate reactor for dehydrogenation-combustion coupling. Chem Eng Sci 2001;56(8):2671–83.
[40] Choudhary TV, B S, Choudhary VR. Catalysts for combustion of methane and lower alkanes review. Appl Catal A 2002;234:1–23.
[41] Li Z, Hoflund GB. A review on complete oxidation of methane at low temperatures. J Nat Gas Chem 2003;12(3):153–60.
[42] Quick LM, Kamitomai S. Catalytic combustion reactor design and test results. Catal Today 1995;26(3–4):303–8.
[43] Anxionnaz Z, Cabassud M, Gourdon C, Tochon P. Heat exchanger/reactors (HEX reactors): concepts, technologies: state-of-the-art. Chem Eng Process 2008;47(12):2029–50.
[44] Kolios G, Gritsch A, Morillo A, Tuttlies U, Bernnat J, et al. Heat-integrated reactor concepts for catalytic reforming and automotive exhaust purification. Appl Catal, B 2007;70(1):16–30.
[45] McCarty JG. Kinetics of PdO combustion catalysis. Catal Today 1995;26(3):283–93.
[46] Norrish RGW, Foord SG. The kinetics of the combustion of methane. Proc R Soc London, Ser A 1936;157(892):503–25.
[47] Otto K. Methane oxidation over Pt on gamma-alumina: kinetics and structure sensitivity. Langmuir 1989;5(6):1364–9.
[48] Dagaut P, Boettner JC, Cathonnet M. Methane oxidation: experimental and kinetic modeling study. Combust Sci Technol 1991;77(1–3):127–48.
[49] Kolb G, Hessel V. Micro-structured reactors for gas phase reactions. Chem Eng J 2004;98(1–2):1–38.
[50] Yue J. Multiphase flow processing in microreactors combined with heterogeneous catalysis for efficient and sustainable chemical synthesis. Catal Today 2018;308:3–19.
[51] Lei Y, Chen W, Lei J. Combustion and direct energy conversion inside a micro-combustor. Appl Therm Eng 2016;100:348–55.
[52] Tian M, Wang XD, Zhang T. Hexaaluminates: a review of the structure, synthesis and catalytic performance. 1984-2004 Catal Sci Technol 2016;6(7).
[53] Zhu J, Li H, Zhong L, Xiao P, Xu X, et al. Perovskite oxides: preparation, characterizations, and applications in heterogeneous catalysis. ACS Catal 2014;4(9):2917–40.
[54] Hepbasli A, Kalinci Y. A review of heat pump water heating systems. Renew Sustain Energy Rev 2009;13(6–7):1211–29.
[55] Ibrahim O, Fardoun F, Younes R, Louahlia-Gualous H. Review of water-heating systems: general selection approach based on energy and environmental aspects. Build Environ 2014;72:259–86.
[56] Kopyscinski J, Schildhauer TJ, Biollaz SM. Production of synthetic natural gas (SNG) from coal and dry biomass - a technology review from 1950 to 2009. Fuel 2010;89(8):1763–83.
[57] Ciuparu D, Lyubovsky MR, Altman E, Pfefferle LD, Datye A. Catalytic combustion of methane over palladium-based catalysts. Catal Rev 2002;44(4):593–649.
[58] Cruellas A, Melchiori T, Gallucci F, van Sint Annaland M. Advanced reactor concepts for oxidative coupling of methane. Catal Rev 2017;59(3):234–94.
[59] Yang J, Guo Y. Nanostructured perovskite oxides as promising substitutes of noble metals catalysts for catalytic combustion of methane. Chin Chem Lett 2018;29(2):252–60.
[60] Sidwell RW, Zhu H, Kibler BA, Kee RJ, Wickham DT. Experimental investigation of the activity and thermal stability of hexaaluminate catalysts for lean methane-air combustion. Appl Catal A 2003;255(2):279–88.
[61] Inoue H, Sekizawa K, Eguchi K, Arai H. Thermal stability of hexaaluminate film coated on SiC substrate for high-temperature catalytic application. J Am Ceram Soc 1997;80(3):584–8.
[62] Inoue H, Sekizawa K, Eguchi K, Arai H. Thick-film coating of hexaaluminate catalyst on ceramic substrates for high-temperature combustion. Catal Today 1999;47(1):181–90.
[63] Groppi G, Cristiani C, Forzatti P. $BaFe_xAl_{(12-x)}O_{19}$ system for high-temperature catalytic combustion: physico-chemical characterization and catalytic activity. J Catal 1997;168(1):95–103.
[64] Iyi N, Takekawa S, Kimura S. Crystal chemistry of hexaaluminates: β-alumina and magnetoplumbite structures. J Solid State Chem 1989;83(1):8–19.
[65] Machida M, Eguchi K, Arai H. Catalytic properties of $BaMAl_{11}O_{19-\alpha}$ (M = Cr, Mn, Fe, Co, and Ni) for high-temperature catalytic combustion. J Catal 1989;120(2):377–86.
[66] Artizzu-Duart P, Brullé Y, Gaillard F, Garbowski E, Guilhaume N, et al. Catalytic combustion of methane over copper- and manganese-substituted barium hexaaluminates. Catal Today 1999;54(1):181–90.
[67] Wickham D, Cook R. Thermally stable catalysts for methane combustion. United States patent US 20030176278. 2003. September 18.
[68] Zhang Y, Wang X, Zhu Y, Liu X, Zhang T. Thermal evolution crystal structure and Fe crystallographic sites in $LaFe_xAl_{12-x}O_{19}$ hexaaluminates. J Phys Chem C 2014;118(20):10792–804.
[69] Wang X, Huang K, Ma W, Cong Y, Ge C, et al. Defect engineering, electronic structure, and catalytic properties of perovskite oxide $La_{0.5}Sr_{0.5}CoO_{3-\delta}$. Chem Eur J 2017;23(5):1093–100.
[70] Shen J, Scott RW, Hayes RE, Semagina N. Structural evolution of bimetallic Pd-Ru catalysts in oxidative and reductive applications. Appl Catal A 2015;502:350–60.
[71] Machida M, Eguchi K, Arai H. Effect of additives on the surface area of oxide supports for catalytic combustion. J Catal 1987;103(2):385–93.

[72] Pena M, Fierro J. Chemical structures and performance of perovskite oxides. Chem Rev 2001;101(7). 1981-2018.
[73] Arai H, Yamada T, Eguchi K, Seiyama T. Catalytic combustion of methane over various perovskite-type oxides. Appl Catal, A 1986;26:265–76.
[74] Cimino S, Lisi L, Pirone R, Russo G, Turco M. Methane combustion on perovskites-based structured catalysts. Catal Today 2000;59(1):19–31.
[75] Laassiri S, Bion N, Duprez D, Royer S, Alamdari H. Clear microstructure-performance relationships in Mn-containing perovskite and hexaaluminate compounds prepared by activated reactive synthesis. Phys Chem Chem Phys 2014;16(9):4050–60.
[76] Miniajluk N, Trawczyński J, Zawadzki M, Tylus W. $LaMnO_3$ ($La_{0.8}Sr_{0.2}MnO_3$) perovskites for lean methane combustion: effect of synthesis method. Adv Mater Phys Chem 2018;8(04):193.
[77] Tao FF, J-j Shan, Nguyen L, Wang Z, Zhang S, et al. Understanding complete oxidation of methane on spinel oxides at a molecular level. Nat Commun 2015;6:7798.
[78] Miao F, Wang F, Mao D, Guo X, Yu J, et al. Effect of different reaction conditions on catalytic activity of La(Mn, Fe)$O_{3+\lambda}$ catalyst for methane combustion. Mater Res Express 2019;6(5):055001.
[79] Li J, Fu H, Fu L, Hao J. Complete combustion of methane over indium tin oxides catalysts. Environ Sci Technol 2006;40(20):6455–9.
[80] Polini R, Falsetti A, Traversa E, Schäf O, Knauth P. Sol-gel synthesis, X-ray photoelectron spectroscopy and electrical conductivity of Co-doped (La, Sr)(Ga, Mg)$O_{3-\delta}$ perovskites. J Eur Ceram Soc 2007;27(13–15):4291–6.
[81] Bhalla A, Guo R, Roy R. The perovskite structure-a review of its role in ceramic science and technology. Mater Res Innov 2000;4(1):3–26.
[82] Polo-Garzon F, Wu Z. Acid-base catalysis over perovskites: a review. J Mater Chem A 2018;6(7):2877–94.
[83] Zhu H, Zhang P, Dai S. Recent advances of lanthanum-based perovskite oxides for catalysis. ACS Catal 2015;5(11):6370–85.
[84] Granger P, Parvulescu VI, Kaliaguine S, Prellier W. Perovskites and related mixed oxides: concepts and applications. Wiley; 2015.
[85] Ersson A, Persson K, Adu IK, Järås SG. A comparison between hexaaluminates and perovskites for catalytic combustion applications. Catal Today 2006;112(1–4):157–60.
[86] Hoflund GB, Li Z, Epling WS, Göbel T, Schneider P, et al. Catalytic methane oxidation over Pd supported on nanocrystalline and polycrystalline TiO_2, Mn_3O_4, CeO_2 and ZrO_2. React Kinet Catal Lett 2000;70(1):97–103.
[87] Ersson A, Kušar H, Carroni R, Griffin T, Järås S. Catalytic combustion of methane over bimetallic catalysts a comparison between a novel annular reactor and a high-pressure reactor. Catal Today 2003;83(1–4):265–77.
[88] Bhagiyalakshmi M, Anuradha R, Park SD, Park TS, Cha WS, et al. Effect of bimetallic Pt-Rh and trimetallic Pt-Pd-Rh catalysts for low temperature catalytic combustion of methane. Bull Korean Chem Soc 2010;31(1):120–4.
[89] Kinnunen N, Suvanto M, Moreno M, Savimäki A, Kallinen K, et al. Methane oxidation on alumina supported palladium catalysts: effect of Pd precursor and solvent. Appl Catal A 2009;370(1–2):78–87.
[90] Farrauto RJ, Hobson M, Kennelly T, Waterman E. Catalytic chemistry of supported palladium for combustion of methane. Appl Catal A 1992;81(2):227–37.
[91] Farrauto RJ, Kennelly T, Waterman EM, Hobson Jr MC. Process conditions for operation of ignition catalyst for natural gas combustion. 1993 [Google Patents].
[92] Pecchi G, Reyes P, López T, Gómez R. Pd-CeO_2 and Pd-La_2O_3/alumina-supported catalysts: their effect on the catalytic combustion of methane. J Non-Cryst Solids 2004;345:624–7.
[93] Toso A, Colussi S, Padigapaty S, de Leitenburg C, Trovarelli A. High stability and activity of solution combustion synthesized Pd-based catalysts for methane combustion in presence of water. Appl Catal, B 2018;230:237–45.
[94] Drozdov VA, Tsyrulnikov PG, Popovskii VV, Bulgakov NN, Moroz EM, et al. Comparative study of the activity of Al-Pd and Al-Pt catalysts in deep oxidation of hydrocarbons. React Kinet Catal Lett 1985;27(2):425–7.
[95] Euzen P, Le Gal J-H, Rebours B, Martin G. Deactivation of palladium catalyst in catalytic combustion of methane. Catal Today 1999;47(1–4):19–27.
[96] Hicks RF, Qi H, Young ML, Lee RG. Structure sensitivity of methane oxidation over platinum and palladium. J Catal 1990;122(2):280–94.
[97] Persson K, Ersson A, Jansson K, Iverlund N, Jaras S. Influence of co-metals on bimetallic palladium catalysts for methane combustion. J Catal 2005;231(1):139–50.
[98] Persson K, Ersson A, Jansson K, Fierro J, Järås SG. Influence of molar ratio on Pd-Pt catalysts for methane combustion. J Catal 2006;243(1):14–24.
[99] Kinnunen NM, Hirvi JT, Suvanto M, Pakkanen TA. Methane combustion activity of Pd-PdOx-Pt/Al2O3 catalyst: the role of platinum promoter. J Mol Catal A Chem 2012;356:20–8.
[100] Stefanov P, Todorova S, Naydenov A, Tzaneva B, Kolev H, et al. On the development of active and stable Pd-Co/γ-Al_2O_3 catalyst for complete oxidation of methane. Chem Eng J 2015;266:329–38.
[101] Zhang S, Kang P, Bakir M, Lapides AM, Dares CJ, et al. Polymer-supported CuPd nanoalloy as a synergistic catalyst for electrocatalytic reduction of carbon dioxide to methane. Proc Natl Acad Sci U S A 2015;112(52):15809–14.
[102] Persson K, Jansson K, Jaras S. Characterisation and microstructure of Pd and bimetallic Pd-Pt catalysts during methane oxidation. J Catal 2007;245(2):401–14.
[103] Persson K, Ersson A, Carrera AM, Jayasuriya J, Fakhrai R, et al. Supported palladium-platinum catalyst for methane combustion at high pressure. Catal Today 2005;100(3–4):479–83.
[104] Briot P, Auroux A, Jones D, Primet M. Effect of particle size on the reactivity of oxygen-adsorbed platinum supported on alumina. Appl Catal 1990;59(1):141–52.
[105] Marceau E, Che M, Saint-Just J, Tatibouët JM. Influence of chlorine ions in Pt/Al_2O_3 catalysts for methane total oxidation. Catal Today 1996;29(1):415–9.
[106] Gremminger AT, Pereira de Carvalho HW, Popescu R, Grunwaldt JD, Deutschmann O. Influence of gas composition on activity and durability of bimetallic Pd-Pt/Al2O3 catalysts for total oxidation of methane. Catal Today 2015;258:470–80.
[107] Hajar Y, Venkatesh B, Baranova E. Electrochemical promotion of nanostructured palladium catalyst for complete methane oxidation. Catalysts 2019;9(1):48.
[108] Hajar YM, Venkatesh B, Houache MS, Liu H, Safari R, et al. Electrochemical promotion of Bi-metallic Ni9Pd core double-shell nanoparticles for complete methane oxidation. J Catal 2019;374:127–35.
[109] Li K, Xu D, Liu K, Ni H, Shen F, et al. Catalytic combustion of lean methane assisted by an electric field over Mn_xCo_y catalysts at low temperature. J Phys Chem C 2019;123(16):10377–88.
[110] Li K, Liu K, Ni H, Guan B, Zhan R, et al. Electric field promoted ultra-lean methane oxidation over Pd-Ce-Zr catalysts at low temperature. Mol Catal 2018;459:78–88.
[111] Liu K, Li K, Xu D, Lin H, Guan B, et al. Catalytic combustion of lean methane assisted by electric field over Pd/Co_3O_4 catalysts at low temperature. J Shanghai Jiaot Univ 2018;23(1):8–17.
[112] Adamowska M, Da Costa P. Structured Pd/γ-Al_2O_3 prepared by washcoated deposition on a ceramic honeycomb for compressed natural gas applications. J Nanopart 2015;2015:1–9.
[113] Li Y, Luo C, Liu Z, Sang L. Catalytic oxidation characteristics of CH_4-air mixtures over metal foam monoliths. Appl Energy 2015;156:756–61.
[114] Cebollada PAR, Garcia Bordejé E. Optimisation of physical properties of γ-alumina coating microreactors used for the growth of a carbon nanofiber layer. Chem Eng J 2009;149(1–3):447–54.
[115] Bravo J, Karim A, Conant T, Lopez GP, Datye A. Wall coating of a CuO/ZnO/Al_2O_3 methanol steam reforming catalyst for micro-channel reformers. Chem Eng J 2004;101(1–3):113–21.
[116] Deutschmann O, Maier LI, Riedel U, Stroemman AH, Dibble RW. Hydrogen assisted catalytic combustion of methane on platinum. Catal Today 2000;59(1):141–50.
[117] Yang H, Li J, Yu H, Peng F, Wang H. Metal-foam-supported Pd/Al_2O_3 catalysts for catalytic combustion of methane: effect of interaction between support and catalyst. Int J Chem React Eng 2015;13(1).
[118] O'Connell M, Kolb G, Zapf R, Men Y, Hessel V. Bimetallic catalysts for the catalytic combustion of methane using microreactor technology. Catal Today 2009;144(3–4):306–11.
[119] Mundhwa M, Parmar RD, Thurgood CP. A comparative parametric study of a catalytic plate methane reformer coated with segmented and continuous layers of combustion catalyst for hydrogen production. J Power Sources 2017;344:85–102.
[120] He L, Fan Y, Luo L, Bellettre J, Yue J. Preparation of Pt/γ-Al_2O_3 catalyst coating in microreactors for catalytic methane combustion. Chem Eng J 2020;380:122424.
[121] Ismagilov ZR, Pushkarev VV, Podyacheva OY, Koryabkina NA, Veringa H. A catalytic heat-exchanging tubular reactor for combining of high temperature exothermic and endothermic reactions. Chem Eng J 2001;82(1):355–60.
[122] Meille V. Review on methods to deposit catalysts on structured surfaces. Appl Catal A 2006;315:1–17.
[123] Zapf R, Becker-Willinger C, Berresheim K, Bolz H, Gnaser H, et al. Detailed characterization of various porous alumina-based catalyst coatings within microchannels and their testing for methanol steam reforming. Chem Eng Res Des 2003;81(7):721–9.
[124] Peela NR, Mubayi A, Kunzru D. Washcoating of γ-alumina on stainless steel microchannels. Catal Today 2009;147:S17–23.
[125] Liauw M, Baerns M, Broucek R, Buyevskaya O, Commenge J, et al. Periodic operation in microchannel reactors: Springer. 2000. p. 224–34.
[126] Xu X, Vonk H, Cybulski A, Moulijn JA. In: Alumina washcoating and metal deposition of ceramic monoliths. Elsevier; 1995. p. 1069–78.
[127] Haas-Santo K, Fichtner M, Schubert K. Preparation of microstructure compatible porous supports by sol-gel synthesis for catalyst coatings. Appl Catal A 2001;220(1):79–92.
[128] Karches M, Morstein M, Rudolf von Rohr P, Pozzo RL, Giombi JL, et al. Plasma-CVD-coated glass beads as photocatalyst for water decontamination. Catal Today 2002;72(3):267–79.
[129] Aaltonen T, Ritala M, Sajavaara T, Keinonen J, Leskelä M. Atomic layer deposition of platinum thin films. Chem Mater 2003;15(9):1924–8.
[130] Pranevicius LL, Valatkevicius P, Valincius V, Montassier C. Catalytic behavior of plasma-sprayed Al-Al_2O_3 coatings doped with metal oxides. Surf Coat Technol 2000;125(1):392–5.
[131] Pranevicius L, Pranevicius LL, Valatkevicius P, Valincius V. Plasma spray deposition of Al-Al_2O_3 coatings doped with metal oxides: catalytic applications. Surf Coat Technol 2000;123(2):122–8.
[132] Zapf R, Kolb G, Pennemann H, Hessel V. Basic study of adhesion of several alumina-based washcoats deposited on stainless steel microchannels. Chem Eng Technol 2006;29(12):1509–12.
[133] Behrendt F, Deutschmann O, Schmidt R, Warnatz JACS. Symposium series. In: Ignition and extinction of hydrogen-air and methane-air mixtures over platinum and palladium. American Chemical Society; 1996. p. 48–57.
[134] Valden M, Pere J, Xiang N, Pessa M. Influence of preadsorbed oxygen on activated chemisorption of methane on Pd(110). Chem Phys Lett 1996;257(3):289–96.
[135] Xu J, Ouyang L, Mao W, Yang XJ, Xu XC, et al. Operando and kinetic study of low-temperature, lean-burn methane combustion over a Pd/γ-Al_2O_3 catalyst. ACS Catal 2012;2(2):261–9.
[136] Yao Y, Yu F. Oxidation of alkanes over noble metal catalysts. Ind Eng Chem Prod Res Dev 1980;19(3):293–8.

[137] Duprat F. Light-off curve of catalytic reaction and kinetics. Chem Eng Sci 2002;57(6):901–11.
[138] Qi W, Ran J, Wang R, Du X, Shi J, et al. Kinetic consequences of methane combustion on Pd, Pt and Pd-Pt catalysts. RSC Adv 2016;6(111):109834–45.
[139] Chin YH, Iglesia E. Elementary steps, the role of chemisorbed oxygen, and the effects of cluster size in catalytic CH_4-O_2 reactions on palladium. J Phys Chem C 2011;115(36):17845–55.
[140] Ma L, Trimm DL, Jiang C. The design and testing of an autothermal reactor for the conversion of light hydrocarbons to hydrogen I. The kinetics of the catalytic oxidation of light hydrocarbons. Appl Catal A 1996;138(2):275–83.
[141] Trimm D, Lam C-W. The combustion of methane on platinum-alumina fibre catalysts-II design and testing of a convective-diffusive type catalytic combustor. Chem Eng Sci 1980;35(8):1731–9.
[142] Gosiewski K, Pawlaczyk A, Warmuzinski K, Jaschik M. A study on thermal combustion of lean methane-air mixtures: simplified reaction mechanism and kinetic equations. Chem Eng J 2009;154(1–3):9–16.
[143] Pawlaczyk A, Gosiewski K. Combustion of lean methane-air mixtures in monolith beds: kinetic studies in low and high temperatures. Chem Eng J 2015;282:29–36.
[144] Tsang W, Hampson R. Chemical kinetic data base for combustion chemistry. Part I. Methane and related compounds. J Phys Chem Ref Data 1986;15(3):1087–279.
[145] Ranzi E, Sogaro A, Gaffuri P, Pennati G, Faravelli T. A wide range modeling study of methane oxidation. Combust Sci Technol 1994;96(4–6):279–325.
[146] Burcat A, Gardiner WCJ, Dixon-Lewis G, Frenklach M, Hanson RK, et al. Combustion chemistry. Springer Nov 7, 1984:197–258. https://doi.org/10.1007/978-1-4684-0188-2. New York.
[147] Oh S, Mitchell P, Siewert R. In: Methane oxidation over noble metal catalysts as related to controlling natural gas vehicle exhaust emissions. Washington, DC: ACS Publication; 1992.
[148] McCabe RW, McCready DF. Formaldehyde oxidation on Pt: kinetic evidence for adsorbed carbon monoxide intermediate. Chem Phys Lett 1984;111(1):89–93.
[149] Lapinski MP, Silver RG, Ekerdt JG, McCabe RW. Formaldehyde oxidation on silica-supported platinum: spectroscopic evidence for adsorbed carbon monoxide intermediate. J Catal 1987;105(1):258–62.
[150] Deutschmann O, Schmidt R, Behrendt F, Warnat J. Numerical modeling of catalytic ignition. Symp (Int) Combust 1996;26(1):1747–54.
[151] Engel T, Ertl G. Elementary steps in the catalytic oxidation of carbon monoxide on platinum metals. Adv Catal 1979;28:1–78.
[152] Frennet A. Chemisorption and exchange with deuterium of methane on metals. Catal Rev Sci Eng 1974;10(1):37–68.
[153] Bond TG, Noguchi BA, Chou C-P, Mongia RK, Chen J-Y, et al. Catalytic oxidation of natural gas over supported platinum: flow reactor experiments and detailed numerical modeling. In: Symposium (international) on combustion, vol. 26. Elsevier; 1996. p. 1771–8.
[154] Firth J, Holland H. Catalytic oxidation of methane over noble metals. Trans Faraday Soc 1969;65:1121–7.
[155] Ahuja OP, Mathur G. Kinetics of catalytic oxidation of methane: application of initial rate technique for mechanism determination. Can J Chem Eng 1967;45(6):367–71.
[156] Groppi G. Combustion of CH_4 over a PdO/ZrO_2 catalyst: an example of kinetic study under severe conditions. Catal Today 2003;77(4):335–46.
[157] Seimanides S, Stoukides M. Catalytic oxidation of methane on polycrystalline palladium supported on stabilized zirconia. J Catal 1986;98(2):540–9.
[158] Garbowski E, Feumi-Jantou C, Mouaddib N, Primet M. Catalytic combustion of methane over palladium supported on alumina catalysts: evidence for reconstruction of particles. Appl Catal A 1994;109(2):277–91.
[159] Müller CA, Maciejewski M, Koeppel RA, Baiker A. Combustion of methane over palladium/zirconia: effect of Pd-particle size and role of lattice oxygen. Catal Today 1999;47(1–4):245–52.
[160] Ciuparu D, Altman E, Pfefferle L. Contributions of lattice oxygen in methane combustion over PdO-Based catalysts. J Catal 2001;203(1):64–74.
[161] Müller CA, Maciejewski M, Koeppel RA, Tschan R, Baiker A. Role of lattice oxygen in the combustion of methane over PdO/ZrO2: combined pulse TG/DTA and MS study with 18O-labeled catalyst. J Phys Chem 1996;100(51):20006–14.
[162] Trimm DL, Lam C-W. The combustion of methane on platinum-alumina fibre catalysts-I: kinetics and mechanism. Chem Eng Sci 1980;35(6):1405–13.
[163] Jodłowski PJ, Jędrzejczyk RJ, Chlebda D, Gierada M, Łojewska J. In situ spectroscopic studies of methane catalytic combustion over Co, Ce, and Pd mixed oxides deposited on a steel surface. J Catal 2017;350:1–12.
[164] Veldsink J, Versteeg G, van Swaaij WPM. Intrinsic kinetics of the oxidation of methane over an industrial copper (II) oxide catalyst on a γ-alumina support. Chem Eng J Biochem Eng J 1995;57(3):273–83.
[165] Hurtado P, Ordóñez S, Sastre H, Dıez FV. Development of a kinetic model for the oxidation of methane over Pd/Al_2O_3 at dry and wet conditions. Appl Catal, B 2004;51(4):229–38.
[166] Jørgensen M. Grönbeck H. First-principles microkinetic modeling of methane oxidation over Pd (100) and Pd (111). ACS Catal 2016;6(10):6730–8.
[167] Au-Yeung J, Chen K, Bell AT, Iglesia E. Isotopic studies of methane oxidation pathways on PdO catalysts. J Catal 1999;188(1):132–9.
[168] Lyubovsky M, Pfefferle L. Methane combustion over the α-alumina supported Pd catalyst: activity of the mixed Pd/PdO state. Appl Catal A 1998;173(1):107–19.
[169] Datye AK, Bravo J, Nelson TR, Atanasova P, Lyubovsky M, et al. Catalyst microstructure and methane oxidation reactivity during the Pd↔ PdO transformation on alumina supports. Appl Catal A 2000;198(1–2):179–96.
[170] Demoulin O, Navez M, Ruiz P. Investigation of the behaviour of a Pd/γ-Al2O3 catalyst during methane combustion reaction using in situ DRIFT spectroscopy. Appl Catal A 2005;295(1):59–70.
[171] Oh SH, Mitchell PJ, Siewert RM. Methane oxidation over alumina-supported noble metal catalysts with and without cerium additives. J Catal 1991;132(2):287–301.
[172] MVd Bossche, Gronbeck H. Methane oxidation over PdO (101) revealed by first-principles kinetic modeling. J Am Chem Soc 2015;137(37):12035–44.
[173] Aghalayam P, Park YK, Fernandes N, Papavassiliou V, Mhadeshwar AB, et al. A C1 mechanism for methane oxidation on platinum. J Catal 2003;213(1):23–38.
[174] Chrzan M, Chlebda D, Jodłowski P, Salomon E, Kołodziej A, et al. Towards methane combustion mechanism on metal oxides supported catalysts: ceria supported palladium catalysts. Top Catal 2019;62(1–4):403–12.
[175] Feng S, Yang W, Wang Z. Synthesis of porous $NiFe_2O_4$ microparticles and its catalytic properties for methane combustion. Mater Sci Eng, B 2011;176(18):1509–12.
[176] Milt VG, Ulla MA, Lombardo EA. Cobalt-containing catalysts for the high-temperature combustion of methane. Catal Lett 2000;65(1):67–73.
[177] Okal J, Zawadzki M, Baranowska K. Methane combustion over bimetallic Ru-Re/γ-Al_2O_3 catalysts: effect of Re and pretreatments. Appl Catal, B 2016;194:22–31.
[178] Iamarino M, Chirone R, Lisi L, Pirone R, Salatino P, et al. Cu/γ-Al_2O_3 catalyst for the combustion of methane in a fluidized bed reactor. Catal Today 2002;75(1):317–24.
[179] Wang Z, Deng J, Liu Y, Yang H, Xie S, et al. Three-dimensionally ordered macroporous $CoCr_2O_4$-supported Au-Pd alloy nanoparticles: highly active catalysts for methane combustion. Catal Today 2017;281(Part 3):467–76.
[180] Cimino S, Pirone R, Lisi L. Zirconia supported $LaMnO_3$ monoliths for the catalytic combustion of methane. Appl Catal, B 2002;35(4):243–54.
[181] Comino G, Gervasini A, Ragaini V, Ismagilov ZR. Methane combustion over copper chromite catalysts. Catal Lett 1997;48(1):39–46.
[182] Chorkendorff I, Niemantsverdriet JW, Niemantsverdriet JW, Niemantsverdriet JW. Kinetics. Concepts of modern catalysis and kinetics. 3rd. Wiley Online Library; 2003. p. 23–77.
[183] Geus JW, van Giezen JC. Monoliths in catalytic oxidation. Catal Today 1999;47(1):169–80.
[184] Shi C, Yang L, Cai J. Cerium promoted Pd/HZSM-5 catalyst for methane combustion. Fuel 2007;86(1–2):106–12.
[185] Barbosa AL, Herguido J, Santamaria J. Methane combustion over unsupported iron oxide catalysts. Catal Today 2001;64(1):43–50.
[186] Lee JH, Trimm DL. Catalytic combustion of methane. Fuel Process Technol 1995;42(2):339–59.
[187] Seo YS, Kang SK, Han MH, Baek YS. Development of a catalytic burner with Pd/NiO catalysts. Catal Today 1999;47(1):421–7.
[188] Anna Poskart M. The control of NO_x concentration in natural gas combustion process. CHEMIK 2013;67(10):848–55.
[189] Farrauto RJ, Lampert JK, Hobson MC, Waterman EM. Thermal decomposition and reformation of PdO catalysts; support effects. Appl Catal, B 1995;6(3):263–70.
[190] Schwartz WR, Ciuparu D, Pfefferle LD. Combustion of methane over palladium-based catalysts: catalytic deactivation and role of the support. J Phys Chem C 2012;116(15):8587–93.
[191] Fleys M, Simon Y, Swierczynski D, Kiennemann A, Marquaire PM. Investigation of the reaction of partial oxidation of methane over Ni/La_2O_3 catalyst. Energy Fuels 2006;20(6):2321–9.
[192] Halabi M, De Croon M, Van Der Schaaf J, Cobden P, Schouten J. Intrinsic kinetics of low temperature catalytic methane-steam reforming and water-gas shift over Rh/$Ce_\alpha Zr_{1-\alpha}O_2$ catalyst. Appl Catal A 2010;389(1–2):80–91.
[193] Mouaddib N, Feumi-Jantou C, Garbowski E, Primet M. Catalytic oxidation of methane over palladium supported on alumina: influence of the oxygen-to-methane ratio. Appl Catal A 1992;87(1):129–44.
[194] Drozdov V, Tsyrulnikov P, Popovskii V, Bulgakov N, Moroz E, et al. Comparative study of the activity of Al-Pd and Al-Pt catalysts in deep oxidation of hydrocarbons. React Kinet Catal Lett 1985;27(2):425–7.
[195] Yao Y-FY. Oxidation of alkanes over noble metal catalysts. Ind Eng Chem Prod Res Dev 1980;19(3):293–8.
[196] Murru M, Gavriilidis A. Catalytic combustion of methane in non-permselective membrane reactors with separate reactant feeds. Chem Eng J 2004;100(1–3):23–32.
[197] Liu W, Xu Y, Tian Z, Xu Z. A thermodynamic analysis on the catalytic combustion of methane. J Nat Gas Chem 2003;12(4):237–42.
[198] Urfels L, Gélin P, Primet M, Tena E. Complete oxidation of methane at low temperature over Pt catalysts supported on high surface area SnO_2. Top Catal 2004;30(1–4):427–32.
[199] Yang Z, Liu J, Zhang L, Zheng S, Guo M, et al. Catalytic combustion of low-concentration coal bed methane over CuO/γ-Al_2O_3 catalyst: effect of SO2. RSC Adv 2014;4(74):39394–9.
[200] Mowery DL, McCormick RL. Deactivation of alumina supported and unsupported PdO methane oxidation catalyst: the effect of water on sulfate poisoning. Appl Catal, B 2001;34(4):287–97.
[201] Wu Z, Deng J, Liu Y, Xie S, Jiang Y, et al. Three-dimensionally ordered mesoporous Co_3O_4-supported Au-Pd alloy nanoparticles: high-performance catalysts for methane combustion. J Catal 2015;332:13–24.
[202] Dixon-Lewis G, Williams D. The oxidation of hydrogen and carbon monoxide. Comprehensive chemical kinetics, 17. Elsevier; 1977. p. 1–248.
[203] Geng H, Yang Z, Zhang L, Ran J, Chen Y. Experimental and kinetic study of methane combustion with water over copper catalyst at low-temperature. Energy Convers Manag 2015;103:244–50.
[204] Ciuparu D, Katsikis N, Pfefferle L. Temperature and time dependence of the water inhibition effect on supported palladium catalyst for methane combustion. Appl Catal A 2001;216(1–2):209–15.

[205] Sadokhina N, Smedler G, Nylén U, Olofsson M, Olsson L. The influence of gas composition on Pd-based catalyst activity in methane oxidation-inhibition and promotion by NO. Appl Catal, B 2017;200:351–60.
[206] Hayashi S, Yamada H, Shimodaira K. High-pressure reaction and emissions characteristics of catalytic reactors for gas turbine combustors. Catal Today 1995; 26(3–4):319–27.
[207] Di Benedetto A, Landi G, Di Sarli V, Barbato PS, Pirone R, et al. Methane catalytic combustion under pressure. Catal Today 2012;197(1):206–13.
[208] Carroni R, Griffin T, Mantzaras J, Reinke M. High-pressure experiments and modeling of methane/air catalytic combustion for power-generation applications. Catal Today 2003;83(1–4):157–70.
[209] Zarur AJ, Ying JY. Reverse microemulsion synthesis of nanostructured complex oxides for catalytic combustion. Nature 2000;403(6765):65.
[210] Li S, Wang X. The Ba-hexaaluminate doped with CeO_2 nanoparticles for catalytic combustion of methane. Catal Commun 2007;8(3):410–5.
[211] Civera A, Negro G, Specchia S, Saracco G, Specchia V. Optimal compositional and structural design of a $LaMnO_3/ZrO_2$/Pd-based catalyst for methane combustion. Catal Today 2005;100(3–4):275–81.
[212] Zhang L, Zhang Y, Dai H, Deng J, Wei L, et al. Hydrothermal synthesis and catalytic performance of single-crystalline $La_{2-x}Sr_xCuO_4$ for methane oxidation. Catal Today 2010;153(3–4):143–9.
[213] Gallucci K, Villa P, Groppi G, Usberti N, Marra G. Catalytic combustion of methane on $BaZr_{(1-x)}Me_xO_3$ perovskites synthesised by a modified citrate method. Catal Today 2012;197(1):236–42.
[214] Hu J, Zhao W, Hu R, Chang G, Li C, et al. Catalytic activity of spinel oxides $MgCr_2O_4$ and $CoCr_2O_4$ for methane combustion. Mater Res Bull 2014;57:268–73.
[215] Wang Y, Arandiyan H, Scott J, Akia M, Dai H, et al. High performance Au-Pd supported on 3D hybrid strontium-substituted lanthanum manganite perovskite catalyst for methane combustion. ACS Catal 2016;6(10):6935–47.
[216] Zaza F, Luisetto I, Serra E, Tuti S, Pasquali M. Catalytic combustion of methane by perovskite-type oxide nanoparticles as pollution prevention strategy. In: AIP conf proc. AIP Publishing; 2016.
[217] Fan X, Li L, Jing F, Li J, Chu W. Effects of preparation methods on $CoAlO_x/CeO_2$ catalysts for methane catalytic combustion. Fuel 2018;225:588–95.
[218] Li X, Liu Y, Deng J, Zhang Y, Xie S, et al. 3DOM LaMnAl11O19-supported AuPd alloy nanoparticles: highly active catalysts for methane combustion in a continuous-flow microreactor. Catal Today 2018;308:71–80.
[219] Li D, Li K, Xu R, Wang H, Tian D, et al. $Ce_{1-x}Fe_xO_{2-\delta}$ catalysts for catalytic methane combustion: role of oxygen vacancy and structural dependence. Catal Today 2018;318:73–85.
[220] Li Y, Armor JN. Catalytic combustion of methane over palladium exchanged zeolites. Appl Catal, B 1994;3(4):275–82.
[221] Kucharczyk B, Tylus W, Kpiński L. Pd-based monolithic catalysts on metal supports for catalytic combustion of methane. Appl Catal, B 2004;49(1):27–37.
[222] Xiao LH, Sun KP, Xu XL, Li XN. Low-temperature catalytic combustion of methane over Pd/CeO_2 prepared by deposition–precipitation method. Catal Commun 2005;6(12):796–801.
[223] Choudhary V, Patil V, Jana P, Uphade B. Nano-gold supported on Fe_2O_3: a highly active catalyst for low temperature oxidative destruction of methane green house gas from exhaust/waste gases. Appl Catal A 2008;350(2):186–90.
[224] Li J, Liang X, Xu S, Hao J. Catalytic performance of manganese cobalt oxides on methane combustion at low temperature. Appl Catal, B 2009;90(1–2):307–12.
[225] Venezia A, Di Carlo G, Pantaleo G, Liotta L, Melaet G, et al. Oxidation of CH_4 over Pd supported on TiO_2-doped SiO_2: effect of Ti(IV) loading and influence of SO_2. Appl Catal, B 2009;88(3–4):430–7.
[226] Specchia S, Palmisano P, Finocchio E, Busca G. Ageing mechanisms on PdO_x-based catalysts for natural gas combustion in premixed burners. Chem Eng Sci 2010;65(1):186–92.
[227] Zhao S, Li J. Silver-cobalt oxides derived from silver nanoparticles deposited on layered double hydroxides for methane combustion. ChemCatChem 2015;7(13): 1966–74.
[228] Yang Z, Yang P, Zhang L, Guo M, Ran J. Experiment and modeling of low-concentration methane catalytic combustion in a fluidized bed reactor. Appl Therm Eng 2016;93:660–7.
[229] Han Z, Zhang H, Dong B, Ni Y, Kong A, et al. High efficient mesoporous Co_3O_4 nanocatalysts for methane combustion at low temperature. Chemistry 2016;1(5): 979–83.
[230] Mahara Y, Tojo T, Murata K, Ohyama J, Satsuma A. Methane combustion over $Pd/CoAl_2O_4/Al_2O_3$ catalysts prepared by galvanic deposition. RSC Adv 2017;7 (55):34530–7.
[231] Jodłowski P, Jędrzejczyk R, Chlebda D, Dziedzicka A, Kuterasiński Ł, et al. Non-noble metal oxide catalysts for methane catalytic combustion: sonochemical synthesis and characterisation. Nanomaterials 2017;7(7):174.
[232] Li L, Chen H, Zhang C, Fei Z. Ultrafine cobalt oxide nanoparticles embedded in porous SiO_2 matrix as efficient and stable catalysts for methane combustion. Mol Catal 2019;469:155–60.
[233] Sadamori H, T T, Matsuhisa T. Proceedings of the international workshop on catalytic combustion. 1994. p. 166–9. Tokyo, Japan.
[234] Kolios G, Frauhammer J, Eigenberger G. Autothermal fixed-bed reactor concepts. Chem Eng Sci 2000;55(24):5945–67.
[235] Kolios G, Frauhammer J, Eigenberger G. Efficient reactor concepts for coupling of endothermic and exothermic reactions. Chem Eng Sci 2002;57(9):1505–10.
[236] Nieken U, Kolios G, Eigenberger G. Control of the ignited steady state in autothermal fixed-bed reactors for catalytic combustion. Chem Eng Sci 1994;49 (24):5507–18.
[237] Glöckler B, Gritsch A, Morillo A, Kolios G, Eigenberger G. Autothermal reactor concepts for endothermic fixed-bed reactions. Chem Eng Res Des 2004;82(2): 148–59.
[238] Devals C, Fuxman A, Bertrand F, Forbes J, Hayes R. Combustion of lean methane in a catalytic flow reversal reactor. In: The proceeding of the Comsol users conference; 2006.
[239] Blanks RF, Wittrig TS, Peterson DA. Bidirectional adiabatic synthesis gas generator. Chem Eng Sci 1990;45(8):2407–13.
[240] Budhi YW, Effendy M, Bindar Y, Subagjo S. Dynamic behavior of reverse flow reactor for lean methane combustion. J Eng Technol Sci 2014;46(3):299–317.
[241] Balaji S, Lakshminarayanan S. Heat removal from reverse flow reactors used in methane combustion. Can J Chem Eng 2005;83(4):695–704.
[242] Gosiewski K, Warmuzinski K. Effect of the mode of heat withdrawal on the asymmetry of temperature profiles in reverse-flow reactors. Catalytic combustion of methane as a test case. Chem Eng Sci 2007;62(10):2679–89.
[243] Gosiewski K, Pawlaczyk A, Jaschik M. Energy recovery from ventilation air methane via reverse-flow reactors. Energy 2015;92:13–23.
[244] Gosiewski K. Efficiency of heat recovery versus maximum catalyst temperature in a reverse-flow combustion of methane. Chem Eng J 2005;107(1–3):19–25.
[245] Marín P, Ordóñez S, Díez FV. Procedures for heat recovery in the catalytic combustion of lean methane-air mixtures in a reverse flow reactor. Chem Eng J 2009;147(2–3):356–65.
[246] Matros YS. Catalytic processes under unsteady-state conditions43. Elsevier; 1988.
[247] Gosiewski K, Matros YS, Warmuzinski K, Jaschik M, Tanczyk M. Homogeneous vs. catalytic combustion of lean methane-air mixtures in reverse-flow reactors. Chem Eng Sci 2008;63(20):5010–9.
[248] Gosiewski K, Pawlaczyk A, Jaschik M. Thermal combustion of lean methane-air mixtures: flow reversal research and demonstration reactor model and its validation. Chem Eng J 2012;207–208:76–84.
[249] Ioannides T, Verykios X. Catalytic partial oxidation of methane in a novel heat-integrated wall reactor. Catal Lett 1997;47(3–4):183–8.
[250] Zanfir M, Gavriilidis A. Catalytic combustion assisted methane steam reforming in a catalytic plate reactor. Chem Eng Sci 2003;58(17):3947–60.
[251] Polman EA, Der Kinderen JM, Thuis FMA. Novel compact steam reformer for fuel cells with heat generation by catalytic combustion augmented by induction heating. Catal Today 1999;47(1):347–51.
[252] Kolios G, Glöckler B, Gritsch A, Morillo A, Eigenberger G. Heat-integrated reactor concepts for hydrogen production by methane steam reforming. Fuel Cells 2005;5 (1):52–65.
[253] Yan Y, Wu G, Huang W, Zhang L, Li L, et al. Numerical comparison study of methane catalytic combustion characteristic between newly proposed opposed counter-flow micro-combustor and the conventional ones. Energy 2019;170: 403–10.
[254] Guo X, Fan Y, Luo L. Multi-channel heat exchanger-reactor using arborescent distributors: a characterization study of fluid distribution, heat exchange performance and exothermic reaction. Energy 2014;69:728–41.
[255] Fan Y, Luo L. Recent applications of advances in microchannel heat exchangers and multi-scale design optimization. Heat Transf Eng 2008;29(5):461–74.
[256] Brandner JJ, Bohn L, Henning T, Schygulla U, Schubert K. Microstructure heat exchanger applications in laboratory and industry. Heat Transf Eng 2007;28(8–9): 761–71.
[257] Kolb G, Schürer J, Tiemann D, Wichert M, Zapf R, et al. Fuel processing in integrated micro-structured heat-exchanger reactors. J Power Sources 2007;171 (1):198–204.
[258] Miesse CM, Masel RI, Jensen CD, Shannon MA, Short M. Submillimeter-scale combustion. AlChE J 2004;50(12):3206–14.
[259] Hua J, Wu M, Kumar K. Numerical simulation of the combustion of hydrogen–air mixture in micro-scaled chambers. Part I: fundamental study. Chem Eng Sci 2005; 60(13):3497–506.
[260] Chen J, Gao X, Xu D. Stability limits and chemical quenching of methane-air flame in plane micro-channels with different walls. RSC Adv 2015;5(49): 39375–83.
[261] Rodrigues JM, Ribeiro MF, Fernandes EC. Catalytic activity of electrodeposited cobalt oxide films for methane combustion in a micro-channel reactor. Fuel 2018; 232:51–9.
[262] Irankhah A, Rahimi M, Rezaei M. Performance research on a methane compact reformer integrated with catalytic combustion. Chem Eng Technol 2014;37(7): 1220–6.
[263] Mundhwa M, Thurgood CP. Numerical study of methane steam reforming and methane combustion over the segmented and continuously coated layers of catalysts in a plate reactor. Fuel Process Technol 2017;158:57–72.
[264] Niu J, Ran J, Li L, Du X, Wang R, et al. Effects of trapezoidal bluff bodies on blow out limit of methane/air combustion in a micro-channel. Appl Therm Eng 2016; 95:454–61.
[265] Jiang P, Lu G, Guo Y, Guo Y, Zhang S, et al. Preparation and properties of a γ-Al_2O_3 washcoat deposited on a ceramic honeycomb. Surf Coat Technol 2005; 190(2–3):314–20.
[266] Govender S, Friedrich H. Monoliths: a review of the basics, preparation methods and their relevance to oxidation. Catalysts 2017;7(2):62.
[267] Llorca J. In: Monolithic reactor. Berlin, Heidelberg: Springer; 2015. p. 1–3. Berlin Heidelberg.
[268] Williams JL. Monolith structures, materials, properties and uses. Catal Today 2001;69(1–4):3–9.
[269] Lyubovsky M, Karim H, Menacherry P, Boorse S, LaPierre R, et al. Complete and partial catalytic oxidation of methane over substrates with enhanced transport properties. Catal Today 2003;83(1):183–97.

[270] Dupont V, Moallemi F, Williams A, Zhang SH. Combustion of methane in catalytic honeycomb monolith burners. Int J Energy Res 2000;24(13):1181–201.
[271] Lin Y. Microporous and dense inorganic membranes: current status and prospective. Separ Purif Technol 2001;25(1):39–55.
[272] Hu T, Zhou H, Peng H, Jiang H. Nitrogen production by efficiently removing oxygen from air using a perovskite hollow-fiber membrane with porous catalytic layer. Front Chem 2018:6.
[273] Falkenstein Smith R, Zeng P, Ahn J. Investigation of oxygen transport membrane reactors for oxy-fuel combustion and carbon capture purposes. Proc Combust Inst 2017;36(3):3969–76.
[274] Habib MA, Nemitallah MA. Design of an ion transport membrane reactor for application in fire tube boilers. Energy 2015;81:787–801.
[275] Vigneault A, Grace JR. Hydrogen production in multi-channel membrane reactor via steam methane reforming and methane catalytic combustion. Int J Hydrogen Energy 2015;40(1):233–43.
[276] Tan X, Li K, Thursfield A, Metcalfe IS. Oxyfuel combustion using a catalytic ceramic membrane reactor. Catal Today 2008;131(1–4):292–304.
[277] Simakov DS, Sheintuch M. Experimental optimization of an autonomous scaled-down methane membrane reformer for hydrogen generation. Ind Eng Chem Res 2009;49(3):1123–9.
[278] Chen J, Yan L. Ammonia decomposition coupled with methane combustion in catalytic microreactors for hydrogen production. Chem Biomol Eng 1994;2(1):19–26.
[279] Yang Z, Yang P, Zhang L, Guo M, Yan Y. Investigation of low concentration methane combustion in a fluidized bed with Pd/Al_2O_3 as catalytic particles. RSC Adv 2014;4(103):59418–26.
[280] Zukowski W. The role of two-stage combustion in the development of oscillations during fluidized bed combustion of gases. Fuel 2000;79(14):1757–65.
[281] Dubinin YV, Tsereshko N, Saraev A, Bulavchenko O, Yakovlev V. Studying the effect of magnesium on the activity of a deep oxidation catalyst for a fluidized bed in methane and CO oxidation reactions. Catal Ind 2018;10(3):237–43.
[282] Dong Q, Zhang S, Duan Z, Zhou Q. An energy analysis of the catalytic combustion burner. Heat Technol Energy Eff 2006;(3).
[283] Specchia S, Ahumada Irribarra MA, Palmisano P, Saracco G, Specchia V. Aging of premixed metal fiber burners for natural gas combustion catalyzed with $Pd/LaMnO_3{\cdot}2ZrO_2$. Ind Eng Chem Res 2007;46(21):6666–73.
[284] Deng C, Yang W, Zhou J, Liu Z, Wang Y, et al. Catalytic combustion of methane, methanol, and ethanol in microscale combustors with Pt/ZSM-5 packed beds. Fuel 2015;150:339–46.